Amyloid Aggregation Behavior of Human Calcitonin

by

Kian Kamgar-Parsi

A dissertation submitted in partial fulfillment
of the requirements for the degree of
Doctor of Philosophy
(Applied Physics)
In the University of Michigan
2018

Doctoral Committee:

Professor Ayyalusamy Ramamoorthy, Chair
Professor Ari Gafni
Professor Jennifer P. Ogilvie
Professor Duncan G. Steel
Professor Sarah Veatch

Kian Kamgar-Parsi

kkamgar@umich.edu

ORCID iD: 0000-0002-6324-8893

Acknowledgements

I first must thank my advisor, Ayyalusamy Ramamoorthy. Rams more than anyone else helped teach me how to become an independent scientist and provided me the freedom to ask and pursue questions wherever my science took me. All the while, he remained available whenever I needed guidance or advice, and the tutelage and support he has provided over the past three years will forever be appreciated.

I also must thank my committee members, Professors Ari Gafni, Jennifer Ogilvie, Duncan Steel, and Sarah Veatch. All of them have provided invaluable support and guidance during my time at Michigan. Jennifer's perceptive questions have led me to expand my lines of inquiry into new and exciting directions. Sarah has motivated me to be aggressive in pursuing my work, and has provided valuable counsel to me throughout the navigation of my graduate studies. I want to give particular thanks to Ari and Duncan for providing me my first opportunity to conduct independent research, and for continuing to be constant sources of support and advice throughout my graduate studies even after I left their lab to join the Ramamoorthy Lab. Their continued mentorship has been invaluable to me during my graduate school career.

I have also been fortunate to collaborate with several brilliant scientists during my years in the Ramamoorthy Lab. I thank Dr. Akira Naito for providing me with the peptide necessary for my experiments at Michigan, and for his willingness to share his expertise. I thank Dr. Liu Hong for his collaboration on developing kinetics models for amyloid aggregation. Our early morning/late-night skype sessions always proved productive and stimulating. I would also like to

thank Dr. Charlie Brooks for his collaboration on molecular dynamics simulations of calcitonin monomers. Charlie's questions inevitably led me to new and exciting avenues of study, and his willingness to discuss our findings together at length is greatly appreciated.

Of course, the majority of my thesis work occurred in the laboratory, and I owe huge thanks to the people of the Ramamoorthy Lab. Dr. Kamal Mroue, Dr. Rongchun Zhang, Dr. Meng Zhang, Dr. Elke Prade, Dr. Thirupati Ravula, Dr. Sam Kotler, Dr. Jeffrey Brender, Dr. Amit Pithadia, Dr. Kyle Korshavn, Dr. Mukesh Mahajan, Dr. Carlo Barnaba, Dr. Bikash Sahoo, Joshua Damron, Katie Gentry, Sarah Cox, Chris MacDonald, Giacomo DiMauro, and Oluseun Oladipo have all been joys to work with and around, and have become friends both inside and outside the lab. Whether discussing confusing experimental results or weekend plans, I always knew I could count on my labmates for help, support, and lunch dates. They will all be sorely missed when I move on in my career. I'd also like to acknowledge Chun-Chieh (Andrew) Chang, for his mentorship in the Gafni-Steel lab when I first started doing graduate research. He taught me a lot about how to be a grad student which served me well over the following four years.

I also want to thank my family for the support they have given me throughout my graduate school career. First and foremost, I would like to thank my parents, Behzad and Faezeh. Getting a PhD is difficult, and knowing that they were always available to talk to about research or life or my struggles meant the world to me. The original reasons I grew to love science, they have supported me in my endeavors since I was old enough to endeavor, and I cannot adequately express my gratitude to them for their continued love and support. I want to thank my sister Saman for keeping me grounded and focused, and being goofy when I most needed it. Her pride in me when I am not proud of myself has been a constant boon for me when things get tough. I also want to thank my grandmother Irandokht, my aunts Firouzeh and Avid, my uncle Behrooz, and my cousins

Nassime, Kurosh, Dariush, Liana, Kaveh, and Pareesa. The occasions where I could visit home were revitalizing, not least of which because I got to see so many people I loved, and that feeling has helped to drive me in my pursuits.

Table of Contents

List of Figures

List of Appendices

Abstract

Under appropriate conditions, certain peptides and proteins, both intrinsically disordered and misfolded from their native state, can self-associate to form long proteinaceous fibrils known as amyloids. This transition forms the molecular basis of several pathologies, through both losses of native functions and cytotoxic effects. Calcitonin (CT) is a 32 amino acid therapeutic hormone peptide that can be considered a molecular paradigm for the central events associated with amyloid misfolding. CT's biological activity is limited by its aggregation along the canonical amyloid aggregation pathway. A better understanding of the misfolding process would not only provide a structural basis to improve CT's long-term stability and activity as a therapeutic, but also provide valuable insights into the pathological aggregation of other amyloids. As such, the aggregation of human CT (hCT) has been studied in this dissertation using a range of biophysical techniques, with a particular focus on native modulators of kinetic behavior.

A direct relationship between human calcitonin (hCT) concentration and aggregation lag time was observed for the first time, contrary to the conventional understanding of amyloid aggregation. This kinetic trend was found to persist over a range of aggregation conditions, as confirmed by Thioflavin-T kinetics assays, CD spectroscopy, and transmission EM. On the basis of kinetics modeling and experimental results, a mechanism whereby structural conversion of hCT monomers is needed before incorporation into the fibril was proposed. Comparative studies of hCT and the canonically aggregating salmon CT (sCT) using experimental and computational techniques suggested that α-helical monomers represent a growth-competent species, whereas unstructured

random coil monomers represent a growth-incompetent species. The kinetic mechanism proposed represents a novel mechanism in amyloid aggregation, and synthesizes several previously disparate amyloid behaviors.

The determinants of hCT lag time were further investigated in a membrane environment, providing the first systematic study of the effect of membranes on CT aggregation. The direct relationship between peptide concentration and lag phase was found to persist in the presence of large unilamellar vesicles (LUVs), and was shown to be dependent on membrane composition. Specifically, lipid compositions encouraging stronger surface interactions increased the concentration dependent differences in lag time. CD experiments suggested adsorption and sequestration of growth-competent helical monomers to play a role in this behavior. An apparent reformatting of mature hCT fibrils was also observed, in a process which appears dependent on not only lipid composition but also the peptide to lipid ratio. The ability of LUVs to remodel fibers grown in solution suggests that interactions between mature fibrils and lipid bilayers are causative in the behavior, rather than membrane-peptide interactions during fiber growth.

The results of this thesis, particularly as they relate to monomer growth competence, represent significant contributions to the amyloid field and CT therapy. The novel kinetic mechanism proposed reveals that intramolecular interactions in disordered monomers, while often transient and weak compared to intermolecular interactions, can play crucial roles in mediating amyloid aggregation. Additionally, the elucidated effects of monomer structure and lipid interactions on hCT aggregation kinetics present possible means by which aggregation kinetics can be modulating while maintaining peptide sequence and thus therapeutic efficacy, a key goal in hCT therapies. Such results present a richer picture of hCT aggregation than had previously been available, and potentially provide novel insights as to more general mechanisms of amyloid aggregation.

Chapter 1

Structural Biology of Calcitonin: from aqueous therapeutic properties to amyloid aggregation

This chapter was adapted from the following publication

> Kamgar-Parsi, K., Tolchard, J., Habenstein, B., Loquet, A., Naito, A., and Ramamoorthy, A. (2016) Structural Biology of Calcitonin: From Aqueous Therapeutic Properties to Amyloid Aggregation. *Isr. J. Chem.* **57**, 634–650

1.1. Introduction to Amyloid Aggregation of Calcitonin

The peptide hormone Calcitonin (CT) was first discovered in 1962 by Copp and colleagues.(1) By monitoring serum calcium levels in fasted and anesthetized dogs, it was found that in concert with the previously identified parathyroid hormone (PTH), an additional hypocalcemic factor named calcitonin was involved in the maintenance of blood calcium levels. These findings were reaffirmed a year later by Kumar et al.(2) Despite initial experimentalists ascribing a parathyroidal origin for CT, it was soon determined to be a thyroid hormone.(3) The 32 amino acid sequence of human calcitonin (hCT) was first determined in 1968, and in the following years several other CT variants were discovered and sequenced, including the oft-studied bovine, porcine, and salmon CTs.(4–7) All sequenced CTs are 32 residues in length and have an intramolecular disulfide bridge (Cys1-Cys7), but sequence homology varies significantly from species to species, with hCT differing from other CTs by as few as 2 residues (murine CT) or as many as 19 residues (ovine CT).(8, 9) CTs retain significant homology in the N-terminal residues, with the N-terminal disulfide bond in particular being conserved across all known

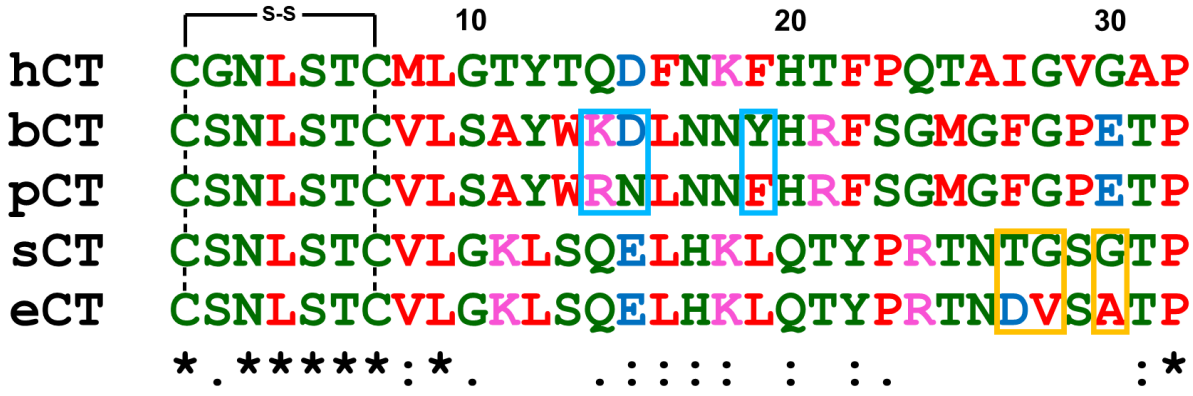

Figure 1.1. Amino-acid sequence alignment of the commonly studied human, bovine, porcine, salmon, and eel calcitonin. All sequences contain a disulfide bridge between residues 1 and 7, with 8 residues being conserved in all species (*), primarily at the N-terminus. C-terminal amino-acid sequences vary significantly between different homologues. Evidence for the evolutionary divergence of different CT sequences can be seen in the relative conservation of CT between more recently diverged species. Eel and salmon CT (eCT and sCT) differ at only 3 locations (orange boxes), with bovine and porcine CT (bCT and pCT) also differing at 3 (blue boxes), whereas mammalian and fish CTs maintain less than 50% sequence homology. Colors describe residues of similar chemistry, asterisks denote fully conserved residues, and periods and colons indicate weak and strong conservation of amino-acid chemistry, respectively.

calcitonin sequences; a feature commonly thought to reduce amyloidogenic aggregation.(10) A comparative alignment of several commonly studied calcitonin peptide sequences is shown in Figure 1.1.

Despite the sequence diversity among CT variants, all CTs have been shown to aggregate into amyloid fibrils when concentrated in aqueous conditions.(11–14) The term “amyloid” references a specific type of supramolecular protein/peptide fibrillar architecture in which monomeric subunits are stacked along the fibril axis through intermolecular hydrogen bonds and electrostatic interactions between β-strands.(15, 16) Such an amyloid fold was structurally characterized for aggregated calcitonin peptides by the presence of β-rich conformation in hCT and the typical cross-β structure in salmon CT by X-ray diffraction.(11, 17) This type of aggregation behavior and secondary structure change is observed in numerous proteins and peptides, and similar conformational diseases have been attributed to a wide variety of pathologies.(18) A significant number of human amyloid peptides have been found to play a role

in conferring pathological conditions to propagate diseases, including the extensively studied amyloid-β, human islet amyloid polypeptide (hIAPP), and α-synuclein peptides, which are implicated in Alzheimer's disease, Type 2 Diabetes Mellitus, and Parkinson's disease respectively.(19–21) Importantly, amyloids have been revealed to possess infectious properties as has been demonstrated for the prion protein.(22) Aggregation products and/or intermediates of these peptides/proteins have been shown to be toxic to various cell types or to drastically perturb their cellular functions.(19–21)

The aggregation process of these peptides is thought to be highly conserved despite differences in primary sequences.(23, 24) For a detailed background and more details on the topic of amyloid aggregation, readers are referred to recent review articles in the literature.(16, 25–31) Briefly, unstructured monomers fold and combine to form small, intermediate aggregates (oligomers) during a period called the lag phase. Oligomers then gradually progress to generate larger protofibrillar species. Upon the formation of a critical nucleating species, amyloids can self-template and undergo rapid fiber growth occurring during the elongation phase. These fibers can subsequently nucleate new protofibrils through numerous secondary nucleation pathways.(31, 32) Eventually, an equilibrium is reached where maximal fiber content is achieved, known as the plateau phase. This description of amyloid aggregation is oversimplified, however; in reality, a complex amalgamation of off-pathway aggregates, species metastability, and heterogeneity serve to obfuscate the determination of the driving factors and intermediate species in the fibrillation and toxicity of amyloidogenic sequences (Fig. 1.2.). Additionally, aggregation is sensitive to a range of environmental factors including buffer composition, salt, pH, lipids, and metals, highlighting the difficulties inherent in generating an all-inclusive model of amyloid aggregation.(16, 20) Although amyloids were originally a species of interest in disease due to their

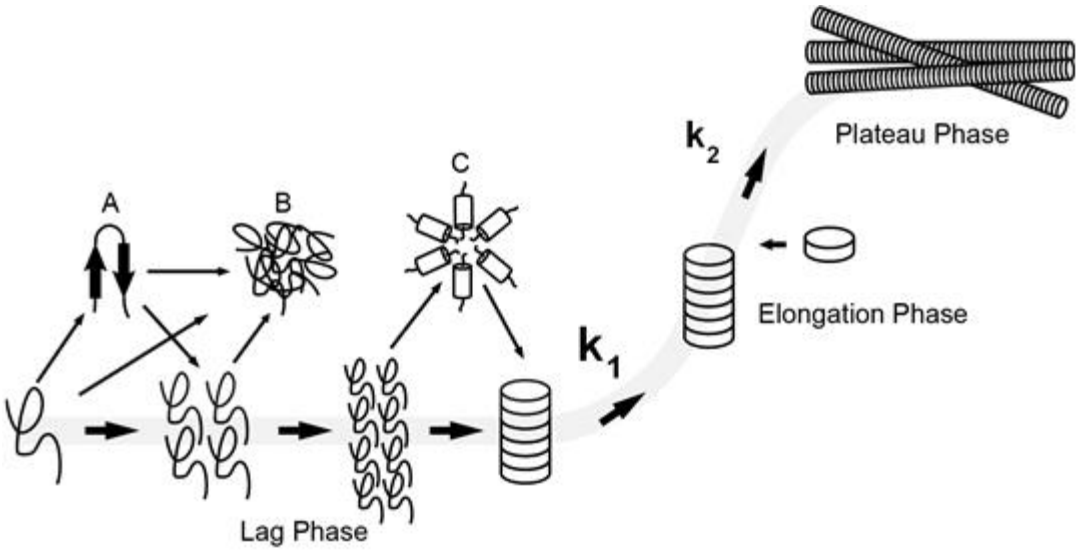

Figure 1.2. Canonical amyloid aggregation pathway. The illustration presents a simplified overview of the process. Initially unstructured monomers aggregate into low molecular weight oligomers, which further aggregate into larger soluble oligomers during the lag phase. Upon formation of a critical nucleus/protofibrillar species, with a first time-determining rate constant, k_1, aggregation is self-templated and fibril elongation progresses rapidly through the addition of monomers or small oligomers in the elongation phase, with a second time-determining rate constant, k_2. Eventually, fiber formation rates equilibrate, with breakage rates and fiber content remaining constant; this is known as the plateau phase. Typically, a majority of initial monomers are sequestered in fibrils, but small aggregates persist even after fibrillation is complete. This picture is complicated by the number of off-pathway intermediates, which provide alternative pathways to fibrils (A, C) and amorphous nonfibrillating aggregates (B). Secondary structural shifts in the monomer to β-sheet morphology (A) and the formation of α-helical peptide micelles (C) as critical species have also been proposed as steps in the amyloid cascade.

propensity to form readily identified plaques, recent evidence has shifted focus away from mature aggregates and towards early oligomers as the putative pathological species in amyloid related diseases.(16, 20, 21, 33) Significant efforts are ongoing to elucidate the mechanism(s) of toxicity and identity the toxic species in amyloid-related diseases.

The amyloidogenic aggregation of CT specifically presents multiple practical challenges, both in normal bodily function and in therapeutic applications. While multiple variants of CT are known to be toxic and form membrane-permeabilizing oligomers *in vitro*, the roles that such behaviors play *in vivo*, if any, are not as well established as in other amyloids.(12, 34–37) To date, such behaviors have not been shown to have any significant roles in disease pathologies, though membrane interactions do hold relevance for both biological function and drug delivery. Studies of CT have revealed that it has skeletoprotective properties mediated through interactions with the

calcitonin receptor (CTR) expressing osteoclasts, leading to its use as an osteoporosis therapeutic agent.(8, 38) Aggregation, however, sequesters and remodels the monomeric subunits of CT and decreases their free concentration, consequently preventing the activation of CTRs.(39, 40) Efforts to combat this limited bioavailability have led to the replacement of hCT as a therapeutic agent with the slower aggregating salmon CT (sCT). However, not only does sCT therapy cause immune response correlated complications, but hCT has also been found to be more potent than sCT under conditions where aggregation was controlled.(40–42) Such considerations highlight why there is significant interest in manipulating the aggregation and structural remodeling of both hCT and sCT for therapeutic purposes. This introduction will examine the role of CT in normal bodily function, its use as a therapeutic agent, and focus on how structural considerations of the aggregation pathway relate to CT biology and therapy.

1.2. Calcitonin production and expression

The first evidence of the existence of a hypocalcemic hormone was provided in 1962 by Copp et al.(1) Using perfusion studies, it was found that decreases in serum calcium levels occurred too rapidly to be caused solely by changes in the expression of the previously known hypercalcemic PTH. This behavior was independently reproduced within the next year, and parathyroidectomy experiments initially suggested a parathyroidal origin for CT.(2) Further experiments revealed the true source of CT (then called thyrocalcitonin to distinguish it from the thought to be separate calcitonin) to be the thyroid.(3) Immunofluorescence experiments later determined CT to be produced solely and specifically in thyroid C-cells.(43)

The synthesis of CT is explained in detail in other reviews.(8, 44) Briefly, CT is coded for by the CALC I gene. Splicing of the gene transcript at exon 4 yields CT in thyroid C-cells, with alternative splicing producing calcitonin gene-related peptide (CGRP), a potent vasodilator, in

neural cells (Fig. 1.3.). Both CT and CGRP are part of the calcitonin family, along with the structurally similar peptides hIAPP and adrenomedullin (AM), although unlike CGRP, hIAPP and AM are not alternative splice products.(45) The 32 residue mature CT, with a disulfide linker between residues 1 and 7, is subsequently released from thyroid C-cells following cleavage from a larger precursor protein.(8, 44)

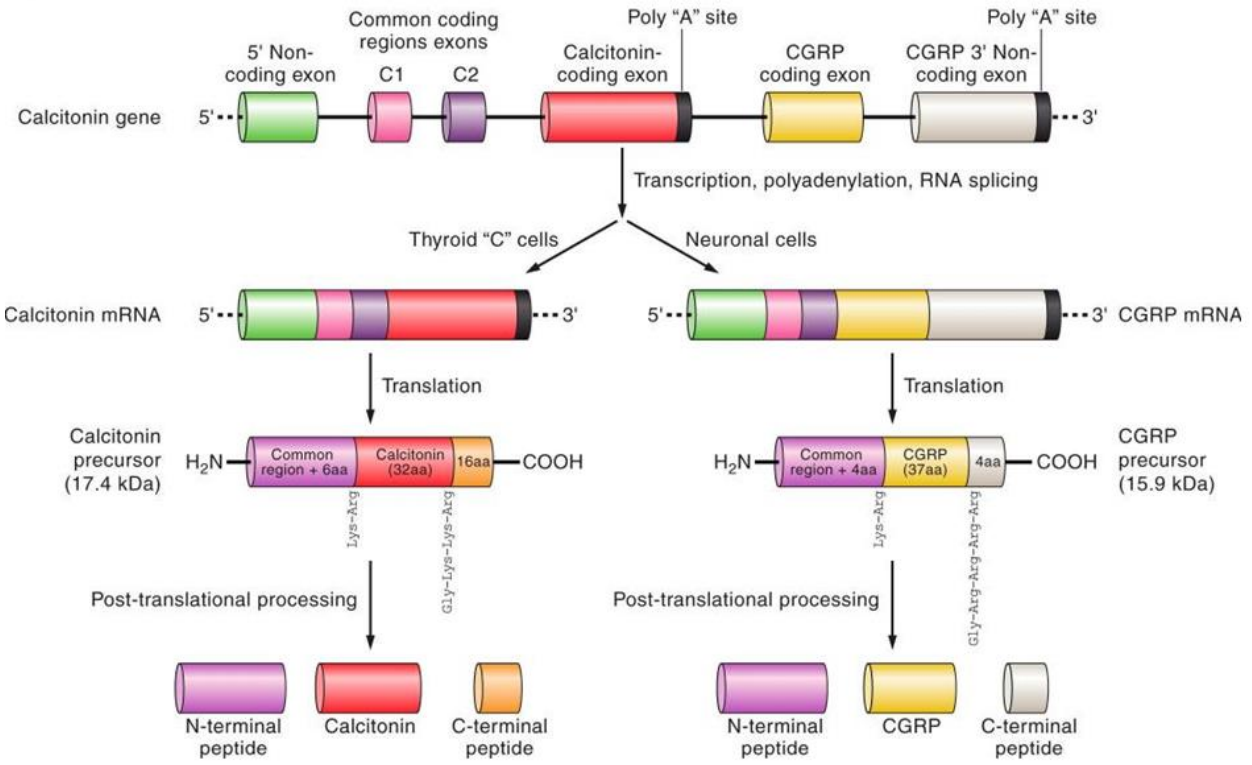

Figure 1.3. Illustration of the synthesis of calcitonin from the CALC I gene. Alternative splicing in thyroid (calcitonin) versus neuronal cells (CGRP) determines the hormone produced. Calcitonin is initially translated as a 17.4 kDa precursor protein, and then sequentially post translationally cleaved (via pre procalcitonin and procalcitonin) to form the 32 residue mature peptide hormone. Figure adapted from (46).

1.3. Physiological roles of Calcitonin

In the decades following CT's discovery, research has revealed it to have additional physiological roles. Most prominent among these is its role in skeletal protection, with hypercalcemia prevention and gastrointestinal interactions being secondary roles. However, some studies have shown minimal metabolic deviations upon removal of CT, leading to speculations

regarding the significance of CT's physiological role.(47) Here we discuss the roles of CT in skeletal protection and hypercalcemia prevention in the body, and consider the evidence for a role in gastrointestinal function.

1.3.1. Skeletal protection

CT's most prominent physiological role is its interaction with the skeleton to moderate calcium homeostasis between blood and bone. CT serves to maintain bone mass primarily by inhibiting osteoclasts, a bone-associated cell type responsible for bone resorption.(48–50) CT's interactions with osteoclasts are mediated by the CTR, a G protein-coupled receptor widely expressed on osteoclast membranes.(51) Upon activation by CT, CTR causes a prompt loss in osteoclast ruffled border, a decreased ability of osteoclasts to acidify the bone-cell interstitial space, and decreased cellular motility.(52–54) All of these effects inhibit osteoclast activity and lead to decreased bone resorption and increased skeletal mass. The related amyloidogenic peptides CGRP and hIAPP have demonstrated an ability to activate CTR mediated inhibitory pathways in osteoclasts, although their interaction and subsequent inhibition is far weaker than the native substrate CT.(8) The relative affinity of the CTR for different members of the calcitonin family is mediated by receptor activity modifying proteins (RAMPs), and as such, elucidating the behavior of RAMPs is the subject of significant scientific effort.(20, 55, 56)

In addition to interactions with the CTR, CT has other direct effects on osteoclast function. CT can alter the phosphorylation state of the focal adhesion proteins paxillin, FAK, and Pyk2.(57) A CT dependent disruption of the actin-ring structure associated with the sealing zone of osteoclasts has also been observed.(57, 58) Loss of focal adhesions leads to decreased efficiency in resorption and eventual decline in overall osteoclast numbers.(8) CT can also form calcium permeable pores in lipid bilayers, with some claiming that such ion flow could lead to osteoclast

detachment from the bone matrix.(36, 37, 59, 60) A role for calcium permeable CT pores *in vivo* requires further exploration, although calcium dependent alterations of osteoclast function are known.(61, 62)

Interactions between CT and two other bone related cell types, osteoblasts and osteocytes, have also been observed, although such interactions are poorly understood. CT administration has the conflicting actions of both decreasing osteoblast function and enhancing osteoinduction.(63, 64) Such behaviors lead to decreased and increased skeletal strength, respectively, confounding efforts to determine the function of CT's interaction with osteoblasts. CT also protects both osteoblasts (no CTR expression) and osteocytes (CTR expression) from apoptosis, indicating an apparently CTR independent interaction with such cells.(65) In addition, osteocyte production of sclerostin, a protein associated with a decrease in bone growth, is induced by sCT.(66) These behaviors have led some to suggest that CT regulates bone turnover through both osteoclast and osteocyte interactions.(67) Overall however, the role of CT in mediating osteoblast and osteocyte function remains unclear.

Several experiments where thyroidectomy had no significant effects on long term bone mass have challenged the significance of CT's role amongst the range of bone regulating hormones.(47, 68) Experiments have also surprisingly shown increased bone mass in CT/CGRPKO mouse models, although such results are confounded by the action of CGRP.(69) Additionally, complications from cortical porosity and overactive bone resorption were observed at 12 months of age in the CT/CGRPKO mouse models.(70, 71) The release of osteoclasts from the inhibitory effects of CT after prolonged exposure and the degradation of hCT in human serum are also well-established phenomena, suggesting the effect of hCT on bone cells is short-lived.(72,

73) It is thus likely that CT's primary contribution to bone physiology is in short-term bone remodeling, or under conditions of significant calcium stress.(67, 74)

In particular, CT is believed to play a significant role in calcium homeostasis during pregnancy and lactation, when maternal bone mass is under pressure from the calcium demands of the fetus or infant. CT stimulates the production of 1,25-dihydroxyvitamin D_3 (1,25D, the active form of vitamin D), with elevated CT and 1,25D levels being associated with pregnancy and lactation, an apparently contradictory relation given the role of 1,25D in promoting resorption.(75–79) However, CT has also shown the ability to increase intestinal absorption of calcium, and thus it appears as if CT could serve the dual roles of increasing dietary calcium uptake, and promoting calcium transfer from bone to serum (through 1,25D) during lactation and pregnancy.(78) This behavior would both protect the maternal skeleton and ensure sufficient calcium delivery to the fetus or infant. In a CT Null mouse model, the bone mineral loss during lactation and the time for bone mass to return to normal were both increased by the lack of CT.(77) Treatment with sCT rescued mineral loss and time to return to baseline.(77) As such, a heightened physiological role for CT during pregnancy and lactation when the mother is under elevated demand for calcium, has been proposed.(75, 77, 80)

1.3.2. Hypercalcemia prevention

The potential for CT to counteract hypercalcemia has been implied since its discovery.(1, 2) While it exhibits no ability to directly sequester or transfer calcium, CT's hypocalcemic function can be explained by its inhibition of osteoclasts; a decrease in bone resorption and transfer of calcium from bone to blood would decrease serum calcium levels. CT in healthy individuals under normal calcium load has a minimal effect, but shows an ability to decrease serum calcium under conditions of endogenous addition of calcium or high bone turnover.(74, 77, 81–83) As such, it

has been theorized that under normal conditions (no exogenous load, normal bone turnover) PTH governs the efflux of calcium from bone, with the influx being governed by the normal concentration gradient of calcium. Meanwhile, under conditions of acute hypercalcemia CT can decrease the efflux of calcium from the skeleton and thus reduce serum calcium levels through its inhibition of osteoclastic activity.(84, 85) Such a view is in keeping with the observed behavior of osteoclastic release from CT inhibition. It is also supported by the upregulation of CT under conditions of high serum calcium, and the susceptibility (and subsequent CT-based rescue) of CT KO mice to hypercalcemia.(67, 86)

1.3.3. Gastrointestinal function

Some evidence suggests that CT could also play a role in gastrointestinal function. Intestinal absorption of calcium is increased by CT.(78) Elcatonin, a synthetic eel calcitonin, has been shown to inhibit gastric and duodenal ulcers.(87) Calcitonin receptor-like receptors have been localized to the human GI tract, and the peptide hormone gastrin, responsible for the secretion of gastric acid by parietal cells, significantly upregulates CT secretion.(80, 88, 89) A similar effect has been found for several other gastrointestinal hormones as well.(90) The studies on GI hormone induced CT secretion were, however, conducted with surgically isolated thyroid glands in situ with direct exposure of the thyroid to GI hormones, thus it is unclear if the response has any biological significance. Overall, the interplay of CT and gastrointestinal function, if any, is still to be determined.

1.4. Structural studies on calcitonin aggregation

CT's aggregation in solution is associated with non-covalent supramolecular assembly leading to the precipitation of the peptide. At the macroscopic level, it results in sample gelation.

Initial structural investigation of CT aggregation was primarily focused on these end-stage aggregates.(11, 91–94) Work by Arvinte and colleagues provided one of the first studies focused on the structure and kinetics of hCT fibrillation.(11) Arvinte found higher peptide concentrations correlate with decreased lag time, a behavior that has been observed for sCT, hCT, and other amyloids, both experimentally and in simulations.(93, 95–97) hCT also showed a propensity to form well-ordered fibrillar aggregates, another common characteristic of other amyloidogenic sequences (Fig. 1.4.).(20, 93, 98–102) TEM images of hCT indicate that short fibrils are observed

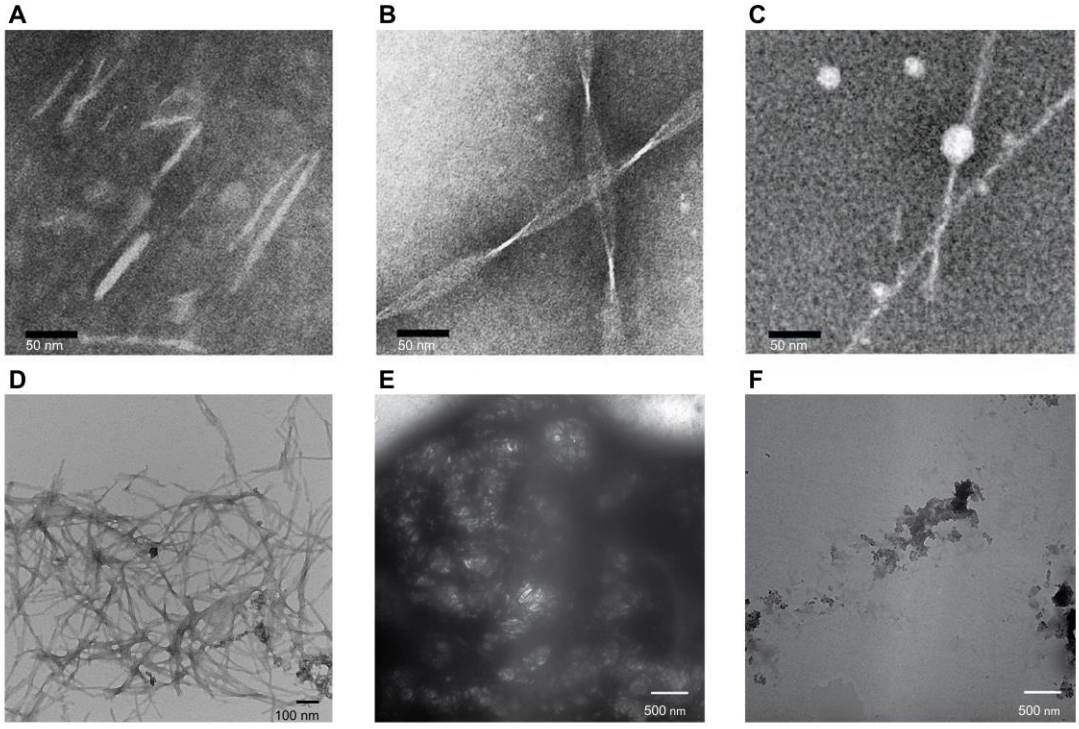

Figure 1.4. Transmission electron microscope images of polymorphic solution structures of human calcitonin aggregates formed under different conditions. A) Short straight fibrils formed 90 min after dissolving 22.5 mg ml^{-1} of hCT in 20 mM sodium phosphate buffer (100 mM NaCl, pH 7.5) at 20 °C. B) Long twisted ribbon type fibrils formed 45 days after dissolving 22.5 mg ml^{-1} of hCT in aqueous acetic acid (15 mM, pH 3.3) at 20 °C. C) Spherical aggregates together with short fibrils formed 4 days after dissolving 40 mg ml^{-1} of hCT in HEPES solution (20 mM, pH 5.6) at 20 °C. D) Dense fibrils of hCT formed from 120 μM initial monomer concentration at 25 °C in 20 mM sodium phosphate buffer (100,000× magnification; unpublished results from the Ramamoorthy group). TEM images of 0.3 mM samples of hCT after 36 hours of incubation at pH 7.4 and 298 K: E) without; and F) with 3 molar equivalents of EGCG (epigallocatechin 3-gallate, a polyphenolic compound extracted from green tea). Absence of amyloid fibers in (F) suggests that EGCG effectively inhibits the aggregation of hCT, which has been further confirmed by NMR experiments; mechanistic details have been reported elsewhere by the Ramamoorthy group (105). TEM images A)–C) were adapted from (98), while E) and F) were adapted from (105).

at pH 7.5, while long twisted fibrils are observed at pH 3.3 (Fig. 1.4.B and C).(103) Interestingly, hCT has exhibited both α-helical and β-sheet structures in end stage fibers, a deviation from the canonical view of amyloid peptides as maintaining a stable, exclusively β-sheet conformation content.(11) Further studies have demonstrated that while α-helical motifs may exist in the final equilibrium mixture (and indeed recent studies have identified primarily helical amyloid fibers), CT fibril morphology primarily relies on β-sheet conformation.(12, 36, 103–109) Figure 1.5. shows typical NMR fingerprints, based on solution and solid-state NMR, of hCT in various forms (soluble and aggregated in mature fibrils).

Subsequent studies have yielded more detailed structural data on the amyloid fibrils of CT. Based on solid-state NMR spectroscopy, Naito and colleagues have revealed distinct behaviors for the central, N-terminal, and C-terminal regions of hCT. Early species contain a central α-helix, with a loop structure at the N-terminus and a random coil C-terminus (Fig. 1.6., monomer).(103) During fibril formation, the central helix converts to a β-strand, with the N-terminal loop remaining unchanged.(103) The formation of this central β-strand also results in a shorter C-terminal in random coil conformation, with residues closer to the central region incorporating into the β-strand (Fig. 1.6., fiber).(104) The observation of a central α-helix to β-strand conversion with a structured N-terminus and unstructured C-terminus has been confirmed in follow up studies by both Naito and others.(91, 92, 98, 108, 110–112) These secondary structural changes in hCT fibrillation persist in both neutral and acidic environments, but pH-dependent differences in the relative length and orientation of β-sheet motifs in the fibril do arise.(98, 104, 112) Specifically, while fibers at pH 7.5 assemble in an antiparallel orientation, fibrils of hCT at low pH form a mixture of parallel and antiparallel β-sheets. It has been suggested that the charge states of the amino acids Asp15,

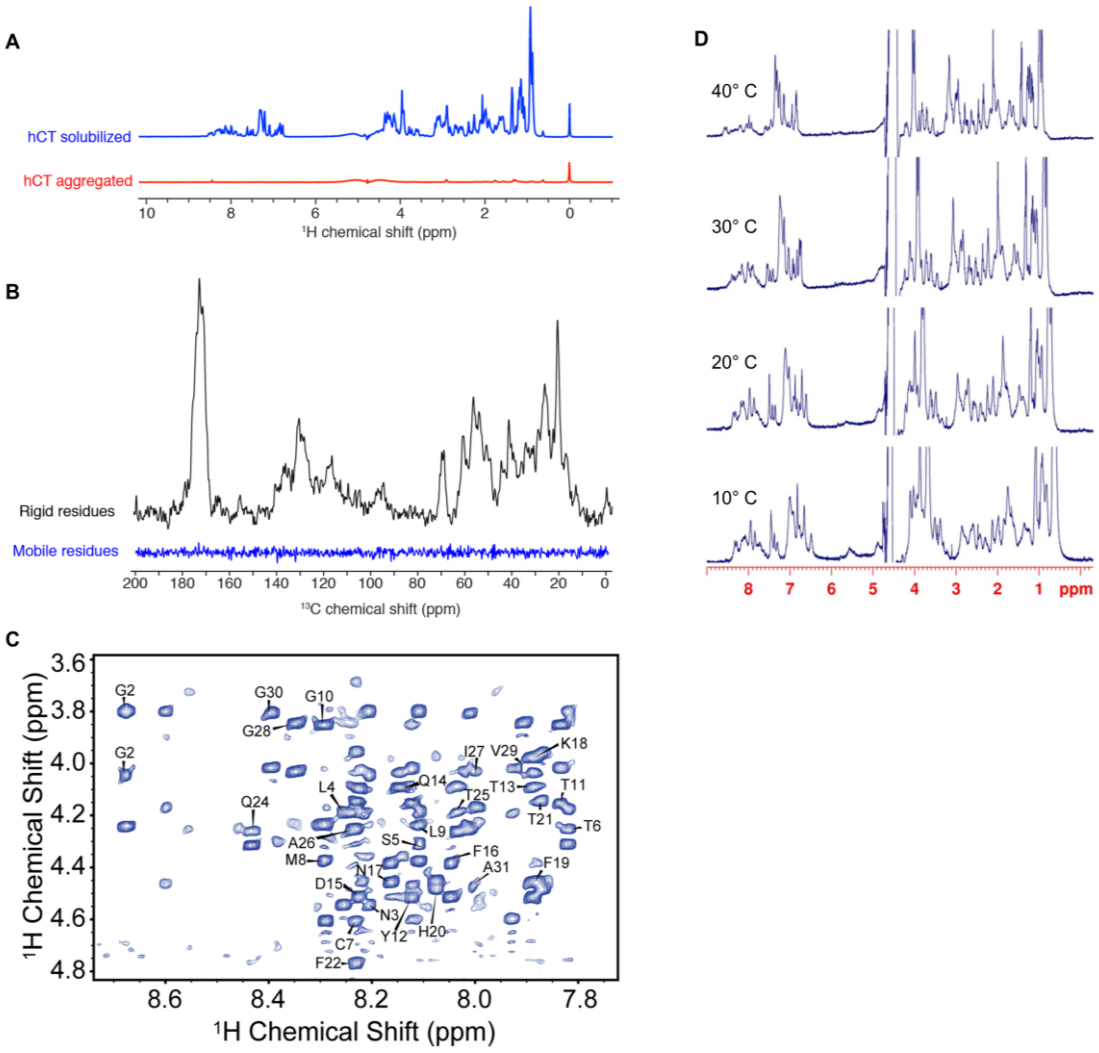

Figure 1.5. Solution and solid-state NMR spectra of hCT in various forms. A) Solution NMR spectra of hCT peptide, in the soluble form (in blue) and in its aggregated form (in red). Signal loss in the spectra of the aggregated form is due to the very slow molecular tumbling that exhibits prefibrillar and fibrillar nanoobjects. B) Solid-state NMR spectra of the hCT fibrils. Cross-polarization experiment (in black) probes the residues in a rigid conformation. The ^{13}C CPMAS spectrum shows relatively high resolution, indicative of a well-ordered core. INEPT-based polarization transfer from ^{1}H to ^{13}C (in blue) is used to probe mobile residues (faster than the microsecond timescale of motion). The absence of signals in the INEPT experiment indicates that all residues within the hCT peptide sequence adapt a rigid conformation. C) Two-dimensional $^{1}H/^{1}H$ NOESY spectrum (the Hα-HN region) of 1mM hCT (in 2 mM sodium phosphate buffer, 7 % D_2O, 50 mM NaCl, pH = 2.9) obtained at 900 MHz proton resonance frequency with a 300 ms mixing time (spectrum adapted from (105)). NOEs were used to determine the structure of the peptide as reported in (105). D) Proton NMR spectra of hCT at pH 7.4 recorded at 600 MHz shows the temperature-dependent spectral resolution; line broadening of amide-NH resonances and line narrowing of aliphatic resonances were observed as the sample temperature was increased from 10 to 40 °C, demonstrating the feasibility of probing the aggregation at atomic-level resolution by NMR spectroscopy (unpublished results from the Ramamoorthy lab).

Lys18, and His20 mediate this effect.(111) It is likely, therefore, that electrostatic interactions play an important role in the structure and packing of CT fibers, as has also been observed for other amyloid peptide assemblies.(113, 114)

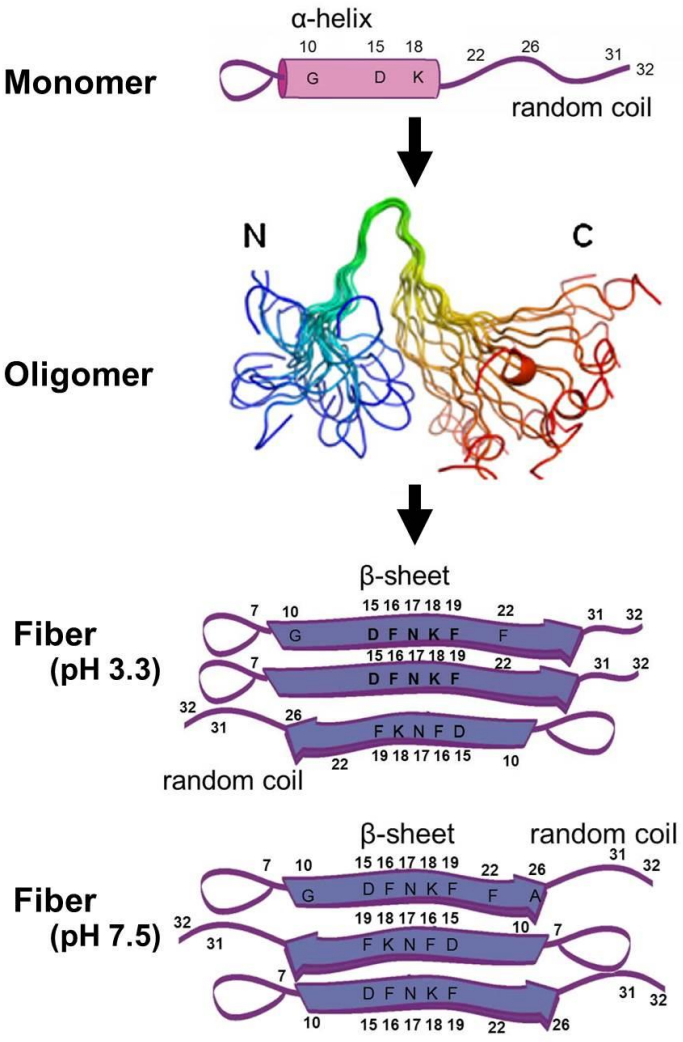

Figure 1.6. NMR-derived structures of monomer, oligomer, and fibril stages of hCT. The monomer and fibril structural models are based on NMR experiments at pH 3.3, and the oligomer structural model is based on NMR experiments at pH 3.3 and 7.5. The monomer exhibits an N-terminal loop, central α-helix, and C-terminal random coil. During early stages of oligomerization, the helix transitions to a β-hairpin, with the N- and C-termini remaining unchanged. This β-structure incorporates more C-terminal residues, with further aggregation, and eventually gives rise to a distinctive β-sheet morphology of amyloid fibrils. At low pH, the charge states on residues 15, 18, and 20 allow for both parallel and antiparallel β-sheet stacking. At neutral pH, residue 15 and 18 possess negative and positive charges, respectively; thus, fibrils show antiparallel β-stacking. The structures show one possible pathway from a monomeric to a fibril structure, although other intermediates along the way are likely.

Several other experiments have been carried out to probe the effect of electrostatic interactions on the aggregation kinetics of CT. At neutral pH, hCT contains a negative charge at Asp15, and positive charges at Lys18 and the C-terminal amide.(111) At acidic pH, His20 (pKa ~6) and Asp15 (pKa ~3.6) both become protonated, changing hCT's charge from +1 to +3.(111)

Increasing peptide charge by decreasing pH has been shown to slow aggregation in CT, yet substitution of the Asp15 with an Asn (increasing the net charge from +1 to +2 at neutral pH) led to accelerated fibrillation kinetics.(105, 111) In contrast, a comparison at neutral pH between hCT (+1 charge) and the slower aggregating sCT (+3 charge) contradicts the behavior of the Asn-hCT mutant relative to the wild-type.(115) The role of electrostatic interactions in CT aggregation kinetics must therefore be more complicated than simple net charge considerations. It is worth noting that all of hCT's charged residues occur in the central region (Fig. 1.1.), associated with rapid formation of α-helices. Consequently, hydrophobic interactions that drive fibril formation likely confound efforts to elucidate the precise role of charged residues in kinetics.

Naito's work has also implicated oligomeric intermediates with a spherical shape as important in seeding fibrils.(98) Such intermediates were found to serve as nucleation sites for the growth and elongation of mature CT fibers, and appeared to be critical for fibril formation. While the structure of these fibers was similar to those previously observed, the biological relevance of the spherical intermediates is uncertain due to the known aggregation-inhibiting properties of the fibrillation environment.(98) Naito's studies have also demonstrated the importance of aromatic residue π-π stacking interactions for maintaining fibril stability.(112) This π-π stacking is viewed as an important driving force during the self-assembly of amyloid fibrils, considering its energetic contribution to the inter-subunit molecular interaction network and its impact into the directionality of the subunit stacking.(116) In this regard, Metrangolo and co. have recently shown that iodination of the two phenylalanine residues of hCT can amplify the fibril formation, leading to a 30-fold more efficient aggregation process.(117) The aromatic stacking is thought to be a major contributor to the difference in aggregation kinetics between sCT and hCT, given that the involved central aromatics Tyr12, Phe16, and Phe19 in hCT all change to Leu in sCT (Figure 1).

Such alterations would eliminate any stabilizing π-π interactions, thus decreasing the stability of critical aggregation species and slowing fibrillation. Indeed a recent crystal structure of hCT showed these π-π interactions to be key in stabilizing the core of hCT amyloid fibrils, and thus also likely key mediators of aggregation rate.(118)

Similar to other central amyloidogenic peptide fragments, the central hCT pentapeptide fragment $D_{15}FNKF_{19}$ has been shown to be required for fibril formation.(108) The central residues of CT are believed to form the fibrillar core of the amyloid fibrils, and the pentapeptide aggregates into fibers with a morphology similar to that formed by the full-length peptide.(103, 106) This fiber formation is noteworthy due to the fairly hydrophilic nature of the pentapeptide, a challenge to the theory that amyloid aggregation is primarily driven by hydrophobic interactions(119) and rather suggests a combined mechanism of hydrophobic and hydrophilic interactions as have been observed for example in polyQ disease related peptides.(120) Like the full-length peptide, it is possible that aromatic interactions play a major role in stabilizing the fibers, although experiments performed with other short peptide fragments from different amyloid peptides counter this claim.(108, 121) Such experiments instead suggest that aromatic interactions are not necessary for fibrillation, but simply alter fibril structure. Regardless, experiments have clearly demonstrated the $D_{15}FNKF_{19}$ hCT fragment to be a key sequence in mediating fibril formation. A second amyloidogenic sequence of hCT towards the N-terminus, T_6CMLGT_{11}, has also been predicted, with an analog having been demonstrated to form amyloid fibrils, though the relevance of this fragment remains up for debate.(122)

A commonly observed feature of both sCT and hCT aggregation is the formation of α-helical motifs.(11, 13, 14, 108, 123–126) Both the full-length hCT and the $D_{15}FNKF_{19}$ pentapeptide have exhibited such structures, with α-helical intermediates forming rapidly and

being highly stable.(103, 104, 108) The specifics of the progression from α-helical intermediates toward the mature fibrillar structure are influenced by a number of factors including pH conditions, the presence of lipids, buffer composition, and the concentrations and types of salts and metal ions.(13, 37, 98, 101, 103, 104) Despite this variability in fibrillation, α-helical intermediates have been observed under a range of conditions and play a significant role in the biological function of CT (discussed below).(11, 14, 108, 121, 127–129) It has also been reported that dimerization of hCT stabilizes the α-helix under aqueous TFE solutions, and that this dimerization is important to the formation of long fibrils.(130) Within individual CT monomers there are often multiple secondary structural motifs present that depend on the aggregation environment and could influence peptide behavior, but given the ubiquity of α-helical intermediates it seems generally accepted that they are a key species in the *in vivo* aggregation of CT.(103, 104, 110)

1.4.1. Kinetic analysis of fibril formation of calcitonin

Kinetic analyses of hCT have been performed by using solid-state ^{13}C NMR to gain insight into the mechanism of fibril formation and inhibition.(98, 103, 104, 111, 112) Increased ^{13}C CP/MAS NMR intensities suggest that the fibrillation can be explained by a two-step autocatalytic reaction mechanism, in which the first step is a homogeneous association to form a nucleus or intermediate and the second step is a catalytic heterogeneous fibrillation to elongate the fibril. The rate constants for the first step (k_1) and the second step (k_2) were analyzed using the following equation,(103)

$$f = \frac{\rho\{\exp[(1+\rho)kt] - 1\}}{\{1 + \rho\exp\{(1+\rho)kt\}}, \qquad (1)$$

where, f represents the fraction of fibril among the total population of peptide among the total population of peptide molecule, $\rho = k_1/k$, $k = ak_2$, and the initial peptide concentration is given by a. The two-step autocatalytic reaction mechanism applied to kinetic analysis of hCT using Eq. (1) was found to be mathematically identical to the Finke-Watzky (W-T) two-step mechanism, which is also used for analysis of the kinetics of fibril formation.(131) This kinetic analysis provided the rate constant of the first step (fibril nucleation), k_1, which is responsible for the lag time of the fibrillation, and the rate constant of the second step (fibril elongation), which is responsible for the rate of fibril elongation. The rate constants for wild-type hCT and several mutants are shown in Table 1. Of note is the fact that k_1 is consistently at least three orders of magnitude smaller than k_2, indicating primary nucleation to be the rate limiting step in hCT aggregation, regardless of pH or point mutations. Additionally, the contributions of central aromatic and charged residues in determining the aggregation rate of hCT, particularly at neutral pH, can be seen.

Table 1.1. pH-dependent rate constants, k_1 and k_2, in a two-step autocatalytic reaction mechanism for hCT fibril formation in solution. *F16L, F19L, Y22L-hCT

Sample	Condition	k_1 (s^{-1})	k_2 ($s^{-1}M^{-1}$)	Ref.
Wt-hCT	pH 7.5	2.8×10^{-6}	2.3	(103)
Wt-hCT	pH 3.3	3.3×10^{-6}	2.4×10^{-3}	(103)
D15N-hCT	pH 7.2	1.6×10^{-5}	5.5	(111)
D15N-hCT	pH 2.9	6.2×10^{-7}	5.4×10^{-3}	(111)
F16L-hCT	pH 7.5	1.9×10^{-7}	4.8×10^{-2}	(112)
F16L-hCT	pH 2.6-3.0	1.8×10^{-6}	6.2×10^{-3}	(112)
F19L-hCT	pH 7.5	7.4×10^{-9}	2.9×10^{-2}	(112)
F19L-hCT	pH 2.6-3.0	1.3×10^{-6}	1.6×10^{-2}	(112)
TL-hCT*	pH 7.5	3.4×10^{-6}	3.0×10^{-3}	(112)
TL-hCT*	pH 2.6-3.0	5.4×10^{-6}	4.8×10^{-3}	(112)
Wt-hCT (HEPES)	pH 5.6	3.0×10^{-10}	2.0×10^{-3}	(98)

1.4.2. Membrane interactions

CT-membrane interactions have been an area of interest both for the possibility of physiological relevance via pore formation, and for the increasing prevalence of lipid-based delivery options for therapies.(36, 37, 110, 132–134) As with other amyloid peptides, CT preferentially interacts with membranes containing anionic lipids, cholesterol, and GM1 ganglioside.(16, 20, 24, 36, 121, 135, 136) α-helical motifs in CT are often detected in membrane environments, and research suggests that helical intermediates are both stabilized by lipids and that such intermediates encourage stronger interactions with membranes, enhancing aggregation.(37, 137, 138) Experiments have also shown that cholesterol-rich lipid environments enhance β-sheet content, likely the result of lipid-mediated fibril formation.(139) It seems that the initial species to interact with the membranes is α-helical and that further aggregation in the membrane environment allows fibrillation to continue, eventually leading to β-sheet containing fibrils. It would therefore appear that α-helical intermediates of CT are key for aggregation in both solution and membrane environments. It is worth noting that several early studies of hCT and sCT membrane interactions used non-native, helix-inducing environments such as sodium dodecyl sulfate micelles, and thus caution should be used when trying to relate structures derived from these studies with biological behaviors of CT.(137, 140)

Additional work by Diociaiuti and colleagues has implicated lipid rafts as having a crucial role in mediating the pore formation of sCT oligomers, a behavior observed in other amyloids as well.(136) The enrichment in lipid rafts for cholesterol and GM1 suggests that these membrane components could play a role in mediating interactions, although a role for lipid raft induced changes in membrane thickness or curvature has not been ruled out.(59) Work by Sheynis and Jelinek showed an interesting behavior of CT to form fibril mats on membrane surfaces without

insertion, in contrast with the amyloid-β whose lipid induced fibrillation is associated with a complete membrane rupture.(102, 135) While the possible implications of lipid raft mediated CT membrane interactions on pore formation are clear, the potential physiological roles for fibril mats, if any, remain unknown.

1.4.3. Prefibrillar oligomers

Compared to other amyloids, there are relatively few studies focused on prefibrillar aggregates of CT. However, some trends have emerged from the literature. Both annular and linear protofibrillar aggregates of sCT have been observed and characterized by Diociauti and colleagues, using both TEM and circular dichroism measurements, showing them to be primarily rich in random coil and β-strand conformation, respectively.(12) Despite the prevalence of these larger species of prefibrillar aggregates, smaller (<20mer) prefibrillar oligomers are the species putatively responsible for membrane permeabilization, exhibiting enhanced pore-formation activity.(12, 59, 105, 115) As with several other amyloid peptides, pore formation by CT oligomers leads to calcium leakage and loss of cell homeostasis, with this behavior being modified by both membrane composition and membrane structure.(36, 37, 59, 60, 94) As mentioned previously, the biological relevance of such pore formation remains unknown. Of greater interest therapeutically is the fact that oligomers are thought to form critical intermediates for further aggregation of CT, making them a potential target for inhibition.(98)

There is a relative lack of structural knowledge on early oligomers in CT compared to mature fibrils beyond the consistent formation of a central α-helix. Among the few characterizations of prefibrillar oligomers, an NMR-based structural model for hCT at acidic pH obtained by Huang and colleagues indicates the formation of a β-hairpin structure in the central

region with an N-terminal loop and unstructured C-terminus.(105) This structure is believed to be stabilized by aromatic residue π-π interactions and is consistent with the structures of Naito and colleagues, representing a potential intermediate in the transition from α-helix to β-strand (Fig. 1.6.). However, intermediates containing random coil, α-helix, and β-hairpin secondary structures have all been detected in CT oligomers, highlighting the heterogeneity and metastability of early aggregation products and the significant effect of environmental conditions.(12, 105, 110) It is likely that the oligomeric intermediate of Huang and colleagues represents only one of a number of oligomeric intermediates formed between monomers and fibers. Amongst these intermediates, micelle-like oligomers have been implicated in the aggregation of several other amyloid peptides, and unpublished results suggest such oligomers may form in the course of CT aggregation as well.(95, 141) Efforts to probe the role of these possible intermediates are ongoing.

1.5. Role of calcitonin structure and aggregation in biological function and therapy

For many of the more widely studied amyloid peptides such as amyloid-β and hIAPP, the biological relevance of their aggregation derives directly from their influence on disease states. Specifically, the formation of cytotoxic oligomers and subsequent cell death is believed to be directly responsible for several types of dementia and other pathologies. While CT has consistently demonstrated the ability to form toxic species in model membrane systems and cultured cells, to date, the aggregation of CT in organisms has neither been shown to directly cause significant toxicity, nor to drive any disease pathology.(13, 34) The relevance of *in vivo* CT aggregation is instead primarily related to its roles in mitigating peptide-receptor interactions and limiting therapeutic efficiency through alterations of peptide structure and bioavailability.

1.5.1. The role of CT structure on biological function

Research points to α-helical intermediates as being key for several essential behaviors of CT. α-helical content is directly proportional to biological activity in several CT variants.(14) In the therapeutically relevant sCT, the consistent formation of an α-helix between residues 9 and 19 may be a key structural determinant in mediating CT-CTR interactions.(60, 125, 126, 142) Interestingly, sCT mutants with excess helical content have exhibited decreased receptor binding affinity and hypocalcemic activity, indicating that the specific length of α-helical domains influences biological function.(128, 143) The central α-helix of hCT is significantly shorter than that of the sCT, and hCT has shown superior hypocalcemic activity under aggregation inhibiting conditions.(40, 142) A potential explanation is that the shorter α-helix of hCT is superior for receptor activation, but either the shorter α-helix or other structural elements of hCT also render it more prone to further aggregate. Thus it appears that there is a balancing act between monomer potency and stability for CT and its various isoforms.

Mechanistically, several ideas exist as to how specific secondary structural elements mediate CT-receptor interactions. The N-terminal tail of CT, the most conserved section of CT across all species (Fig. 1), is believed to be critical for receptor activation, binding to the CTR and initiating its cAMP cascade.(55, 60, 123, 128, 129) This N-terminal region forms a loop structure in hCT as mentioned, with this structural motif persisting in a range of solution conditions. Studies with hCT peptide fragment 9-32 have shown helix formation upon interactions with membranes, but have failed to demonstrate spontaneous membrane insertion without the N-terminal residues, indicating the potential dual role of such residues in both receptor activation and membrane insertion.(123) As mentioned previously, the presence and structure of α-helical motifs is also correlated with CT biological activity. Additionally, NMR experiments, along with the well-established ability of α-helical CT to insert into the membrane, led Rawat and Kumar to propose

that CT could interact with intermembrane receptor domains, although such a behavior would be rare amongst GPCRs.(110) Overall, it is likely that both the central α-helix and N-terminal loop contribute to receptor activation.

A role for the C-terminal residues of CT in receptor binding and activation is less clear, although recent results suggest their involvement. Johansson and colleagues recently managed to crystalize sCT C-terminal peptide fragments bound to the ectodomain of the CTR.(144) Using X-ray crystallography, it was found that a type II β-turn formed involving residues 28-31 of sCT, with this turn being complementary to a loop consisting of residues 121-128 of the CTR. Hydrogen bonding between sCT and CTR was also mapped, with stacking between Pro32 of sCT and Trp79 of CTR in particular being implicated as a potential key interaction. Working with similarly truncated sCT and CTR models, Lee and colleagues likewise found C-terminal residues of sCT to form a turn and hydrogen bond with CTR residues.(55) This work also implicated the stacking of Pro32 of sCT and Trp79 of CTR as a potentially key mediator of CT-CTR interactions, with a P32Y mutation in the sCT sequence significantly weakening binding to the CTR ectodomain. These results suggest that C-terminal residues of CT could mediate interactions with the CTR.

Despite these recent discoveries, prior evidence also exists that the C-terminus is not relevant for receptor interactions. The unstructured nature of the CT C-terminus, along with the lack of sequence conservation between species, suggests a minimal role in receptor activation.(60, 91, 92) C-terminally mutated hCT peptides have shown no decrease in receptor binding or hypocalcemic effect, calling into question whether or not the binding exhibited by Johansson and Lee was sufficient for receptor activation.(128, 145) The use of truncated versions of sCT and CTR by Johansson and Lee along with the lack of a membrane environment and non-evaluation of activation also presents questions as to the biological relevance of the interactions observed.(55,

144) Clearly, further experiments involving CT and CTRs are necessary to clarify the structure-function relationship in CT mediated CTR activation.

1.5.2. The role of CT aggregation in therapeutic applications

Owing to its roles in mediating bone reformatting, CT has been used as a therapeutic in the treatment of the bone-related diseases osteoporosis and Paget's disease to decrease the loss of bone mass and rate of bone reformatting, respectively.(38, 146) For details on the history of CT therapy, the reader is directed to a review by Henrikson et al.(147) Typically, sCT has been the most commonly used isoform in therapeutic applications, owing to its slower aggregation rate relative to hCT, which increases the amount of soluble, bioavailable monomeric peptide.(39) Despite its slower aggregation relative to hCT, sCT still aggregates, making it an improvement over hCT but still an inefficient therapeutic.(11, 112) sCT therapy is also associated with several side effects including anorexia and vomiting, and has been shown to cause antibody formation and immune response.(41, 42, 148, 149) Such reactions further decrease the efficacy of sCT treatments.(150) hCT is not associated with an immune response, and therefore modifications to the hCT peptide to increase its bioavailability are an attractive alternative to current sCT therapies.(151)

A promising target for improving hCT bioavailability is the central aromatic residues Tyr12, Phe16, and Phe19. Mutation studies replacing these central aromatic residues in hCT with Leu (thus increasing homology with sCT) led to a decrease in aggregation rate by 2-3 orders of magnitude.(112) The more conservative F19Y mutation had no effect on aggregation kinetics, indicating that the effect of the central aromatics is general and not specific to any one amino acid.(112) These findings were supported by MD simulations.(112) Crucially, such mutants of hCT maintain their biological function, likely through stabilization of helical motifs, with both hypocalcemic potency and duration being enhanced over wt-hCT in rat models.(152, 153) Given

their significant homology to wt-hCT, it is also unlikely that such mutants would elicit immune response. Additionally, polyphenols, a popular class of small molecule inhibitors of amyloid aggregation, have proven effective in modulating the aggregation of CT.(105, 154) It is believed that such inhibitors operate through interference with π-π interactions, validating this region as a potential site for pharmaceutical optimization and further strengthening arguments for a strong role for aromatic residues in CT aggregation and remodeling.(105)

Other modifications to hCT could also be made to decrease its aggregation propensity. The oxidation state of methionine at residue 8 in hCT has been shown to alter its aggregation rate in a pH-independent manner.(155) The absence of methionine in sCT suggests that a mutation at residue 8 of hCT could present another avenue for kinetics modification. Investigation by Fowler and colleagues found that five amino acid substitutions (T11R, N17R, N24R, I27T, V29S) in hCT could slow its aggregation to the rate of sCT, mainly through increasing α-helix stability and decreasing peptide hydrophobicity.(128) Additionally, more of this α-helix promoting hCT mutant remained soluble once aggregation equilibrium was achieved, compared to wild-type, and the peptide modifications did not adversely affect receptor binding or the hypocalcemic effect. Another study by Andreotti and colleagues found that the mutation of five central and C-terminally located residues in hCT to their sCT equivalents (Y12L, N17H, A26N, I27T, A31T) both decreased the rate of aggregation and maintained structure and biological function.(145) This modified hCT also had the ability to inhibit the aggregation of wild-type hCT when the two were co-incubated.(145) As with the mutations to the aromatic residues of hCT, the mutants of Fowler and Andreotti would also be expected to decrease the immune responses endemic of sCT therapy, given the rarity of antibody formation against hCT.(151) The decreased immune response and

subsequently decreased secondary resistance would further enhance the effectiveness of CT therapies. Such mutated hCT variants thus present another potential alternative to sCT therapies.

CT's interactions with lipid vesicles are also of significant interest due to the increasing prevalence of lipid based delivery systems for biomolecular therapeutics.(132, 133, 156, 157) Significant efforts have been made to modify CTs to enhance their permeability through epithelial layers in order to increase their effective bioavailability. It appears that α-helical intermediates would be beneficial to that end due to their enhanced membrane insertion abilities. The formation of α-helices by CT is enhanced by anionic lipids and cholesterol within the bilayer, and while such CT structures are believed to be key for receptor interactions, α-helical intermediates in the presence of lipid bilayers also have been shown to drive fibril formation. A universal answer as to whether or not α-helices are desirable during drug application thus appears unlikely, and would depend heavily on other factors (other peptide modifications, mode of intake, dosage, etc.). The choice of lipids in a lipid based delivery system, particularly the head group charge, could prove to be an attractive and simple means of controlling aggregation during peptide delivery.

Despite the prevalence of helical intermediates, mature CT fibrils are found to contain primarily a β-sheet secondary structure.(12, 36, 103–108) The progression of CT monomers to β-sheet fibrils via α-helical intermediates would seem to mark such intermediates as a target species for fibrillation inhibition, but any modifications of CT fibrillation must be performed with receptor interactions in mind. As discussed, significant evidence exists showing α-helical intermediates to be key in mediating peptide-receptor interactions. Therefore, direct inhibition of helix formation would likely render CT ineffective as a therapeutic. However, prevention of a further progression to β-strand morphologies and fiber formation would leave biological activity intact. The

stabilization of helical intermediates has already been demonstrated in other systems to prevent fibrillation *in vivo* and enhance CT pore formation, indicating an increased bioavailability.(94, 153, 158–160) Furthermore, decreased fibrillation and improved bioavailability and function are observed in α-helix promoting hCT mutants, and residue specific data exists on the effect that modifying helix length and location has on peptide function.(128, 142, 143) Therefore, stabilizing the formation of α-helical intermediates of CT appears to be one of the simplest and least invasive methods by which to enhance bioavailability and efficacy of CT as a therapeutic.

1.6. Current calcitonin therapy

The availability of other osteoporosis drugs such as bisphosphonates has led to CT therapy primarily being used for the short-term mediation of acute pain from osteoporosis, although combination treatments involving CT have shown efficacy in mediating both hypercalcemia and bone quality under circumstances in which other treatments were ineffective.(161–164) In particular, CT has seen significant use as a therapeutic for the treatment of postmenopausal osteoporosis.(39, 161, 165, 166) Efforts to improve CT efficacy in recent years have primarily focused on peptide modifications and alternative delivery methods.

1.6.1. Peptide alterations

In addition to preventing aggregation, therapeutic forms of CT must overcome the obstacle of proteolytic clearance. This clearance is especially rapid in the presence of gastrointestinal enzymes, with full degradation of both hCT and sCT occurring within a few hours.(167–169) Experiments by Doschak and colleagues also revealed a 75% loss of radiolabeled sCT within 3 hours in major tissues in rat, with near complete loss within 24 hours.(170) Indeed, the rapid degradation of CT particularly in the digestive track is a major obstacle to the development of oral

formulations. Many prominent alternative oral delivery methods (detailed below) and peptide modifications are therefore focused on improving uptake and longevity. PEGylated and N-terminally acylated sCT have both shown improved resistance and intestinal permeability, with PEGylated sCT also showing increased longevity and a ~3-5x improvement in hypocalcemic effect in rat models.(169, 171, 172) Lipidization has also been used to improve trans-epithelial transport, with both reversible and non-reversible additions being explored.(173, 174) Reversible lipidization of sCT maintains more peptide in serum for longer, with correspondingly longer hypocalcemic activity.(175) Additionally, non-reversible lipidization has been shown to alter peptide secondary structure, which would likely inhibit receptor activation.(173) As such, reversible lipidizations of sCT appear to be the more promising of the two for peptide modification.

1.6.2. Alternative delivery methods

Alternatives to injected and nasal spray sCT (the current preferred methods of administration) are being explored. The majority of these efforts focus on oral administration through novel delivery vessels. An oral mucoadhesive polymer delivery system developed by Gupta and colleagues demonstrated significant load delivery in rat intestine, and a 50-fold improvement in bioavailability versus direct intestinal injection.(176) Biodegradable nanoparticles, coated liposomes, and lipid nanocapsules have all also been shown to produce improved sCT delivery, both in cultured cells and through oral delivery *in vivo*.(132, 133, 156, 157, 177) Despite these advances, phase III clinical trials of oral delivery methods have failed to demonstrate statistically significant increases in bone mineral density over nasal applications, and thus the development of oral delivery methods for sCT remains in progress.(165, 166, 178). The efficacy of all sCT treatment methods, including oral delivery, is likely still limited by sCT's aggregation and limited bioavailability upon absorption.

1.6.3. CT Therapy and medullary thyroid carcinoma

A commonly mentioned concern regarding the use of CT in osteoporosis therapy is the association between CT fibrils with medullary thyroid carcinoma (MTC) tumor cells.(179–181) It has been strongly suggested that CT fibrillation is a driver of tumor formation and progression.(34, 119, 139, 154) Several problems exist with this interpretation, however. MTC is a cancer of the CT-expressing C-cells, thus one would expect unmitigated cell proliferation to result in excessive local production of CT and subsequent fibril formation. To our knowledge, as of this writing there is no evidence in the literature showing CT, fibrillar or otherwise, to cause MTC, with this idea being further challenged by the existence of CT-negative MTC tumors.(182, 183) CT's use as a biomarker for MTC also suggests it to be an effect, rather than a cause, of MTC since elevated CT serum levels occur after tumor formation.(184, 185) Additionally, elevated CT levels do not necessarily correspond to the presence of MTC.(186, 187) The strongest case for an active role in MTC for CT is an analysis by the Food and Drug Administration and European Medicines Agency finding CT therapy to correlate with cancer risk.(188) However, this correlation was weak (<1% increase), involved clinical trials much longer than current typical dosing regimens for short-term use, and showed no specificity to MTC versus other carcinomas.(188) Overall, the fibrillation of CT seems like a consequence, rather than a driver, of MTC.

1.7. Dissertation Objectives

While significant advances have been made, there are still gaps in our understanding of hCT as it pertains to the amyloid formation process. Given the role of CTs as a therapeutic, significant effort has been put into structural characterizations and modifications to improve bioavailability. However, given the current dominance of sCT in the therapeutic market, studies aiming to elucidate the molecular underpinnings behind hCT aggregation have been rare, despite

the promise that modified hCT holds as a therapeutic. There is thus a need to elucidate the role of the therapeutically relevant hCT monomer structure in aggregation kinetics in order to improve CT therapeutics. Additionally, for the amyloid field as a whole there is a need to determine early drivers of the aggregation process in order to mediate or prevent aggregation before the formation of toxic oligomer species. In this dissertation, I first study an abnormal kinetic aggregation behavior of wild-type hCT in solution (Chapter 2). The observation of a direct relationship between peptide concentration and lag time, contrary to the typical trend in amyloids, was explained by self-inhibition of hCT by growth-incompetent monomers. A kinetic model for a novel mechanism of amyloid aggregation was devised, synthesizing several disparate previously observed/predicted phenomenon in amyloid aggregation.(189–191) Given the predicted importance of helical structural motifs in determining growth-competence, along with the aforementioned importance of hCT membrane interactions, I next characterized the effect of model membranes of varied phospholipid composition on hCT aggregation kinetics (Chapter 3). The kinetic trend from Chapter 2 was found to persist, and in addition several previously unreported behaviors of hCT in a membrane environment were elucidated. This study represents the first systematic study of the effect of phospholipid bilayers on hCT aggregation, and helps to both elucidate more general amyloid-membrane interactions as well as potentially informing future therapeutic efforts based on lipid delivery systems which are growing in prevalence and popularity.(132–134, 156, 157, 192, 193)

1.8. References

1. Copp, D. H., Cameron, E. C., Cheney, B. A., Davidson, A. G., and Henze, K. G. (1962) Evidence for calcitonin--a new hormone from the parathyroid that lowers blood calcium. *Endocrinology*. **70**, 638–49

2. Ashwini Kumar, M., Foster, G. V., and Macintyre, I. (1963) Further evidence for Calcitonin: a hormone which lowers plasma-calcium. *Lancet*. **282**, 480–482

3. Hirsch, P. F., Gauthier, G. F., and Munson, P. L. (1963) Thyroid hypocalcemic principle and recurrent laryngeal nerve injury as factors affecting the response to parathyroidectomy in rats. *Endocrinology*. **73**, 244–52

4. Brewer, H. B., and Ronan, R. (1969) Amino acid sequence of bovine thyrocalcitonin. *Proc. Natl. Acad. Sci. U. S. A.* **63**, 940–7

5. Niall, H. D., Keutmann, H. T., Copp, D. H., and Potts, J. T. (1969) Amino acid sequence of salmon ultimobranchial calcitonin. *Proc. Natl. Acad. Sci. U. S. A.* **64**, 771–8

6. Potts, J. T., Niall, H. D., Keutmann, H. T., Brewer, H. B., and Deftos, L. J. (1968) The amino acid sequence of porcine thyrocalcitonin. *Proc. Natl. Acad. Sci. U. S. A.* **59**, 1321–8

7. Riniker, B., Brugger, M., Kamber, B., Rittel, W., Sieber, P., and Neher, R. (1969) Structure and synthesis of human calcitonin M. *Biochem. J.* **111**, 14P

8. Zaidi, M., Inzerillo, A. ., Moonga, B. ., Bevis, P. J. ., and Huang, C. L.-H. (2002) Forty years of calcitonin—where are we now? A tribute to the work of Iain Macintyre, FRS. *Bone*. **30**, 655–663

9. Raulais, D., Hagaman, J., Ontjes, D. A., Lundblad, R. L., and Kingdon, H. S. (1976) The complete amino-acid sequence of rat thyrocalcitonin. *Eur. J. Biochem.* **64**, 607–11

10. Li, Y., Yan, J., Zhang, X., and Huang, K. (2013) Disulfide bonds in amyloidogenesis diseases related proteins. *Proteins Struct. Funct. Bioinforma.* **81**, 1862–1873

11. Arvinte, T., Cudd, A., and Drake, A. F. (1993) The structure and mechanism of formation of human calcitonin fibrils. *J. Biol. Chem.* **268**, 6415–22

12. Diociaiuti, M., Macchia, G., Paradisi, S., Frank, C., Camerini, S., Chistolini, P., Gaudiano, M. C., Petrucci, T. C., and Malchiodi-Albedi, F. (2014) Native metastable prefibrillar oligomers are the most neurotoxic species among amyloid aggregates. *Biochim. Biophys. Acta*. **1842**, 1622–9

13. Rymer, D. L., and Good, T. A. (2001) The role of G protein activation in the toxicity of amyloidogenic Abeta-(1-40), Abeta-(25-35), and bovine calcitonin. *J. Biol. Chem.* **276**, 2523–30

14. Siligardi, G., Samorí, B., Melandri, S., Visconti, M., and Drake, A. F. (1994) Correlations between biological activities and conformational properties for human, salmon, eel, porcine calcitonins and Elcatonin elucidated by CD spectroscopy. *Eur. J. Biochem.* **221**, 1117–25

15. Hamley, I. W. (2012) The amyloid beta peptide: a chemist's perspective. Role in Alzheimer's and fibrillization. *Chem. Rev.* **112**, 5147–92

16. Harrison, R. S., Sharpe, P. C., Singh, Y., and Fairlie, D. P. (2007) Amyloid peptides and proteins in review. *Rev. Physiol. Biochem. Pharmacol.* **159**, 1–77

17. Gilchrist, P. J., and Bradshaw, J. P. (1993) Amyloid formation by salmon calcitonin. *Biochim. Biophys. Acta*. **1182**, 111–4

18. Chiti, F., and Dobson, C. M. (2006) Protein misfolding, functional amyloid, and human disease. *Annu. Rev. Biochem.* **75**, 333–66

19. Spillantini, M. G., Schmidt, M. L., Lee, V. M., Trojanowski, J. Q., Jakes, R., and Goedert, M. (1997) Alpha-synuclein in Lewy bodies. *Nature*. **388**, 839–40

20. Westermark, P., Andersson, A., and Westermark, G. T. (2011) Islet amyloid polypeptide, islet amyloid, and diabetes mellitus. *Physiol. Rev.* **91**, 795–826

21. Murphy, M. P., and LeVine, H. (2010) Alzheimer's disease and the amyloid-beta peptide. *J. Alzheimers. Dis.* **19**, 311–23

22. Prusiner, S. B. (1982) Novel proteinaceous infectious particles cause scrapie. *Science*. **216**, 136–44

23. DeToma, A. S., Salamekh, S., Ramamoorthy, A., and Lim, M. H. (2012) Misfolded proteins in Alzheimer's disease and type II diabetes. *Chem. Soc. Rev.* **41**, 608–21

24. Brender, J. R., Salamekh, S., and Ramamoorthy, A. (2012) Membrane disruption and early events in the aggregation of the diabetes related peptide IAPP from a molecular perspective. *Acc. Chem. Res.* **45**, 454–62

25. Knowles, T. P. J., Vendruscolo, M., and Dobson, C. M. (2014) The amyloid state and its association with protein misfolding diseases. *Nat. Rev. Mol. Cell Biol.* **15**, 384–96

26. Straub, J. E., and Thirumalai, D. (2011) Toward a molecular theory of early and late events in monomer to amyloid fibril formation. *Annu. Rev. Phys. Chem.* **62**, 437–63

27. Patel, H. R., Pithadia, A. S., Brender, J. R., Fierke, C. A., and Ramamoorthy, A. (2014) In Search of Aggregation Pathways of IAPP and Other Amyloidogenic Proteins: Finding Answers through NMR Spectroscopy. *J. Phys. Chem. Lett.* **5**, 1864–70

28. Kotler, S. A., Brender, J. R., Vivekanandan, S., Suzuki, Y., Yamamoto, K., Monette, M., Krishnamoorthy, J., Walsh, P., Cauble, M., Holl, M. M. B., Marsh, E. N. G., and Ramamoorthy, A. (2015) High-resolution NMR characterization of low abundance oligomers of amyloid-β without purification. *Sci. Rep.* **5**, 11811

29. Meisl, G., Kirkegaard, J. B., Arosio, P., Michaels, T. C. T., Vendruscolo, M., Dobson, C. M., Linse, S., and Knowles, T. P. J. (2016) Molecular mechanisms of protein aggregation from global fitting of kinetic models. *Nat. Protoc.* **11**, 252–72

30. Eisenberg, D. S., and Sawaya, M. R. (2017) Structural Studies of Amyloid Proteins at the Molecular Level. *Annu. Rev. Biochem.* **86**, 69–95

31. Chiti, F., and Dobson, C. M. (2017) Protein Misfolding, Amyloid Formation, and Human

Disease: A Summary of Progress Over the Last Decade. *Annu. Rev. Biochem.* **86**, 27–68

32. Cohen, S. I. A., Linse, S., Luheshi, L. M., Hellstrand, E., White, D. A., Rajah, L., Otzen, D. E., Vendruscolo, M., Dobson, C. M., and Knowles, T. P. J. (2013) Proliferation of amyloid-β42 aggregates occurs through a secondary nucleation mechanism. *Proc. Natl. Acad. Sci. U. S. A.* **110**, 9758–63

33. Hardy, J., and Selkoe, D. J. (2002) The Amyloid Hypothesis of Alzheimer's Disease: Progress and Problems on the Road to Therapeutics. *Science (80-.).* **297**, 353–356

34. Schubert, D., Behl, C., Lesley, R., Brack, A., Dargusch, R., Sagara, Y., and Kimura, H. (1995) Amyloid peptides are toxic via a common oxidative mechanism. *Proc. Natl. Acad. Sci. U. S. A.* **92**, 1989–93

35. Morimoto, K., Nagata, S., Kubo, T., Oda, T., and Kaneko, I. (1998) [Amyloidogenic peptides such as beta-amyloid, amylin and calcitonin strongly enhance the susceptibility of rat hippocampal neurons to excitatory amino acids in vivo]. *Nihon Yakurigaku Zasshi.* **112 Suppl**, 83P–87P

36. Diociaiuti, M., Polzi, L. Z., Valvo, L., Malchiodi-Albedi, F., Bombelli, C., and Gaudiano, M. C. (2006) Calcitonin forms oligomeric pore-like structures in lipid membranes. *Biophys. J.* **91**, 2275–81

37. Meleleo, D., and Picciarelli, V. (2016) Effect of calcium ions on human calcitonin. Possible implications for bone resorption by osteoclasts. *Biometals.* **29**, 61–79

38. Robin, J. C., and Ambrus, J. L. (1982) Studies on osteoporosis VI. Effect of human and salmon calcitonin on experimental osteoporosis. *Res. Commun. Chem. Pathol. Pharmacol.* **35**, 491–8

39. Chesnut, C. H., Azria, M., Silverman, S., Engelhardt, M., Olson, M., and Mindeholm, L. (2008) Salmon calcitonin: a review of current and future therapeutic indications. *Osteoporos. Int.* **19**, 479–91

40. Cudd, A., Arvinte, T., Gaines Das, R. E., Chinni, C., and MacIntyre, I. (1995) Enhanced Potency of Human Calcitonin When Fibrillation is Avoided. *J. Pharm. Sci.* **84**, 717–719

41. Singer, F. R., Fredericks, R. S., and Minkin, C. (1980) Salmon calcitonin therapy for paget's disease of bone the problem of acquired clinical resistance. *Arthritis Rheum.* **23**, 1148–1154

42. Singer, F. R., Aldred, J. P., Neer, R. M., Krane, S. M., Potts, J. T., and Bloch, K. J. (1972) An evaluation of antibodies and clinical resistance to salmon calcitonin. *J. Clin. Invest.* **51**, 2331–8

43. Bussolati, G., and Pearse, A. G. (1967) Immunofluorescent localization of calcitonin in the "C" cells of pig and dog thyroid. *J. Endocrinol.* **37**, 205–9

44. Masi, L., and Brandi, M. L. (2007) Calcitonin and calcitonin receptors. *Clin. Cases Miner. Bone Metab.* **4**, 117–22

45. Wimalawansa, S. J. (1997) Amylin, calcitonin gene-related peptide, calcitonin, and adrenomedullin: a peptide superfamily. *Crit. Rev. Neurobiol.* **11**, 167–239

46. Russell, F. A., King, R., Smillie, S.-J., Kodji, X., and Brain, S. D. (2014) Calcitonin gene-related peptide: physiology and pathophysiology. *Physiol. Rev.* **94**, 1099–142

47. Hirsch, P. F., and Baruch, H. (2003) Is calcitonin an important physiological substance? *Endocrine*. **21**, 201–8

48. Foster, G. V. (1968) Calcitonin: A review of experimental and clinical investigations. *Postgrad. Med. J.* **44**, 411–422

49. Friedman, J., and Raisz, L. G. (1965) Thyrocalcitonin: inhibitor of bone resorption in tissue culture. *Science*. **150**, 1465–7

50. Wallach, S., Rousseau, G., Martin, L., and Azria, M. (1999) Effects of calcitonin on animal and in vitro models of skeletal metabolism. *Bone*. **25**, 509–16

51. Nicholson, G. C., Moseley, J. M., Sexton, P. M., Mendelsohn, F. A., and Martin, T. J. (1986) Abundant calcitonin receptors in isolated rat osteoclasts. Biochemical and autoradiographic characterization. *J. Clin. Invest.* **78**, 355–60

52. Holtrop, M. E., Raisz, L. G., and Simmons, H. A. (1974) The effects of parathyroid hormone, colchicine, and calcitonin on the ultrastructure and the activity of osteoclasts in organ culture. *J. Cell Biol.* **60**, 346–55

53. Chambers, T. J., and Magnus, C. J. (1982) Calcitonin alters behaviour of isolated osteoclasts. *J. Pathol.* **136**, 27–39

54. Chambers, T. J., Fuller, K., and Darby, J. A. (1987) Hormonal regulation of acid phosphatase release by osteoclasts disaggregated from neonatal rat bone. *J. Cell. Physiol.* **132**, 90–6

55. Lee, S.-M., Hay, D. L., and Pioszak, A. A. (2016) Calcitonin and Amylin Receptor Peptide Interaction Mechanisms: Insights into Peptide-binding Modes and Allosteric Modulation of the Calcitonin Receptor by Receptor Activity-modifying Proteins. *J. Biol. Chem.* **291**, 8686–8700

56. Hay, D. L., Walker, C. S., Gingell, J. J., Ladds, G., Reynolds, C. A., and Poyner, D. R. (2016) Receptor activity-modifying proteins; multifunctional G protein-coupled receptor accessory proteins. *Biochem. Soc. Trans.* **44**, 568–73

57. Zhang, Z., Neff, L., Bothwell, A. L. M., Baron, R., and Horne, W. C. (2002) Calcitonin induces dephosphorylation of Pyk2 and phosphorylation of focal adhesion kinase in osteoclasts. *Bone*. **31**, 359–65

58. Shyu, J.-F., Shih, C., Tseng, C.-Y., Lin, C.-H., Sun, D.-T., Liu, H.-T., Tsung, H.-C., Chen, T.-H., and Lu, R.-B. (2007) Calcitonin induces podosome disassembly and detachment of osteoclasts by modulating Pyk2 and Src activities. *Bone*. **40**, 1329–42

59. Malchiodi-Albedi, F., Contrusciere, V., Raggi, C., Fecchi, K., Rainaldi, G., Paradisi, S., Matteucci, A., Santini, M. T., Sargiacomo, M., Frank, C., Gaudiano, M. C., and Diociaiuti, M. (2010) Lipid raft disruption protects mature neurons against amyloid oligomer toxicity. *Biochim. Biophys. Acta*. **1802**, 406–15

60. Stipani, V., Gallucci, E., Micelli, S., Picciarelli, V., and Benz, R. (2001) Channel formation by salmon and human calcitonin in black lipid membranes. *Biophys. J.* **81**, 3332–8

61. Kajiya, H. (2012) Calcium signaling in osteoclast differentiation and bone resorption. *Adv. Exp. Med. Biol.* **740**, 917–32

62. Cheng, X., Hookway, E. S., Kashima, T., Oppermann, U., Galione, A., and Athanasou, N. A. (2015) The role of calcium and nicotinic acid adenine dinucleotide phosphate (NAADP) in human osteoclast formation and resorption. *Calcif. Tissue Int.* **96**, 73–9

63. Okubo, Y., Bessho, K., Fujimura, K., Kusumoto, K., Ogawa, Y., and Iizuka, T. (2000) Effect of elcatonin on osteoinduction by recombinant human bone morphogenetic protein-2. *Biochem. Biophys. Res. Commun.* **269**, 317–21

64. Monier-Faugere, M. C., Geng, Z., Qi, Q., Arnala, I., and Malluche, H. H. (1996) Calcitonin prevents bone loss but decreases osteoblastic activity in ovariohysterectomized beagle dogs. *J. Bone Miner. Res.* **11**, 446–55

65. Plotkin, L. I., Weinstein, R. S., Parfitt, A. M., Roberson, P. K., Manolagas, S. C., and Bellido, T. (1999) Prevention of osteocyte and osteoblast apoptosis by bisphosphonates and calcitonin. *J. Clin. Invest.* **104**, 1363–74

66. Gooi, J. H., Pompolo, S., Karsdal, M. A., Kulkarni, N. H., Kalajzic, I., McAhren, S. H. M., Han, B., Onyia, J. E., Ho, P. W. M., Gillespie, M. T., Walsh, N. C., Chia, L. Y., Quinn, J. M. W., Martin, T. J., and Sims, N. A. (2010) Calcitonin impairs the anabolic effect of PTH in young rats and stimulates expression of sclerostin by osteocytes. *Bone*. **46**, 1486–97

67. Davey, R. A., and Findlay, D. M. (2013) Calcitonin: physiology or fantasy? *J. Bone Miner. Res.* **28**, 973–9

68. Hurley, D. L., Tiegs, R. D., Wahner, H. W., and Heath, H. (1987) Axial and appendicular bone mineral density in patients with long-term deficiency or excess of calcitonin. *N. Engl. J. Med.* **317**, 537–41

69. Hoff, A. O., Catala-Lehnen, P., Thomas, P. M., Priemel, M., Rueger, J. M., Nasonkin, I., Bradley, A., Hughes, M. R., Ordonez, N., Cote, G. J., Amling, M., and Gagel, R. F. (2002) Increased bone mass is an unexpected phenotype associated with deletion of the calcitonin

gene. *J. Clin. Invest.* **110**, 1849–57

70. Huebner, A. K., Keller, J., Catala-Lehnen, P., Perkovic, S., Streichert, T., Emeson, R. B., Amling, M., and Schinke, T. (2008) The role of calcitonin and alpha-calcitonin gene-related peptide in bone formation. *Arch. Biochem. Biophys.* **473**, 210–7

71. Huebner, A. K., Schinke, T., Priemel, M., Schilling, S., Schilling, A. F., Emeson, R. B., Rueger, J. M., and Amling, M. (2006) Calcitonin deficiency in mice progressively results in high bone turnover. *J. Bone Miner. Res.* **21**, 1924–34

72. Baylin, S. B., Bailey, A. L., Hsu, T.-H., and Foster, G. V. (1977) Degradation of human calcitonin in human plasma. *Metabolism*. **26**, 1345–1354

73. Heersche, J. N. M. (1992) Calcitonin effects on osteoclastic resorption: the "escape phenomenon" revisited. *Bone Miner.* **16**, 174–177

74. Davey, R. A., Turner, A. G., McManus, J. F., Chiu, W. S. M., Tjahyono, F., Moore, A. J., Atkins, G. J., Anderson, P. H., Ma, C., Glatt, V., MacLean, H. E., Vincent, C., Bouxsein, M., Morris, H. A., Findlay, D. M., and Zajac, J. D. (2008) Calcitonin receptor plays a physiological role to protect against hypercalcemia in mice. *J. Bone Miner. Res.* **23**, 1182–93

75. Stevenson, J. C., Hillyard, C. J., MacIntyre, I., Cooper, H., and Whitehead, M. I. (1979) A physiological role for calcitonin: protection of the maternal skeleton. *Lancet (London, England)*. **2**, 769–70

76. Kumar, R., Cohen, W. R., Silva, P., and Epstein, F. H. (1979) Elevated 1,25-dihydroxyvitamin D plasma levels in normal human pregnancy and lactation. *J. Clin. Invest.* **63**, 342–4

77. Woodrow, J. P., Sharpe, C. J., Fudge, N. J., Hoff, A. O., Gagel, R. F., and Kovacs, C. S. (2006) Calcitonin plays a critical role in regulating skeletal mineral metabolism during lactation. *Endocrinology*. **147**, 4010–21

78. Jaeger, P., Jones, W., Clemens, T. L., and Hayslett, J. P. (1986) Evidence that calcitonin stimulates 1,25-dihydroxyvitamin D production and intestinal absorption of calcium in vivo. *J. Clin. Invest.* **78**, 456–61

79. Raisz, L. G., Trummel, C. L., Holick, M. F., and DeLuca, H. F. (1972) 1,25-dihydroxycholecalciferol: a potent stimulator of bone resorption in tissue culture. *Science*. **175**, 768–9

80. Felsenfeld, A. J., and Levine, B. S. (2015) Calcitonin, the forgotten hormone: does it deserve to be forgotten? *Clin. Kidney J.* **8**, 180–187

81. Martin, T. J., and Melick, R. A. (1969) The acute effects of porcine calcitonin in man. *Australas. Ann. Med.* **18**, 258–63

82. Cooper, C. W., Hirsch, P. F., Toverud, S. U., and Munson, P. L. (1967) An improved method for the biological assay of thyrocalcitonin. *Endocrinology*. **81**, 610–6

83. Hirsch, P. F., and Munson, P. L. (1969) Thyrocalcitonin. *Physiol. Rev.* **49**, 548–622

84. Parfitt, A. M. (2003) Misconceptions (3): calcium leaves bone only by resorption and enters only by formation. *Bone*. **33**, 259–263

85. Atkins, G. J., and Findlay, D. M. (2012) Osteocyte regulation of bone mineral: a little give and take. *Osteoporos. Int.* **23**, 2067–79

86. Brown, E. M. (2013) Role of the calcium-sensing receptor in extracellular calcium homeostasis. *Best Pract. Res. Clin. Endocrinol. Metab.* **27**, 333–43

87. Ohno, H., Noguchi, M., and Takayanagi, N. (1985) Effect of elcatonin on experimental gastric and duodenal ulcers. *Jpn. J. Pharmacol.* **37**, 67–75

88. Cooper, C. W., Schwesinger, W. H., Mahgoub, A. M., and Ontjes, D. A. (1971) Thyrocalcitonin: stimulation of secretion by pentagastrin. *Science*. **172**, 1238–40

89. Cottrell, G. S., Alemi, F., Kirkland, J. G., Grady, E. F., Corvera, C. U., and Bhargava, A. (2012) Localization of calcitonin receptor-like receptor (CLR) and receptor activity-modifying protein 1 (RAMP1) in human gastrointestinal tract. *Peptides*. **35**, 202–11

90. Care, A. D., Bruce, J. B., Boelkins, J., Kenny, A. D., Conaway, H., and Anast, C. S. (1971) Role of pancreozymin-cholecystokinin and structurally related compounds as calcitonin secretogogues. *Endocrinology*. **89**, 262–71

91. Kanaori, K., and Nosaka, A. Y. (1995) Study of human calcitonin fibrillation by proton nuclear magnetic resonance spectroscopy. *Biochemistry*. **34**, 12138–43

92. Moriarty, D. F., Vagts, S., and Raleigh, D. P. (1998) A role for the C-terminus of calcitonin in aggregation and gel formation: a comparative study of C-terminal fragments of human and salmon calcitonin. *Biochem. Biophys. Res. Commun.* **245**, 344–8

93. Avidan-Shpalter, C., and Gazit, E. (2006) The early stages of amyloid formation: biophysical and structural characterization of human calcitonin pre-fibrillar assemblies. *Amyloid*. **13**, 216–25

94. Micelli, S., Meleleo, D., Picciarelli, V., Stoico, M. G., and Gallucci, E. (2004) Effect of nanomolar concentrations of sodium dodecyl sulfate, a catalytic inductor of alpha-helices, on human calcitonin incorporation and channel formation in planar lipid membranes. *Biophys. J.* **87**, 1065–75

95. Brender, J. R., Krishnamoorthy, J., Sciacca, M. F. M., Vivekanandan, S., D'Urso, L., Chen, J., La Rosa, C., and Ramamoorthy, A. (2015) Probing the Sources of the Apparent Irreproducibility of Amyloid Formation: Drastic Changes in Kinetics and a Switch in Mechanism Due to Micellelike Oligomer Formation at Critical Concentrations of IAPP. *J.*

Phys. Chem. B. **119**, 2886–2896

96. Hong, L., Qi, X., and Zhang, Y. (2012) Dissecting the kinetic process of amyloid fiber formation through asymptotic analysis. *J. Phys. Chem. B.* **116**, 6611–7

97. Arosio, P., Knowles, T. P. J., and Linse, S. (2015) On the lag phase in amyloid fibril formation. *Phys. Chem. Chem. Phys.* **17**, 7606–18

98. Itoh-Watanabe, H., Kamihira-Ishijima, M., Kawamura, I., Kondoh, M., Nakakoshi, M., Sato, M., and Naito, A. (2013) Characterization of the spherical intermediates and fibril formation of hCT in HEPES solution using solid-state 13C-NMR and transmission electron microscopy. *Phys. Chem. Chem. Phys.* **15**, 16956–64

99. Gaudiano, M. C., Colone, M., Bombelli, C., Chistolini, P., Valvo, L., and Diociaiuti, M. (2005) Early stages of salmon calcitonin aggregation: effect induced by ageing and oxidation processes in water and in the presence of model membranes. *Biochim. Biophys. Acta*. **1750**, 134–45

100. Gaudiano, M. C., Diociaiuti, M., Bertocchi, P., and Valvo, L. (2003) Effects induced by hydroxyl radicals on salmon calcitonin: a RP-HPLC, CD and TEM study. *Biochim. Biophys. Acta*. **1623**, 33–40

101. Rastogi, N., Mitra, K., Kumar, D., and Roy, R. (2012) Metal ions as cofactors for aggregation of therapeutic peptide salmon calcitonin. *Inorg. Chem.* **51**, 5642–50

102. Sciacca, M. F. M., Kotler, S. A., Brender, J. R., Chen, J., Lee, D., and Ramamoorthy, A. (2012) Two-step mechanism of membrane disruption by Aβ through membrane fragmentation and pore formation. *Biophys. J.* **103**, 702–10

103. Kamihira, M., Naito, A., Tuzi, S., Nosaka, A. Y., and Saitô, H. (2000) Conformational transitions and fibrillation mechanism of human calcitonin as studied by high-resolution solid-state 13C NMR. *Protein Sci.* **9**, 867–77

104. Naito, A., Kamihira, M., Inoue, R., and Saitô, H. (2004) Structural diversity of amyloid fibril formed in human calcitonin as revealed by site-directed 13C solid-state NMR spectroscopy. *Magn. Reson. Chem.* **42**, 247–57

105. Huang, R., Vivekanandan, S., Brender, J. R., Abe, Y., Naito, A., and Ramamoorthy, A. (2012) NMR characterization of monomeric and oligomeric conformations of human calcitonin and its interaction with EGCG. *J. Mol. Biol.* **416**, 108–20

106. Reches, M., Porat, Y., and Gazit, E. (2002) Amyloid fibril formation by pentapeptide and tetrapeptide fragments of human calcitonin. *J. Biol. Chem.* **277**, 35475–80

107. Zanuy, D., Haspel, N., Tsai, H.-H. G., Ma, B., Gunasekaran, K., Wolfson, H. J., and Nussinov, R. (2004) Side chain interactions determine the amyloid organization: a single layer beta-sheet molecular structure of the calcitonin peptide segment 15-19. *Phys. Biol.* **1**, 89–99

108. Lakshmanan, A., Cheong, D. W., Accardo, A., Di Fabrizio, E., Riekel, C., and Hauser, C. A. E. (2013) Aliphatic peptides show similar self-assembly to amyloid core sequences, challenging the importance of aromatic interactions in amyloidosis. *Proc. Natl. Acad. Sci. U. S. A.* **110**, 519–24

109. Tayeb-Fligelman, E., Tabachnikov, O., Moshe, A., Goldshmidt-Tran, O., Sawaya, M. R., Coquelle, N., Colletier, J.-P., and Landau, M. (2017) The cytotoxic Staphylococcus aureus PSMα3 reveals a cross-α amyloid-like fibril. *Science (80-.).* **355**, 831–833

110. Rawat, A., and Kumar, D. (2013) NMR investigations of structural and dynamics features of natively unstructured drug peptide - salmon calcitonin: implication to rational design of potent sCT analogs. *J. Pept. Sci.* **19**, 33–45

111. Kamihira, M., Oshiro, Y., Tuzi, S., Nosaka, A. Y., Saitô, H., and Naito, A. (2003) Effect of electrostatic interaction on fibril formation of human calcitonin as studied by high resolution solid state 13C NMR. *J. Biol. Chem.* **278**, 2859–65

112. Itoh-Watanabe, H., Kamihira-Ishijima, M., Javkhlantugs, N., Inoue, R., Itoh, Y., Endo, H., Tuzi, S., Saitô, H., Ueda, K., and Naito, A. (2013) Role of aromatic residues in amyloid fibril formation of human calcitonin by solid-state 13C NMR and molecular dynamics simulation. *Phys. Chem. Chem. Phys.* **15**, 8890–901

113. Guo, M., Gorman, P. M., Rico, M., Chakrabartty, A., and Laurents, D. V. (2005) Charge substitution shows that repulsive electrostatic interactions impede the oligomerization of Alzheimer amyloid peptides. *FEBS Lett.* **579**, 3574–3578

114. Marshall, K. E., Morris, K. L., Charlton, D., O'Reilly, N., Lewis, L., Walden, H., and Serpell, L. C. (2011) Hydrophobic, aromatic, and electrostatic interactions play a central role in amyloid fibril formation and stability. *Biochemistry*. **50**, 2061–71

115. Diociaiuti, M., Gaudiano, M. C., and Malchiodi-Albedi, F. (2011) The slowly aggregating salmon Calcitonin: a useful tool for the study of the amyloid oligomers structure and activity. *Int. J. Mol. Sci.* **12**, 9277–95

116. Gazit, E. (2002) A possible role for pi-stacking in the self-assembly of amyloid fibrils. *FASEB J.* **16**, 77–83

117. Bertolani, A., Pirrie, L., Stefan, L., Houbenov, N., Haataja, J. S., Catalano, L., Terraneo, G., Giancane, G., Valli, L., Milani, R., Ikkala, O., Resnati, G., and Metrangolo, P. (2015) Supramolecular amplification of amyloid self-assembly by iodination. *Nat. Commun.* **6**, 7574

118. Metrangolo, P., Terraneo, G., Cavallo, G., Pizzi, A., Morra, G., Bertolani, A., Gazzera, L., Pirrie, L., Meli, M., Colombo, G., and Genoni, A. (2016) Crystal structure of the DFNKF segment of human calcitonin unveils aromatic interactions between phenylalanines. *Chem. - A Eur. J.* **23**, 2051–2058

119. Tsai, H.-H., Zanuy, D., Haspel, N., Gunasekaran, K., Ma, B., Tsai, C.-J., and Nussinov, R.

(2004) The stability and dynamics of the human calcitonin amyloid peptide DFNKF. *Biophys. J.* **87**, 146–58

120. Ramirez-Alvarado, M., Kelly, J. W., and Dobson, C. M. (2010) *Protein misfolding diseases : current and emerging principles and therapies*, Wiley

121. Shtainfeld, A., Sheynis, T., and Jelinek, R. (2010) Specific Mutations Alter Fibrillation Kinetics, Fiber Morphologies, and Membrane Interactions of Pentapeptides Derived from Human Calcitonin. *Biochemistry*. **49**, 5299–5307

122. Iconomidou, V. A., Leontis, A., Hoenger, A., and Hamodrakas, S. J. (2013) Identification of a novel "aggregation-prone"/'amyloidogenic determinant' peptide in the sequence of the highly amyloidogenic human calcitonin. *FEBS Lett.* **587**, 569–74

123. Wagner, K., Van Mau, N., Boichot, S., Kajava, A. V., Krauss, U., Le Grimellec, C., Beck-Sickinger, A., and Heitz, F. (2004) Interactions of the Human Calcitonin Fragment 9–32 with Phospholipids: A Monolayer Study. *Biophys. J.* **87**, 386–395

124. Bauer, H. H., Müller, M., Goette, J., Merkle, H. P., and Fringeli, U. P. (1994) Interfacial adsorption and aggregation associated changes in secondary structure of human calcitonin monitored by ATR-FTIR spectroscopy. *Biochemistry*. **33**, 12276–82

125. Arvinte, T., and Drake, A. F. (1993) Comparative study of human and salmon calcitonin secondary structure in solutions with low dielectric constants. *J. Biol. Chem.* **268**, 6408–14

126. Meyer, J. P., Pelton, J. T., Hoflack, J., and Saudek, V. (1991) Solution structure of salmon calcitonin. *Biopolymers*. **31**, 233–41

127. Micelli, S., Meleleo, D., Picciarelli, V., and Gallucci, E. (2006) Effect of pH-variation on insertion and ion channel formation of human calcitonin into planar lipid bilayers. *Front. Biosci.* **11**, 2035–44

128. Fowler, S. B., Poon, S., Muff, R., Chiti, F., Dobson, C. M., and Zurdo, J. (2005) Rational design of aggregation-resistant bioactive peptides: reengineering human calcitonin. *Proc. Natl. Acad. Sci. U. S. A.* **102**, 10105–10

129. Stroop, S. D., Nakamuta, H., Kuestner, R. E., Moore, E. E., and Epand, R. M. (1996) Determinants for calcitonin analog interaction with the calcitonin receptor N-terminus and transmembrane-loop regions. *Endocrinology*. **137**, 4752–6

130. Kawashima, H., Katayama, M., Yoshida, R., Akaji, K., Asano, A., and Doi, M. (2016) A dimer model of human calcitonin13-32 forms an α-helical structure and robustly aggregates in 50% aqueous 2,2,2-trifluoroethanol solution. *J. Pept. Sci.* **22**, 480–4

131. Morris, A. M., Watzky, M. A., Agar, J. N., and Finke, R. G. (2008) Fitting neurological protein aggregation kinetic data via a 2-step, minimal/"Ockham's razor" model: the Finke-Watzky mechanism of nucleation followed by autocatalytic surface

growth. *Biochemistry*. **47**, 2413–27

132. Umerska, A., Matougui, N., Groo, A.-C., and Saulnier, P. (2016) Understanding the adsorption of salmon calcitonin, antimicrobial peptide AP114 and polymyxin B onto lipid nanocapsules. *Int. J. Pharm.* **506**, 191–200

133. Matougui, N., Boge, L., Groo, A.-C., Umerska, A., Ringstad, L., Bysell, H., and Saulnier, P. (2016) Lipid-based nanoformulations for peptide delivery. *Int. J. Pharm.* **502**, 80–97

134. Baginski, L., Gobbo, O. L., Tewes, F., Salomon, J. J., Healy, A. M., Bakowsky, U., and Ehrhardt, C. (2012) In vitro and in vivo characterisation of PEG-lipid-based micellar complexes of salmon calcitonin for pulmonary delivery. *Pharm. Res.* **29**, 1425–34

135. Sheynis, T., and Jelinek, R. (2010) Lipid-Induced Calcitonin Fibrillation Blocks Membrane Interactions of a Peptide Antibiotic. *J. Phys. Chem. B.* **114**, 15530–15535

136. Malchiodi-Albedi, F., Paradisi, S., Matteucci, A., Frank, C., and Diociaiuti, M. (2011) Amyloid oligomer neurotoxicity, calcium dysregulation, and lipid rafts. *Int. J. Alzheimers. Dis.* **2011**, 906964

137. Motta, A., Andreotti, G., Amodeo, P., Strazzullo, G., and Castiglione Morelli, M. A. (1998) Solution structure of human calcitonin in membrane-mimetic environment: the role of the amphipathic helix. *Proteins.* **32**, 314–23

138. Epand, R. M., Epand, R. F., Orlowski, R. C., Schlueter, R. J., Boni, L. T., and Hui, S. W. (1983) Amphipathic helix and its relationship to the interaction of calcitonin with phospholipids. *Biochemistry*. **22**, 5074–5084

139. Wang, S. S.-S., Good, T. A., and Rymer, D. L. (2005) The influence of phospholipid membranes on bovine calcitonin secondary structure and amyloid formation. *Protein Sci.* **14**, 1419–28

140. Motta, A., Pastore, A., Goud, N. A., and Castiglione Morelli, M. A. (1991) Solution conformation of salmon calcitonin in sodium dodecyl sulfate micelles as determined by two-dimensional NMR and distance geometry calculations. *Biochemistry*. **30**, 10444–10450

141. Sabaté, R., and Estelrich, J. (2005) Evidence of the existence of micelles in the fibrillogenesis of beta-amyloid peptide. *J. Phys. Chem. B.* **109**, 11027–32

142. Amodeo, P., Motta, A., Strazzullo, G., and Castiglione Morelli, M. A. (1999) Conformational flexibility in calcitonin: the dynamic properties of human and salmon calcitonin in solution. *J. Biomol. NMR.* **13**, 161–74

143. Andreotti, G., Méndez, B. L., Amodeo, P., Morelli, M. A. C., Nakamuta, H., and Motta, A. (2006) Structural determinants of salmon calcitonin bioactivity: the role of the Leu-based amphipathic alpha-helix. *J. Biol. Chem.* **281**, 24193–203

144. Johansson, E., Hansen, J. L., Hansen, A. M. K., Shaw, A. C., Becker, P., Schäffer, L., and Reedtz-Runge, S. (2016) Type II Turn of Receptor-bound Salmon Calcitonin Revealed by X-ray Crystallography. *J. Biol. Chem.* **291**, 13689–13698

145. Andreotti, G., Vitale, R. M., Avidan-Shpalter, C., Amodeo, P., Gazit, E., and Motta, A. (2011) Converting the highly amyloidogenic human calcitonin into a powerful fibril inhibitor by three-dimensional structure homology with a non-amyloidogenic analogue. *J. Biol. Chem.* **286**, 2707–18

146. Schneider, D., Hofmann, M. T., and Peterson, J. A. (2002) Diagnosis and treatment of Paget's disease of bone. *Am. Fam. Physician*. **65**, 2069–72

147. Henriksen, K., Bay-Jensen, A.-C., Christiansen, C., and Karsdal, M. A. (2010) Oral salmon calcitonin--pharmacology in osteoporosis. *Expert Opin. Biol. Ther.* **10**, 1617–29

148. Feletti, C., and Bonomini, V. (1979) Effect of calcitonin on bone lesions in chronic dialysis patients. *Nephron*. **24**, 85–8

149. Yamamoto, Y., Nakamuta, H., Koida, M., Seyler, J. K., and Orlowski, R. C. (1982) Calcitonin-induced anorexia in rats: a structure-activity study by intraventricular injections. *Jpn. J. Pharmacol.* **32**, 1013–7

150. Levy, F., Muff, R., Dotti-Sigrist, S., Dambacher, M. A., and Fischer, J. A. (1988) Formation of neutralizing antibodies during intranasal synthetic salmon calcitonin treatment of Paget's disease. *J. Clin. Endocrinol. Metab.* **67**, 541–5

151. Grauer, A., Reinel, H. H., Ziegler, R., and Raue, F. (1993) Neutralizing antibodies against calcitonin. *Horm. Metab. Res.* **25**, 486–8

152. Maier, R., Kamber, B., Riniker, B., and Rittel, W. (1976) Analogues of human calcitonin. IV. Influence of leucine substitutions in positions 12, 16 and 19 on hypocalcaemic activity in the rat. *Clin. Endocrinol. (Oxf).* **5 Suppl**, 327S–332S

153. Andreotti, G., and Motta, A. (2003) Modulating calcitonin fibrillogenesis: an antiparallel alpha-helical dimer inhibits fibrillation of salmon calcitonin. *J. Biol. Chem.* **279**, 6364–6370

154. Guo, C., Ma, L., Zhao, Y., Peng, A., Cheng, B., Zhou, Q., Zheng, L., and Huang, K. (2015) Inhibitory effects of magnolol and honokiol on human calcitonin aggregation. *Sci. Rep.* **5**, 13556

155. Mulinacci, F., Poirier, E., Capelle, M. A. H., Gurny, R., and Arvinte, T. (2011) Enhanced physical stability of human calcitonin after methionine oxidation. *Eur. J. Pharm. Biopharm. Off. J. Arbeitsgemeinschaft für Pharm. Verfahrenstechnik e.V.* **78**, 229–38

156. Sang Yoo, H., and Gwan Park, T. (2004) Biodegradable nanoparticles containing protein-fatty acid complexes for oral delivery of salmon calcitonin. *J. Pharm. Sci.* **93**, 488–95

157. Werle, M., and Takeuchi, H. (2009) Chitosan-aprotinin coated liposomes for oral peptide delivery: Development, characterisation and in vivo evaluation. *Int. J. Pharm.* **370**, 26–32

158. Zurdo, J. (2005) Polypeptide models to understand misfolding and amyloidogenesis and their relevance in protein design and therapeutics. *Protein Pept. Lett.* **12**, 171–87

159. Kallberg, Y., Gustafsson, M., Persson, B., Thyberg, J., and Johansson, J. (2001) Prediction of amyloid fibril-forming proteins. *J. Biol. Chem.* **276**, 12945–50

160. Villegas, V., Zurdo, J., Filimonov, V. V, Avilés, F. X., Dobson, C. M., and Serrano, L. (2000) Protein engineering as a strategy to avoid formation of amyloid fibrils. *Protein Sci.* **9**, 1700–8

161. Tella, S. H., and Gallagher, J. C. (2014) Prevention and treatment of postmenopausal osteoporosis. *J. Steroid Biochem. Mol. Biol.* **142**, 155–70

162. Tagiyev, A., Demirbilek, H., Tavil, B., Buyukyilmaz, G., Gumruk, F., and Cetin, M. (2016) Severe Hypercalcemia in a Child With Acute Lymphoblastic Leukemia Relapse: Successful Management With Combination of Calcitonin and Bisphosphonate. *J. Pediatr. Hematol. Oncol.* **38**, 232–234

163. Abbassy, M. A., Watari, I., Bakry, A. S., Ono, T., and Hassan, A. H. (2016) Calcitonin and vitamin D3 have high therapeutic potential for improving diabetic mandibular growth. *Int. J. Oral Sci.* **8**, 39–44

164. Wei, J., Wang, J., Gong, Y., and Zeng, R. (2015) Effectiveness of combined salmon calcitonin and aspirin therapy for osteoporosis in ovariectomized rats. *Mol. Med. Rep.* **12**, 1717–26

165. Binkley, N., Bolognese, M., Sidorowicz-Bialynicka, A., Vally, T., Trout, R., Miller, C., Buben, C. E., Gilligan, J. P., and Krause, D. S. (2012) A phase 3 trial of the efficacy and safety of oral recombinant calcitonin: the Oral Calcitonin in Postmenopausal Osteoporosis (ORACAL) trial. *J. Bone Miner. Res.* **27**, 1821–9

166. Bandeira, L., Lewiecki, E. M., and Bilezikian, J. P. (2016) Pharmacodynamics and pharmacokinetics of oral salmon calcitonin in the treatment of osteoporosis. *Expert Opin. Drug Metab. Toxicol.* **12**, 1–9

167. Wang, J., Yadav, V., Smart, A. L., Tajiri, S., and Basit, A. W. (2015) Toward oral delivery of biopharmaceuticals: an assessment of the gastrointestinal stability of 17 peptide drugs. *Mol. Pharm.* **12**, 966–73

168. Tozaki, H., Emi, Y., Horisaka, E., Fujita, T., Yamamoto, A., and Muranishi, S. (1995) Metabolism of peptide drugs by the microorganisms in rat cecal contents. *Biol. Pharm. Bull.* **18**, 929–31

169. Youn, Y. S., Jung, J. Y., Oh, S. H., Yoo, S. D., and Lee, K. C. (2006) Improved intestinal delivery of salmon calcitonin by Lys18-amine specific PEGylation: stability, permeability,

pharmacokinetic behavior and in vivo hypocalcemic efficacy. *J. Control. Release*. **114**, 334–42

170. Yang, Y., Bhandari, K. H., Panahifar, A., and Doschak, M. R. (2014) Synthesis, Characterization and Biodistribution Studies of 125I-Radioiodinated di-PEGylated Bone Targeting Salmon Calcitonin Analogue in Healthy Rats. *Pharm. Res.* **31**, 1146–1157

171. Mero, A., Schiavon, M., Veronese, F. M., and Pasut, G. (2011) A new method to increase selectivity of transglutaminase mediated PEGylation of salmon calcitonin and human growth hormone. *J. Control. Release*. **154**, 27–34

172. Trier, S., Linderoth, L., Bjerregaard, S., Strauss, H. M., Rahbek, U. L., and Andresen, T. L. (2015) Acylation of salmon calcitonin modulates in vitro intestinal peptide flux through membrane permeability enhancement. *Eur. J. Pharm. Biopharm. Off. J. Arbeitsgemeinschaft für Pharm. Verfahrenstechnik e.V*. **96**, 329–37

173. Cheng, W., Satyanarayanajois, S., and Lim, L.-Y. (2007) Aqueous-soluble, non-reversible lipid conjugate of salmon calcitonin: synthesis, characterization and in vivo activity. *Pharm. Res.* **24**, 99–110

174. Wang, J., Chow, D., Heiati, H., and Shen, W.-C. (2003) Reversible lipidization for the oral delivery of salmon calcitonin. *J. Control. Release*. **88**, 369–80

175. Cheng, W., and Lim, L.-Y. (2008) Comparison of reversible and nonreversible aqueous-soluble lipidized conjugates of salmon calcitonin. *Mol. Pharm.* **5**, 610–21

176. Gupta, V., Hwang, B. H., Lee, J., Anselmo, A. C., Doshi, N., and Mitragotri, S. (2013) Mucoadhesive intestinal devices for oral delivery of salmon calcitonin. *J. Control. Release*. **172**, 753–62

177. Wu, R., Ma, B., Zhou, Q., and Tang, C. (2017) Salmon calcitonin-loaded PLGA microspheres/calcium phosphate cement composites for osteoblast proliferation. *J. Appl. Polym. Sci.* **134**, 45486

178. Varamini, P., and Toth, I. (2016) Recent advances in oral delivery of peptide hormones. *Expert Opin. Drug Deliv.* **13**, 507–22

179. Khurana, R., Agarwal, A., Bajpai, V. K., Verma, N., Sharma, A. K., Gupta, R. P., and Madhusudan, K. P. (2004) Unraveling the amyloid associated with human medullary thyroid carcinoma. *Endocrinology*. **145**, 5465–70

180. Tubiana, M., Milhaud, G., Coutris, G., Lacour, J., Parmentier, C., and Bok, B. (1968) Medullary carcinoma and thyrocalcitonin. *Br. Med. J.* **4**, 87–9

181. Sletten, K., Westermark, P., and Natvig, J. B. (1976) Characterization of amyloid fibril proteins from medullary carcinoma of the thyroid. *J. Exp. Med.* **143**, 993–8

182. Schmid, K. W., and Ensinger, C. (1998) “Atypical” medullary thyroid carcinoma with

little or no calcitonin expression. *Virchows Arch.* **433**, 209–15

183. Samà, M. T., Rossetto Giaccherino, R., Gallo, M., Felicetti, F., Maletta, F., Bonelli, N., Piovesan, A., Palestini, N., Ghigo, E., and Arvat, E. (2016) Clinical challenges with calcitonin-negative medullary thyroid carcinoma. *J. Cancer Res. Clin. Oncol.* **142**, 2023–9

184. Ito, Y., Miyauchi, A., Kihara, M., Kudo, T., and Miya, A. (2016) Calcitonin doubling time in medullary thyroid carcinoma after the detection of distant metastases keenly predicts patients' carcinoma death. *Endocr. J.* **63**, 663–7

185. Bae, Y. J., Schaab, M., and Kratzsch, J. (2015) Calcitonin as Biomarker for the Medullary Thyroid Carcinoma. *Recent results cancer Res. Fortschritte der Krebsforsch. Progrès dans les Rech. sur le cancer*. **204**, 117–37

186. Rosario, P. W., and Calsolari, M. R. (2016) Usefulness of Serum Calcitonin in Patients Without a Suspicious History of Medullary Thyroid Carcinoma and with Thyroid Nodules Without an Indication for Fine-Needle Aspiration or with Benign Cytology. *Horm. Metab. Res. = Horm. und Stoffwechselforsch. = Horm. métabolisme*. **48**, 372–276

187. Zhou, Q., Yue, S., Cheng, Y., Jin, J., and Xu, H. (2017) Clinical and pathological analysis of 19 cases of medullary thyroid carcinoma without an increase in calcitonin. *Exp. Toxicol. Pathol.* **69**, 575–579

188. Overman, R. A., Borse, M., and Gourlay, M. L. (2013) Salmon Calcitonin Use and Associated Cancer Risk. *Ann. Pharmacother.* **47**, 1675–1684

189. Blancas-Mejía, L. M., Misra, P., and Ramirez-Alvarado, M. (2017) Differences in protein concentration dependence for nucleation and elongation in light chain amyloid formation. *Biochemistry*. **56**, 757–766

190. Zhijie Qin, Dongmei Hu, Min Zhu, A., and Fink, A. L. (2007) Structural Characterization of the Partially Folded Intermediates of an Immunoglobulin Light Chain Leading to Amyloid Fibrillation and Amorphous Aggregation. *Biochemistry*. **46**, 3521–3531

191. Kashchiev, D. (2017) Modeling the Effect of Monomer Conformational Change on the Early Stage of Protein Self-Assembly into Fibrils. *J. Phys. Chem. B.* **121**, 35–46

192. Lin, C.-H., Chen, C.-H., Lin, Z.-C., and Fang, J.-Y. (2017) Recent advances in oral delivery of drugs and bioactive natural products using solid lipid nanoparticles as the carriers. *J. Food Drug Anal.* **25**, 219–234

193. Chono, S., Togami, K., and Itagaki, S. (2017) Aerosolized liposomes with dipalmitoyl phosphatidylcholine enhance pulmonary absorption of encapsulated insulin compared with co-administered insulin. *Drug Dev. Ind. Pharm.* **43**, 1892–1898

Chapter 2

Growth-incompetent monomers of human calcitonin lead to a non-canonical direct relationship between peptide concentration and lag time

This chapter was adapted from the following publication

> Kamgar-Parsi, K., Hong, L., Naito, A., Brooks, C. L., and Ramamoorthy, A. (2017) Growth-incompetent monomers of human calcitonin lead to a noncanonical direct relationship between peptide concentration and aggregation lag time. *J. Biol. Chem.* **292**, 14963–14976

2.1. Introduction

Calcitonin (CT) is a 32 amino acid peptide hormone produced in thyroidal c-cells.(1) Originally discovered due to its hypocalcemic effects, further studies showed CT's main function to be skeletoprotective.(1) CT inhibits bone resorption and maintains bone mass through G protein-coupled receptor-mediated interactions with osteoclasts, and it has therefore been used as a therapeutic for the bone diseases osteoporosis and Paget's disease.(1–4) However, CT-based therapies have been limited by the intrinsic tendency of CT to aggregate in solution as both the structural reformatting and sequestration of CT during its aggregation decrease bioavailability and efficacy.(5, 6)

The characteristics of CT's aggregation mark it as a member of the amyloid family. These peptides and proteins are characterized by their propensity to form amyloid fibrils, in which monomeric subunits adopt β-strand structures and stack along the fibril axis through inter-molecular hydrogen bonding and electrostatic interactions.(7) The structure of these fibrils and the general process by which they form from their respective monomeric subunits is thought to be

relatively conserved across different primary sequences.(7, 8) Briefly, during the initial phase of aggregation known as the lag phase, peptide monomers self-associate to form small, soluble aggregates (oligomers), with continued aggregation leading to the production of protofibrils. Such protofibrils then seed rapid elongation through monomer addition, leading to the formation of mature amyloid fibrils. Crucially, the fibrillation of amyloidogenic peptides has been shown to play a role in a number of disease pathologies. At least 60 such peptides have been identified in humans, with over half having been implicated in diseases including Alzheimer's, Parkinson's, and Type 2 Diabetes Mellitus.(9–13) Despite extensive investigations, significant confusion remains as to the details of aggregation and the specific roles that such peptide aggregates play in disease pathology. The heterogeneous and metastable nature of the prefibrillar aggregates, as well as the large effects that subtle shifts in environmental factors have on aggregation, have combined to obfuscate the identification of critical aggregation intermediates or specific toxic species. A detailed elucidation of amyloid aggregation would both aid in disease understanding and provide guidance in efforts to inhibit aggregation and toxicity.

For CT in particular there is a need to slow aggregation to improve therapeutic efficacy. To this end, the rapidly aggregating human calcitonin (hCT) has been replaced by the slower aggregating salmon calcitonin (sCT) as the current standard in calcitonin-based osteoporosis therapy.(2, 14) Despite improvements over hCT, sCT-based therapies are associated with side effects and immune responses that interfere with therapeutic efficacy.(4, 15, 16) Additionally, hCT maintains improved therapeutic efficacy compared to sCT when aggregation is controlled, and is free of the side effects and immune responses associated with sCT.(5, 17) Significant interest therefore exists in slowing the aggregation of hCT to improve its utility as a therapeutic agent.

Here a direct relationship between peptide concentration and lag time in the aggregation of

hCT is shown for the first time. Such a trend goes against the conventional wisdom of the amyloid field, where increasing concentrations lead to faster aggregation.(18–21) In several other amyloids, including the closely related human islet amyloid polypeptide (hIAPP), "micelle-like" oligomers formed above a critical micelle concentration (CMC) have emerged as potential key kinetics-modulating intermediates, however such intermediates in hCT were found to be kinetically inactive.(19, 20, 22–25) Instead, these results point to the need for monomer structural conversion as responsible for the trend. The concentration dependent and structural differences in these species were investigated and a novel kinetic model for amyloid formation by hCT was proposed. Further elucidation of this aggregation pathway could identify key intermediates and inform future efforts in kinetics modification in the therapeutic applications of CT.

2.2. Results

2.2.1. hCT presents an atypical direct relationship between initial monomer concentration and lag time

Thioflavin-T (ThT) assays have become the standard for kinetic monitoring of amyloid fibril growth due to the quantum yield increase in ThT upon binding to β-sheet rich structures.(26–30) ThT assays were used in order to probe the concentration dependence of hCT aggregation rate. ThT kinetic curves were measured for a range of initial monomer concentrations (Fig. 2.1.A). The ThT traces of hCT show the typical sigmoidal fibril growth pattern characteristic of amyloids, however the direct relationship between peptide concentration and lag time (time duration of the lag phase) is contrary to the expected behavior (Fig. 2.1. B). Amyloids typically present an inverse relationship between initial monomer concentration and lag time as reported in the literature.(18–21) It is well established that the aggregation characteristics of amyloids depend heavily on their

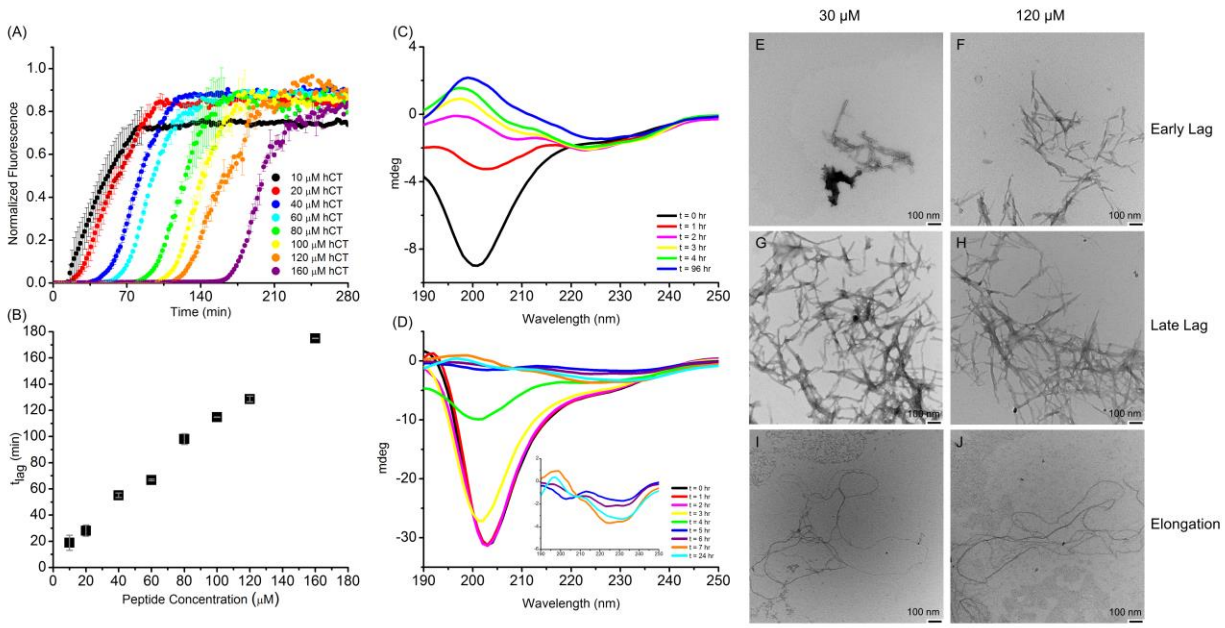

Figure 2.1. hCT aggregation exhibits a direct relationship between initial monomer concentration and lag time. A) Normalized averaged ThT curves of hCT fibrillation at different initial monomer concentrations. Experiments were performed in duplicate at 25 ºC in 20 mM phosphate buffer, pH 7.4 with orbital shaking and 1 equivalent of ThT. Error bars represent standard deviation. B) Quantification of dependence of lag time on peptide concentration from A. Error bars represent standard deviation. Transition away from random coil to betasheet-like structure is seen for C) 30 μM hCT and D) 120 μM hCT. Spectra represent averages of 5 scans. Inset shows compressed y-scale of 120 μM spectra at later time points. Representative TEM images of hCT at three distinct time points (early lag phase, late lag phase, and elongation phase) at high (120 μM) and low (30 μM) concentrations confirm fibril formation. Note that no concentration-dependent morphological differences are evident at any stage of aggregation.

aggregation environment, yet the atypical trend observed for hCT is found to persist through changes of buffer (concentration and type), salt concentration, pH, agitation, and temperature (Fig. 2.2.).(31, 32) This consistency indicates the behavior to be characteristic of hCT, rather than a consequence of a specific set of environmental conditions.

To ensure that the ThT data was reflective of the macroscopic peptide behavior, rather than a report on a limited sub-population, population wide secondary structure was determined via CD spectroscopy. The time evolution of secondary structure was measured for 30 μM and 120 μM initial monomer concentrations (Fig. 2.1.C-D). At both concentrations, hCT initially displayed a primarily random coil secondary structure, typical for monomers of CT.(33–35) Aggregation was accompanied by a depletion in the random coil peak, and subsequent increase in β-sheet signal for

both peptide concentrations, confirming the ThT-detected increase in β-sheet to be representative of the overall peptide population. The β-sheet signal was stable for at least 24 hours, indicating the hCT to have reached its mature fibrillar state. Consistent with the trend found from ThT fluorescence data, the 120 μM hCT took approximately four times longer to undergo the transition to a β-sheet conformation than the 30 μM hCT. For both conditions, significant signal loss occurred due to the aggregation and gelation of the peptide, a phenomenon previously described

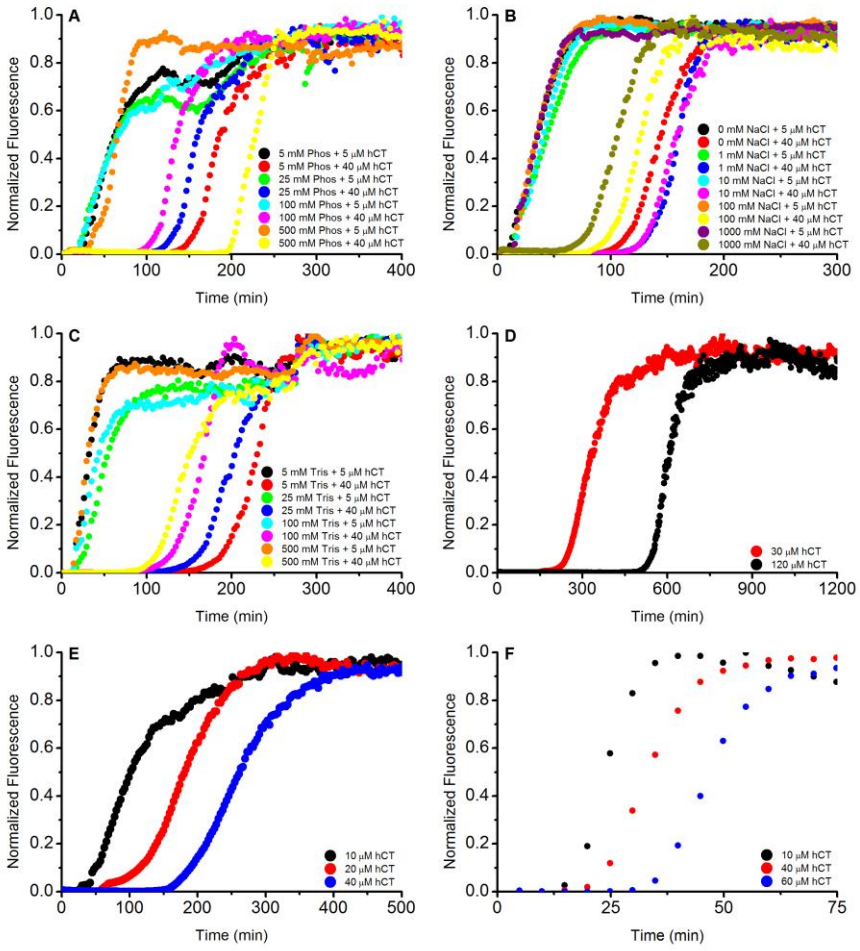

Figure 2.2. hCT aggregates slower at higher concentrations under a range of conditions. ThT kinetic assays were performed with A) A range of sodium phosphate buffer concentrations without salt, pH 7.4 B) 20 mM sodium phosphate buffer with a range of salt (NaCl) concentrations, pH 7.4 C) A range of Tris buffer concentrations, pH 7.4 D) In 20 mM sodium phosphate buffer under quiescent conditions, pH 7.4 E) 20 mM sodium bicarbonate buffer, pH 10.0 F) 20 mM sodium phosphate buffer, pH 7.4. All experiments were performed with orbital shaking and 2 equivalents of ThT other than D (no shaking, one equivalent of ThT). All plates were run at 25 °C with the exception of F), run at 37 °C. As can be seen, all conditions consistently show higher concentrations to aggregate slower.

for CT.(36) To ensure signal loss did not introduce artifacts into secondary structure determinations, end stage β-sheet morphology was verified by single-point ThT fluorescence.

TEM images were also taken to further confirm the validity of the ThT and CD results. Aggregation of 30 μM and 120 μM hCT was tracked by ThT fluorescence, and samples were removed for imaging at equivalent stages of aggregation for both concentrations (Fig. A.1.). Early and late lag phase images show short, ThT-negative, protofibrillar aggregates of a few hundred nanometers in length (Fig. 2.1.E-H). The protofibrils are morphologically indistinguishable between early and late lag phase for both concentrations, with the exception of concentration-dependent density differences. Final stage aggregates show long, thin amyloid aggregates forming fibrils (Fig. 2.1.I-J). Again, the aggregate morphology remains the same in both samples. Both concentrations exhibited the canonical progression of fibril formation via nucleating protofibrils and elongation, with no discernable concentration dependent differences in morphology at any stage. Combined with the ThT assays, these CD and TEM results confirm the direct relationship between peptide concentration and lag time to be a genuine behavior.

2.2.2. Anomalous lag time dependence on peptide concentration is not entirely primary nucleus dependent

The observed hCT concentration dependent differences in lag time, combined with the conserved elongation rates, are consistent with theoretical predictions of differences in primary nucleation rate.(37) The lack of concentration dependent morphological differences in protofibrillar or fibrillar aggregates by TEM or CD supports the idea that concentration dependent changes in lag time involve the rate of nucleus formation, rather than the characteristics of the nucleus itself.(38) To probe this hypothesis, seeded ThT kinetics assays were performed.(39–41)

Although the addition of seeds accelerated fibril formation, an extended lag phase remained even in the presence of high seed concentrations (Fig. A.2.A). Additionally, in the presence of seed, the monomer concentration dependence of the lag phase was abolished (Fig. A.2.B). A lag time independent of free monomer concentration is expected for seeded ThT assays, and is consistent with differences in primary nucleation rate contributing to the direct relationship between lag time and peptide concentration. However, the persistence of an extended lag time even with 15% seeding by volume implies that the existence of primary nuclei is not sufficient for fibril formation and elongation, with such a phenomenon having been previously shown in other systems.(42)

2.2.3. hCT oligomer behavior changes with concentration

The results of seeded ThT kinetics assays focused further analysis on the presence and interconversion of oligomeric intermediates which dominate the lag phase. In order to probe the kinetics of oligomerization, rather than fibril formation, the time evolution of hCT aggregate size was monitored using DLS experiments. Despite peptide preparations minimizing the number of non-monomeric species initially present, peaks representing small oligomeric species and larger aggregates appear rapidly after sample preparation, at both high (120 μM) and low (30 μM) hCT concentrations (Fig. 2.3.A). In order to confirm the detected species as hCT aggregates rather than artifacts, Epigallocatechin gallate (EGCG), a natural product known to interact with and break apart amyloid aggregates including oligomers of hCT, was added.(33, 43, 44) The addition of EGCG shifted the small oligomeric peak from 2-5 nm to less than 1 nm in radius, confirming the source of the peak to be small soluble aggregates (Fig. 2.3.A). The peak associated with larger, potentially protofibrillar aggregates was unaffected by EGCG. Previous studies have revealed the effect of EGCG on hCT aggregates to be mediated primarily by interactions between the aromatic rings of EGCG with those of Tyr12 and Phe16.(33) The ability of EGCG to remodel only low

molecular weight aggregates by DLS would suggest the larger aggregates to be significantly more stable, potentially due to the sequestration and subsequent solvent inaccessibility of the aromatic residues.

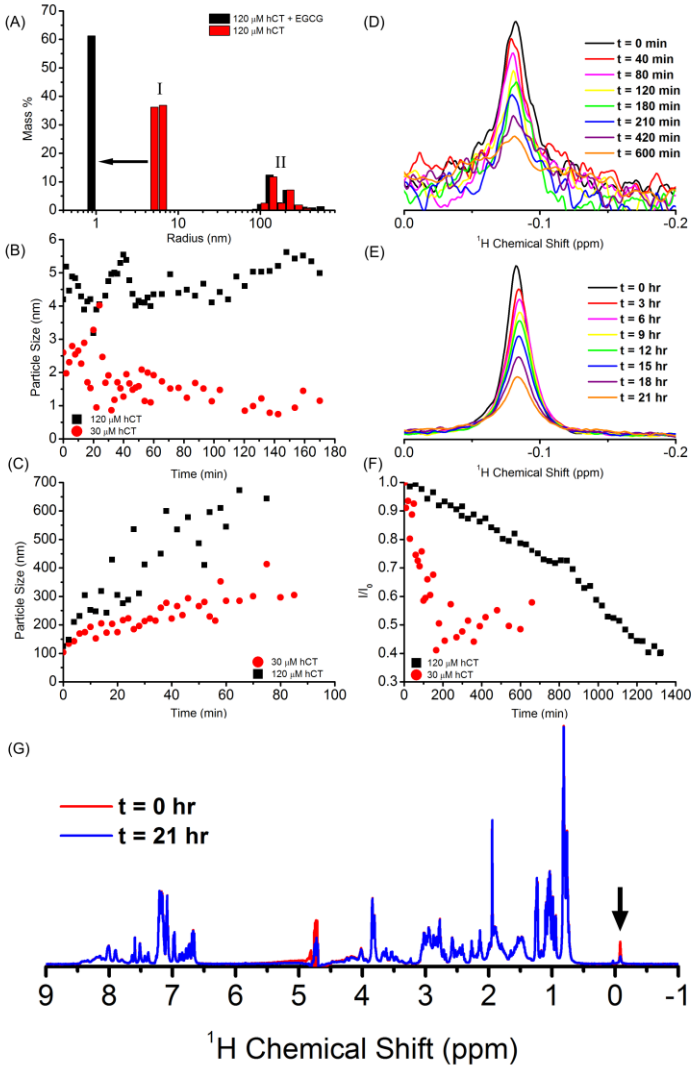

Figure 2.3. Concentration-dependent differences in early aggregates of hCT. A) Representative sample of hCT DLS profile at early time-points with and without EGCG. Peak I represents low molecular weight soluble oligomers, while Peak II represents larger aggregate species. B) Time-course measurement of oligomer radius shows a consistently larger radius at higher concentrations, indicating a concentration dependent change in small oligomer formation. C) Time-course measurement of protofibril peak shows accelerated growth at higher concentrations. Note that initial protofibril peak size is equivalent for both concentrations, thus differences in size at later time points are indicative of post aggregate formation changes. All DLS profiles represent averages of 10 independent acquisitions. The time evolution of the oligomer peak at 30 μM hCT (D) and 120 μM hCT (E) indicates differences in oligomer reformatting. F) Plot of oligomer peak intensity normalized to oligomer peak intensity at t=0 versus time for both 30 μM hCT and 120 μM hCT, determined via fixed bound integration. G) 1H NMR spectra for 120 μM hCT. Spectra show negligible intensity loss over the course of the experiment outside of the peak at -0.1 ppm (black arrow).

In EGCG-free preparations, two clear differences in aggregate size appear. First, the smaller peak representing low molecular weight oligomer species shows consistently larger aggregates for 120 μM hCT (4-5 nm radius) as opposed to 30 μM (1-2 nm radius) (Fig. 2.3.B). Such a finding suggests that the oligomeric population is concentration dependent, favoring larger oligomers at higher concentrations. Second, the observed changes in the larger peak initially appearing at ~100 nm for both conditions indicate a significantly faster growth for samples containing 120 μM hCT compared to those containing 30 μM, which suggests a more rapid re-organization of aggregates to larger species at higher concentrations (Fig. 2.3.C). DLS results do not exhibit any statistically significant concentration- or time-dependent differences in mass distribution between peaks. The majority of peptide mass (~80%) is contained in peak I as expected for early aggregation stages (Fig. A.4.), indicating that the relative percentage of peptide in each peak remains fixed over the time course measured in the experiment.

To further probe the concentration dependent time evolution of hCT oligomers, a time course 1D ^{1}H NMR experiment was used to track the progression of oligomerization by monitoring the peak at -0.1 ppm. This peak appears in the NMR spectra of amyloidogenic peptides when aliphatic protons are shielded from solvent, as occurs when they are sequestered in oligomeric aggregates.(30, 33, 45) Monitoring the time evolution of this peak at high and low concentrations provides information on the concentration dependence of oligomerization kinetics specifically, an alternative to typical kinetic assays which track only fibrillation kinetics.

At both concentrations, an oligomer peak was found immediately, consistent with the DLS data. Over time, the oligomer peak intensity decreased for both peptide concentrations (Fig. 2.3.D-E). Interestingly, the ^{1}H NMR spectra revealed a slower loss of oligomer peak intensity at higher concentrations (Fig. 2.3.F). This would initially appear a trivial result, given that the ThT and CD

time course experiments both exhibit slower aggregation at higher concentrations, implying a longer period of oligomer-dominated peptide distribution and slower loss of signal intensity to NMR-invisible species. However, the overall spectrum signal intensity for both concentrations is unchanged over the course of the experiment (Fig. 2.3.G), indicating the differential rates in oligomer peak intensity loss to be independent of fibrillation, and instead representative of concentration dependent differences in oligomeric reformatting. It is important to note that given the NMR-invisible size of the larger, rapidly growing aggregate species detected by DLS (peak II), the changes in the oligomer peak detected by NMR must represent a different process, involving changes in either oligomer packing or prevalence. Taken together, both the DLS and the NMR data confirm concentration dependent differences in early oligomeric behavior, independent of primary nucleus formation. Specifically, higher hCT concentrations exhibit larger and longer lived oligomers during the lag phase than lower hCT concentrations.

2.2.4. The effect of micelle-like oligomers on hCT aggregation

Given a postulated oligomeric culprit driving the abnormal hCT aggregation, a potential role for micelle-like oligomers was investigated. In contrast to amyloid oligomers as typically described, which form over a range of concentrations with varied sizes and morphologies, micelle-like oligomers form exclusively above their critical micelle concentration (CMC). Additionally, such oligomers consistently result in the shielding of hydrophobic peptide regions in the oligomeric interior, analogously to lipid micelles. Studies have reported that several amyloid proteins including amyloid-β, hIAPP, and PrP form such oligomers, with these oligomers exhibiting significant effects on aggregation kinetics.(19, 20, 22–25) The formation of micelle-like oligomers has also been proposed, but not detected, for hCT and provides a potential mechanism for the concentration versus lag time trend.(32, 46) At higher concentrations an

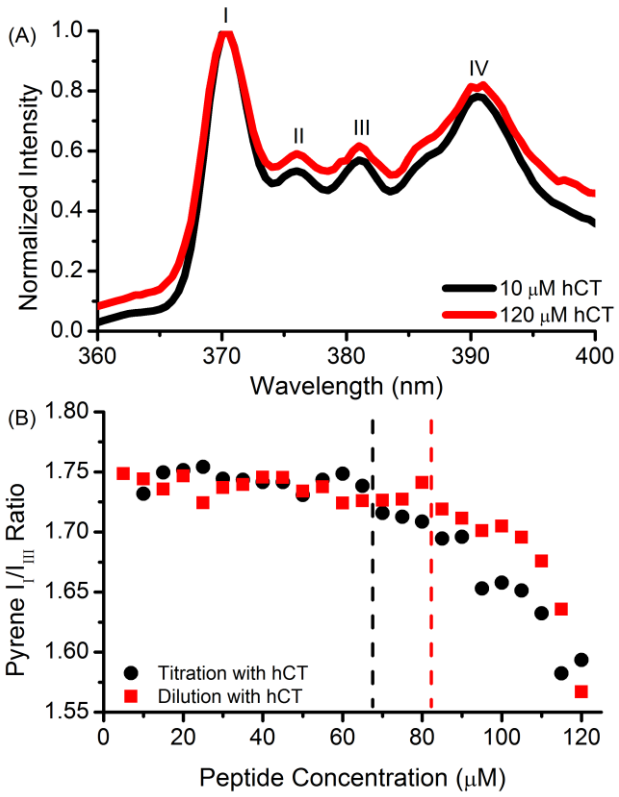

Figure 2.4. Pyrene detects a micelle-like oligomer in hCT. A) Fluorescence spectra of pyrene normalized to peak I. The shift in peak III at different concentrations relative to peak I is indicative of micelle formation. B) Plot of pyrene I/III ratio over indicated hCT concentration range. Dashed lines indicate initial formation (titration) or final dissolution (dilution) of hCT micelle-like oligomers. I/III ratio determined from average of three scans.

elevated number of micelle-like oligomers could pull progressively larger amounts of monomers off-pathway, providing a sink for monomers and resulting in slower aggregation.

The formation of micelle-like hCT oligomers was determined by monitoring the fluorescence spectrum of pyrene, a well-established technique for detecting micelle formation.(19, 47, 48) Pyrene emission spectra were collected with changing peptide concentrations, and the peak I/peak III intensity ratio plotted against concentration (Fig. 2.4.). This ratio undergoes a sharp decrease upon crossing ~80 μM peptide, indicating that micelle-like hCT oligomers form above this CMC. The pyrene spectral shift occurs at roughly the same concentration with both increasing (titration) and decreasing (dilution) peptide concentrations, indicating that the formation of the micelle-like oligomer is reversible. This formation of a reversible micelle-like oligomer of hCT is

consistent with the behavior of similar aggregates in other amyloids, and represents the first direct confirmation of micelle formation by hCT.(19, 20, 22)

Despite confirming their formation, results to this point suggest that micelle-like oligomers of hCT play no role in the anomalous concentration dependent aggregation trend observed. The relationship between lag time and peptide concentration displays no discontinuity at or above the CMC, as would be expected if micelle-like oligomers were involved (Fig. 2.1.B). This kinetic inactivity of the micelle-like oligomer of hCT is at odds with the behavior of similar aggregates in other amyloids, and casts doubt as to its role in previously proposed hCT aggregation pathways.

2.2.5. Inhibition by growth-incompetent hCT monomers explains the anomalous trend in concentration versus lag time

The micelle independence of the atypical concentration versus lag time trend, combined with the persistence of a long lag phase in the presence of seeds, necessitates another determinant of lag time. The existence of no apparent concentration dependent morphological differences in protofibrillar or mature fibril species suggests the canonical elongation and fragmentation mechanisms for amyloid fibril kinetics to be at work.(37) Additionally, the persistence of a prominent lag time in the presence of seeds would suggest that initial hCT peptides are different from classical monomers in that they cannot immediately be incorporated into fibrils during elongation. Such a difference could arise through the need for a structural conversion step in the monomers before they are growth-competent. As such, the inverse dependence of lag time on the monomer concentration can be explained by the existence of two distinct types of monomers, growth-competent and growth-incompetent (see Section 2.4.8. for model details). Such promiscuity in monomer conformation inhibits the formation of mature fibrils by both limiting the availability of growth-competent monomers and through the formation of slowly reversible

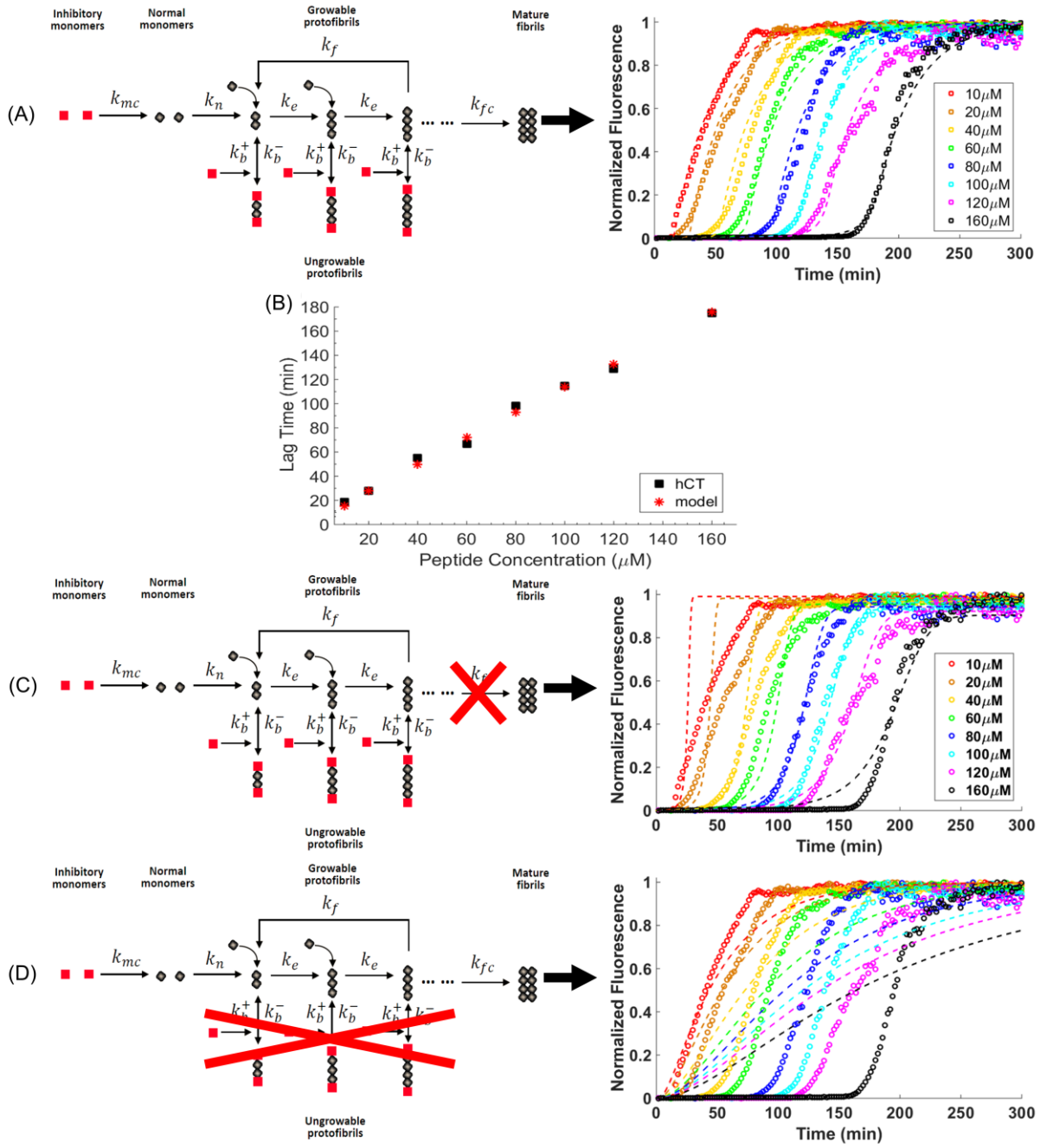

Figure 2.5. Monomer conversion allows accurate kinetic modeling of observed trend between peptide concentration and lag time. A) Reaction diagram for hCT fibrillation and comparison between experimental (colored squares) and computational (dashed lines) evolutions shows model to recapitulate experimental trend. Global fitting (dashed lines) was performed according to Eq. 1 with $k_n = 1.8 \times 10^{-4}\ h^{-1}$, $k_e = 1 \times 10^{5}\ \mu M^{-1}\ h^{-1}$, $k_{mc} = 3.5 \times 10^{2}\ h^{-1}$, $k_{fc} = 1.9\ h^{-1}$, $k_b^+ = 1.2 \times 10^{5}\ \mu M^{-1}\ h^{-1}$, $k_b^- = 1.4 \times 10^{-7}\ h^{-1}$, $k_f = 1 \times 10^{-2}\ h^{-1}$, and $n_c = 1$. B) Comparison of dependence of lag time on peptide concentration between experimental and computational results. Lag time for both computational and experimental data is determined according to fitting with Eq. 1. C) Removal of lateral structure conversion from protofibril to mature fibril will cause a gradual decrease in predicted curve slopes. The best global fitting is shown according to Eq. 1 with $k_n = 2.2 \times 10^{-3}\ h^{-1}$, $k_e = 1 \times 10^{5}\ \mu M^{-1}\ h^{-1}$, $k_{mc} = 98.6\ h^{-1}$, $k_b^+ = 2.7 \times 10^{4}\ \mu M^{-1}\ h^{-1}$, $k_b^- = 1.87 \times 10^{-9}\ h^{-1}$, $k_f = 7.3 \times 10^{-2}\ h^{-1}$, and $n_c = 1$. D) Removal of the monomer inhibition step on protofibril elongation will cause the disappearance of the inverse relationship between lag time and peptide concentration. Curves are drawn based on best global fitting with $k_n = 4.9 \times 10^{-3}\ h^{-1}$, $k_e = 1 \times 10^{5}\ \mu M^{-1}\ h^{-1}$, $k_{mc} = 58.3\ h^{-1}$, $k_{fc} = 1.3\ h^{-1}$, $k_f = 1.6 \times 10^{-3}\ h^{-1}$, and $n_c = 2.3$.

growth-incompetent aggregates (Fig. 2.5.A). Such a model accurately reproduces the experimental data showing a direct relationship between lag time and monomer concentration (Fig. 2.5.A-B). Details of model species evolution, rate constant influence, and sensitivity analysis are provided in Appendix A (Fig. A.4.-A.6.).

Comparisons between the current model and other unsuccessful models are shown in Fig. 2.5.C-D, highlighting the necessity of key model elements. Note that the removal of the monomer conversion step in the current model leads to a reversion to the canonical relationship between peptide concentration and lag time, as has been previously shown in the literature.(37, 49)

2.2.6. MD simulations implicate α-helical structure as critical for monomer growth-competence

In order to correlate this study with other kinetics studies focused on maintaining monomeric CT for therapeutic applications, the behavior of hCT was compared with the therapeutically preferred sCT (Fig. 2.6.A). As expected, sCT exhibited significantly longer lag times than hCT under identical conditions (Fig. 2.6.B). However, despite the significant sequence homology, under identical conditions sCT displays the canonical relation between lag time and peptide concentration for amyloids, in contrast to hCT. According to the kinetics modeling, the reversion of sCT to the canonical relation between peptide concentration and lag phase should be correlated with a difference in the initial structures in sCT as compared to hCT. Experimental methods to distinguish specific monomer or oligomer conformations in the interconverting and heterogeneous pre-fibrillar milieu have yet to be achieved in amyloid research. In order to circumvent these limitations, molecular dynamics (MD) simulations were utilized to probe the relative distributions of hCT and sCT monomers in solution. MD simulations show sCT to sample a more compact region of conformational space and occupy fewer structural basins (clusters) on

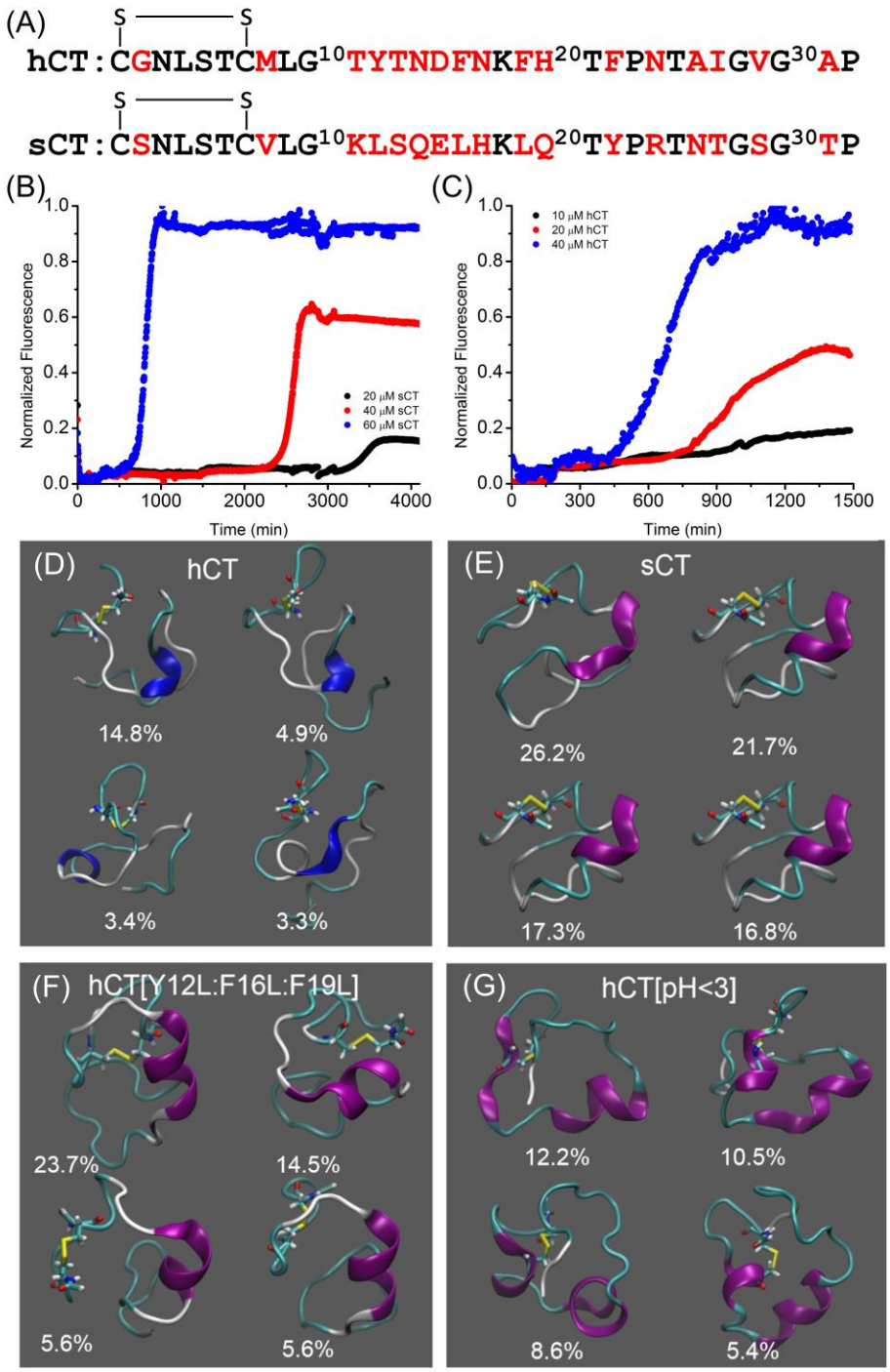

Figure 2.6. Molecular dynamics simulations implicate α-helical structure as key in determining monomer growth-competence. A) Comparison between the sequences of hCT and sCT. Non-conserved residues shown in red. B) sCT and C) hCT at low pH display the typical relationship between lag phase and peptide concentration. Experiments performed in duplicate at 25 ºC in 20 mM phosphate buffer, pH 7.4 for sCT and 20 mM citric acid buffer, pH 3.3 for hCT. Curves normalized to 60 μM max fluorescence and 40 μM max fluorescence for sCT and hCT, respectively. Structural models representing the 4 most populated clusters and the relative percentage of monomer found in each cluster for D) hCT, E) sCT, F) hCT mutant, and G) low pH hCT. Models show sCT with the highest helical propensity, hCT the lowest, with the hCT-mutant and low pH hCT again being intermediate to hCT and sCT (sCT > hCT mutant = hCT (low pH) > hCT).

its energy landscape than hCT, with 82% of sCT conformations falling in the 4 most populated clusters compared to just 26.4% for hCT (Fig. 2.6.D-E, Fig. A.7.). sCT monomer conformations had smaller radii of gyration and a more compact distribution of end-to-end distances than hCT (Fig. A.7.C-D). sCT also shows several discrete overrepresented end-to-end distance values relative to a normal Gaussian distribution, further hinting at increased structure. Significantly, sCT monomers show increased numbers of helix-incorporated residues as compared to hCT, a finding in keeping with previous comparative studies (Fig. A.7.B).(50, 51) This increased helical structure in sCT versus hCT immediately after peptide solubilization was confirmed by CD measurements (Fig. 2.7.). The decreased conformational heterogeneity and more structured helical sCT monomer as compared to hCT is consistent with the kinetic model predictions of differing degrees of monomer heterogeneity, leading to the canonical inverse relationship between lag time and concentration in sCT. Specifically, the increased helical structure in the sCT monomer would suggest that this more structured, "sCT-like" monomer represents the growth-competent species, whereas the less ordered "hCT-like" species represent the growth-incompetent species, which requires conversion through oligomeric intermediates to gain structure and proceed to fibril incorporation.

While the precise causes for these differences between hCT and sCT remain unknown, one possible explanation lies in the mutation of the three central aromatic residues in hCT (Tyr12, Phe16, Phe19) to Leu in sCT. The associated π-π stacking interactions in hCT have been confirmed by NMR and crystallography as crucial in driving fibrillation, with mutations in these three residues increasing hCT lag times to be comparable with sCT.(52, 53) The ability for EGCG to dissociate early aggregates in hCT believed to be associated with monomer conversion suggests that aromatic residues play a key role in said conversion as well. As such, MD simulations were

performed on a hCT mutant (Y12L, F16L, F19L) to probe the role of these residues in the monomer conformational heterogeneity and structure. Interestingly, the mutated hCT behaved in a fashion intermediate to hCT and sCT: the mutant displayed decreased conformational heterogeneity, increased α-helical content, and decreased radii of gyration and end-to-end distances as compared to wild-type hCT, rendering it more "sCT-like" (Fig. 2.6.F, Fig. A.7.). The MD simulations thus support the idea that these residues are important for not only interpeptide stabilizing interactions, but also as intrapeptide conformational constraints.

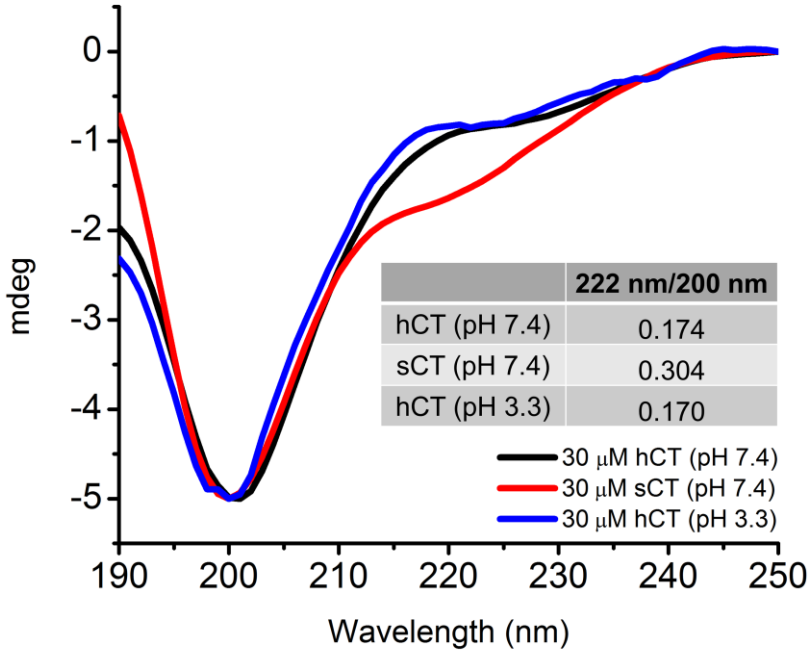

Figure 2.7. Circular Dichroism measurements support MD simulations on α-helical propensity. CD spectra of hCT (pH 7.4), sCT (pH 7.4), and hCT (pH 3.3) are shown immediately after sample preparation. Curves are normalized to -5 mdeg at 200 nm to allow direct visualization of α-helical content relative to random coil. Spectra represent averages of 5 scans. As is quantified in the inset, sCT shows the strongest α-helical signal relative to random coil, with hCT (pH 7.4) and hCT (pH 3.3) showing lower helical content. Looking at lineshapes indicates hCT (pH 3.3) to have a more pronounced shoulder at 222nm as compared to hCT (pH 7.4), indicating increased helical content despite similarity in the 222nm/200nm ratio and showing the CD results to agree with simulations.

Similarly to the hCT mutant, hCT under low pH conditions (pH 3.3) was also observed in MD simulations to exhibit increased helical structure in the monomer and become more "sCT-like" (Fig. 2.6.G, Fig. A.7.).(32, 33, 46) Critically, ThT experiments with hCT at low pH actually show a reversion back to the canonical amyloid relationship with this increased monomer

structure, similarly to sCT (Fig. 2.6.C). Further, CD experiments confirm freshly dissolved hCT at low pH to contain α-helical structure intermediate to sCT and hCT at neutral pH, consistently with MD simulations (Fig. 2.7.). This data provides further evidence that more structured, "sCT-like" monomers, specifically with α-helical motifs, represent a growth-competent species that allows fibrillation along the canonical amyloid pathway.

2.3. Discussion

A direct relationship between amyloid concentration and lag time has only been observed twice prior, both times in light chain amyloids.(54, 55) In these studies, a dimer-monomer exchange mediating the relative native state population was proposed, with higher concentrations favoring the non-fibrillating dimer and slower aggregation. The formation of an anti-parallel helical dimer has been shown to slow aggregation in sCT as well, however the experiments performed in this study give no evidence for such dimer formation being causative in the trend.(56) Indeed, if such a helix mediated dimer were the causative species, one would expect the more helical sCT, rather than hCT, to display the direct relationship between lag time and concentration. This study instead suggests that while helix formation is key in hCT aggregation, structural differences in free monomers, rather than an aggregate mediated sequestration, result in the increase in lag time with higher peptide concentration.

The existence of growth-competent and growth-incompetent monomers has been proposed previously, however several novel aspects of the current model warrant further consideration.(57) The reproduction of the reported trend requires the monomer conversion rate to depend inversely on initial peptide concentration, with a relatively slow rate constant. Such a phenomenon is unsurprising if one assumes monomer conversion to occur indirectly through the formation and

dissociation of low molecular weight oligomeric intermediates. According to the Ostwald ripening mechanism, the dissociation of larger particles is slower than that of smaller ones, with the time being roughly proportional to particle size.(58, 59) As such, one would expect the rate of oligomeric reformatting, and thus monomer conversion, to be inversely proportional to oligomer size. Not only is this differential rate of oligomer reformatting seen in the time-course NMR experiments, but the larger size of initial small oligomers observed at higher concentrations by DLS provides direct evidence for the existence of such an intermediate species. The inverse dependence of the kinetic term k_{mc} on m_{tot} incorporates these results into the kinetic model.

Additionally, the current model proposes the existence of off-pathway protofibrillar species, which persist without immediately elongating to fibrils. In particular, these off-pathway species could be formed by the addition of growth-incompetent monomers to growth-competent aggregates, essentially providing a means by which such monomers inhibit further growth and elongation. The detection of larger ThT-negative aggregates in the lag phase by DLS and TEM such as those predicted by the model during the lag phase, before mature fibril formation and elongation, is consistent with this model. Interestingly, the lack of a ThT-detectable β-sheet signal from these protofibrils as well as the marked morphological differences between protofibrils and mature fibrils hints at possible structural conversion steps in addition to the monomer conversion. Such a lateral structure conversion is fully consistent with previous hCT studies and the requirement of a unimolecular reaction, which accounts for the concentration independence of elongation rate observed in the ThT traces.(60)

Despite the support our kinetic model enjoys from both previous and current works, it is important to note that the complexity of the amyloid aggregation process likely is not fully encapsulated in the kinetic parameters described; other rate-determining species and conversions

in addition to those explicitly described are likely present. Furthermore, again owing to the metastability and heterogeneity of aggregate species, a direct experimental isolation and quantification of individual rate constants is not possible. An evaluation of the ability of the model to predict and reproduce experimentally induced changes in aggregation kinetics, e.g. through alterations of aggregation environment, would be valuable in determining model validity. Thus while the current model does present a viable and supported explanation for the kinetic trend, further experiments are required.

Interestingly, MD simulations show both the hCT mutant and hCT at low pH to form an amphipathic α-helix in the central region between Asp15 and Phe19, while such a helix is absent in the wild-type hCT. This central DFNKF region (DLNKL in the hCT mutant) forms the core of hCT fibrils, and has previously been shown to adopt a helical conformation in monomers, as determined by NMR.(46, 61, 62) The results in this study suggest that the helical structure of the

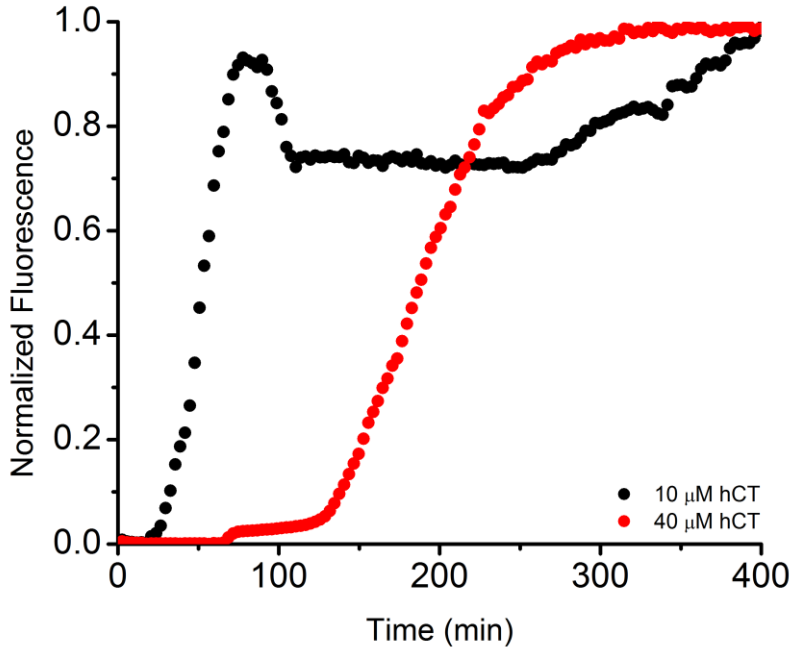

Figure 2.8. ThT kinetics assays at pH 5.4 indicate the direct relationship to remain, implicate Asp15 in determining growth-competence. Assays were performed in triplicate using citric acid buffer, pH 5.4, at 25 ºC, with orbital shaking and 2 equivalents of ThT. The similar relationship between lag time and concentration at pH 7.4 and 5.4 indicates the behavior to be independent of the charge state of His20 (pKa = 6).

DFNKF region may be key in determining the growth competence of hCT monomers, potentially by driving initial monomer self-recognition events through hydrophobic interactions. Low pH environments and leucine residues have both previously been shown to enhance helical propensity, consistent with the above findings.(63, 64) In particular for hCT going from pH 7.4 to pH 3.3, the side chains of Asp15 and His20 both become protonated. Given the proximity of these residues to the central helix forming region, they present likely causes for the pH dependent change. ThT kinetics experiments at pH 5.4 (where His20 is protonated but Asp15 is not) reveal the maintenance of the direct relationship between concentration and lag time, suggesting that the charge state of Asp15 plays the larger role in the pH-determined growth-competence of hCT monomers(Fig. 2.8.). Further experiments involving the above-mentioned hCT mutant and other, more structured hCT monomers will be valuable in fully understanding the role of monomer structure and concentration in determining lag time.

Previous studies have reported both hCT and sCT to exhibit α-helical structural motifs during the progression to mature β-strand conformations, consistently with the predictions of this study.(6, 65–70) Note that the dominance of random coil structure in this study's CD experiments, with smaller amounts of helical structure are not contradictory to previous studies. The predicted monomer structures of hCT and sCT, both here and in other studies, maintain extended unstructured regions, with limited numbers of helical residues. Additionally, the relatively rapid incorporation of converted monomers into fibrils, a mechanism consistent with previous amyloid research and exemplified in Figure A.4.A, would serve to preferentially sequester helical monomers in favor of less structured monomers.

In light of the fact that low pH conditions and mutated hCT have been shown to slow the aggregation of hCT, it is important to note that the shift to a more "sCT-like" growth-competent

monomer is not proposed to represent an overall acceleration of the aggregation pathway, but rather a loss of need for monomer reformatting, and thus a return to the canonical relation between peptide concentration and lag time. Despite this, a correlation does exist between the degree of monomer structure and lag time. A hypothesized explanation is that the more stable helices in "sCT-like" monomers, while encouraging initial monomer interactions and aggregation events, could resist conversion to β-sheet structures thus delaying overall lag times. This explanation finds support in the reported delay of sCT aggregation by helical dimers, mediated by the helical propensity of the monomer and stabilizing hydrophobic leucine interactions between helices.(56, 71) It seems likely that the observations of monomer helical stability being correlated with slower lag times are due to the formation of similar stable helical structures, but further studies are required to confirm the persistence of this behavior in the above experiments.

Interestingly, it appears that micelle-like oligomers play no significant role in hCT aggregation, in contrast to other amyloids. In addition to being kinetically inactive, the above CD, NMR, and TEM experiments showed no structural or morphological differences upon the introduction of micelle-like oligomers through increased concentration. TEM measurements do show punctate proteinaceous aggregates in the late lag phase above the CMC only, with such aggregates being absent at low concentrations (Fig. A.8.). Such aggregates may be the micelle-like oligomers, but show no spatial association with other aggregates, further suggesting a non-functional role. Naito and colleagues previously observed spherical aggregates of hCT to form in HEPES buffer.(32) Such oligomers were shown to seed fibril formation, and micelle-like oligomers were proposed as a preceding species to these spherical aggregates. Given the lack of kinetic influence or fibril association of the micelle-like oligomers detected in this study, it would seem that the spherical aggregates formed in HEPES buffer could form in a micelle-independent

fashion. The kinetic inactivity of micelle-like oligomers of hCT observed in this study is especially confounding given recent work highlighting the role of such oligomers in the aggregation of the related peptide hIAPP.(20) Both hCT and hIAPP belong to the calcitonin family, bind to the same receptor, contain an N-terminal disulfide bond, and possess similar numbers of residues and charges. The causes for this deviation in oligomer influence are unknown, and are confounded by the reversible formation of oligomers and the difficulty in isolating them from the pre-fibrillar milieu.

The reported relationship between concentration and lag time in hCT also holds therapeutic promise through the possibility for higher effective doses of hCT without the correlated hindrance of decreased bioavailability. Indeed such a phenomenon has broad interest for all fibrillating therapeutic peptides, e.g. insulin, where large local peptide concentrations and subsequent aggregation pre-uptake, for example within nanoparticles, pose obstacles to therapeutic efficacy and alternative therapeutic delivery methods.(72–77) With the increasing prevalence of therapeutic peptides in the pharmaceutical market, such issues are taking on progressively more importance. The direct relationship seen here between lag time and peptide concentration could inform future efforts to design appropriate peptide delivery systems, and allow the packaging of higher dosages of peptide without loss of efficacy.

2.4. Materials and Methods

2.4.1. Peptide preparation

Human calcitonin peptide was synthesized via Fmoc chemistry as described previously.(33) The disulfide bond between Cys1 and Cys7 of hCT was formed by air oxidation at pH 8.0-8.5 at diluted concentration and in the presence of 6 M urea to prevent fibrillation. To

ensure consistent monomeric starting conditions, peptide was dissolved in hexafluoroisopropanol (HFIP) at a concentration of 1 mg/ml. Peptide was then separated into 100 μL aliquots, flash frozen in liquid nitrogen, and lyophilized for a period of 48 hours. After lyophilization, peptide aliquots were stored at -20 ºC until use. Peptide solutions were prepared by resolubilizing the lyophilized aliquots in 100 μL of HCl pH 4 at 4 ℃ to a concentration of ~300 μM, followed by brief sonication to ensure peptide dissolution. Peptide solutions were then warmed to room temperature and subsequently used.

2.4.2. Thioflavin-T Kinetic Assay

Thioflavin-T (ThT) experiments were run on a Biotek Synergy 2 microplate reader (BioTek Instruments, Inc., Winooski, VT, USA) on uncoated Fisherbrand 96-well polystyrene plates. Peptide was added to final concentrations of 20 mM buffer and ThT at 25 ºC, and immediately prior to acquisition. Experiments were performed in duplicate with two equivalents of ThT and 100 μL total volume unless otherwise indicated. Wells were bottom read with an excitation wavelength of 440 nm (30 nm bandwidth) and emission wavelength of 485 nm (20 nm bandwidth). Curves were normalized, averaged, and kinetic parameters t_{50} and t_{lag} calculated via fitting to the equations:(26)

$$P(t) = P_{\infty} + \frac{P_0 - P_{\infty}}{1 + e^{k(t - t_{50})}} \quad , \quad t_{lag} = t_{50} - \frac{2}{k} \qquad (2)$$

For seeded assays, seeds were generationally created to ensure uniform morphology(78) 1st generation seeds were created at 120 μM in 20 mM phosphate buffer at 50 μL volume, at 37 ℃ shaking at 1000 rpm for 24 hrs. Subsequent generations were seeded by the previous generation at

10% by volume, and incubated under identical conditions. 4th generation seed was seeded identically with 200 μL final volume. 4th generation seeds were used for ThT kinetics assays

2.4.3. Circular Dichroism

Circular dichroism (CD) spectra were taken on a Jasco J-1500 Circular Dichroism Spectrometer (JASCO, Inc., Easton, MD, USA). Spectra were recorded at 25 °C with 120 μM hCT and 30 μM hCT concentrations in 20 mM phosphate buffer pH 7.4 in a 1 mm quartz cuvette unless otherwise indicated. Spectra were recorded with 2 nm bandwidth, 1 nm step size, scan speed of 100 nm/min, baseline corrected, and averaged over 5 scans. Smoothing was performed using the Savitzky-Golay method, with a convolution width of 15. Between reads, peptide samples were transferred to a microcentrifuge tube and vortexed for 2 s every 10 minutes.

2.4.4. Transmission Electron Microscopy

Samples for transmission electron microscopy (TEM) were removed at 3 separate time points from a single well of a ThT plate and flash frozen in liquid nitrogen. Glow-discharged grads (Formar/Carbon 300-mesh, Electron Microscopy Sciences, Hatfield, PA, USA) were treated with the samples for 2 min at room temperature. Excess sample was removed with filter paper and washed three times with ddH_20. Each grid was stained with uranyl acetate (1% w/v, ddH_20, 5μL, 1 min), blotted to remove excess stain, and dried for 15 min at room temperature. TEM images were recorded on a JEOL 1400-plus TEM (80kV) (Microscopy and Image Analysis Laboratory, University of Michigan, Ann Arbor, MI, USA).

2.4.5. Dynamic Light Scattering

Dynamic light scattering (DLS) measurements were taken at 25 ºC using a DynaPro NanoStar Dynamic Light Scattering Spectrometer (Wyatt Technology, Santa Barbara, CA, USA). All reagents and buffers were syringe filtered (0.22 μm pore size) prior to sample preparation. Initially monomeric aliquots of hCT were added to a final peptide concentration of 120 μM or 30 μM in 20 mM phosphate buffer, pH 7.4 and immediately loaded into the cuvette for analysis. Scattering was measured every 2 minutes for the first hour, every 6 minutes for the following 2 hours, and every 10 minutes for the subsequent 2 hours. All reported measurements are averages of 10 acquisitions. Trials with indistinguishable oligomer and larger aggregate peaks, or with poor fits, were disregarded in analysis.

2.4.6. Nuclear Magnetic Resonance

All NMR spectra were obtained on a Bruker 600 MHz spectrometer (Bruker Corporation, Billerica, MA, USA). 300 μL of peptide solution in 20 mM phosphate buffer pH 7.4 with 10% D_2O (v/v) was prepared. Spectra were collected every two minutes at 25 ºC with a spectral width of 8992.8 Hz and 64 or 32 scans for the 30 μM and 120 μM samples, respectively. Spectra were processed using Topspin 2.1 (Bruker), where normalized oligomer peak intensities were determined via fixed bound integration.

2.4.7. Pyrene Fluorescence Assay

Pyrene solutions were prepared by dissolving pyrene powder in DMSO followed by serial dilution down to 1 μM in 20 mM phosphate buffer, pH 7.4. Samples were prepared by dilution of peptide stock to final peptide concentration in 20 mM phosphate buffer, pH 7.4, with 1 μM pyrene to ensure constant pyrene concentration throughout titration/dilution. Pyrene emission spectra were recorded with a FluoroMax-4 Spectrofluorometer (Horiba, Ltd., Kyoto, Japan), with final

spectra being obtained via averaging of three scans taken at 25 ºC. Excitation was at 334 nm with a bandwidth of 2 nm, emission bandwidth was 1 nm. The intensities of peaks I and III were recorded at 370 nm and 381 nm, respectively. The I/III intensity ratio was plotted vs peptide concentration, and the CMC was determined by fitting the data to an inverse logarithmic decay and determining the point at which the ratio dropped beyond low concentration average.

2.4.8. Kinetics Modeling

The kinetics modeling equations are given below.

$$\begin{cases} \dot{m}_i(t) = -k_{mc} m_i(t) / m_{tot} - k_b^+ m_i(t) P_n(t) + k_b^- P_b(t), \\ \dot{m}_n(t) = k_{mc} m_i(t) / m_{tot} - n_c k_n m_n(t)^{n_c} - 2k_e m_n(t) P_n(t), \\ \dot{P}_n(t) = k_n m_n(t)^{n_c} + k_f M_p(t) - k_b^+ m_i(t) P_n(t) + k_b^- P_b(t), \\ \dot{P}_b(t) = k_b^+ m_i(t) P_n(t) - k_b^- P_b(t), \\ \dot{M}_p(t) = n_c k_n m_n(t)^{n_c} + 2k_e m_n(t) P_n(t) - k_{fc} M_p(t), \\ \dot{M}_f(t) = k_{fc} M_p(t). \end{cases} \quad (3)$$

In these equations, $m_i(t)$ and $m_n(t)$ represent the concentrations of hCT peptides before and after structure conversion, $P_b(t)$ and $P_n(t)$ represent the number concentration of growth-incompetent and growth-competent aggregates, and $M_p(t)$ and $M_f(t)$ represent the mass concentrations of protofibrils and mature fibrils, respectively. m_{tot} represents the total concentration of hCT peptides in the system. It is noticeable that $m_{tot} = m_i(t)+m_n(t)+M_p(t)+M_f(t)$ due to the conservation law of mass. k_{mc}, k_{fc}, k_n, k_b^+, k_b^-, k_e, and k_f are the rate constants governing the structure conversion of monomers and protofibrils, the primary nucleation of hCT monomers, the conversion from growth-competent to growth-incompetent aggregates by binding with pre-converted hCT monomers and its inverse reaction the growth of fibrils through elongation, and the fragmentation of protofibrils, respectively (Fig. 4A). n_c represents the critical nucleus size for primary nucleation.

2.4.9. Molecular Dynamics Simulations

Molecular dynamics (MD) simulations were carried out for sequences representing hCT and sCT at neutral pH, hCT at pH 3, and a hCT mutant (T12L, F16L, F19L hCT). All sequences used methylated acetyl and methylated amide as blocking groups at the N- and C-termini, respectively (ACE and CT3 patches in CHARMM). The simulations were performed using the CHARMM software package and force fields.(79, 80) In order to sample the conformational distributions adopted by each peptide in solution, simulations were performed utilizing the replica exchange methodology and an implicit, generalized Born solvent model adopted to run on GPUs.(81, 82) The peptide was represented in an implicit (Debye-Hückel) ionic environment representing 100 mM NaCl.(83) All heavy atom – hydrogen bonds were constrained using the SHAKE algorithm, and the each temperature window of the replica exchange sampling was coupled to a Langevin temperature bath at the desired temperature.(84, 85) Twelve temperature windows, which were exponentially distributed between 310K and 400 K, were employed. Each replica was sampled for 100 ns, or a total sampling of 1.2 μs. For each replica 5000 snapshots were saved at each temperature for subsequent analysis. The conformational distribution for each sequence was characterized at 310K by computing the distribution of structural characteristics, i.e., end-to-end distance, helical content and radius of gyration. Additionally, the ensemble of structures at 310K from each sequence was visualized by clustering the structures from replica-exchange steps 1000-5000 using K-means clustering with 4.5 Å Cα + Cβ rmsd based with the MMTSB Tool cluster.pl criterion.(86)

2.5. Acknowledgements

This study was supported by funds from NIH (AG048934 to A.R.) and Protein Folding Disease center at the University of Michigan. L.H. acknowledges financial support from Tsinghua University Initiative Scientific Research Program (Grants 20151080424) and the program of China Scholarships Council (CSC). Support from the NIH (GM107233 to CLBIII) is gratefully acknowledged. The authors thank Kyle Korshavn for help with TEM and NMR measurements and Oluseun Oladipo for help with ThT experiments.

2.6. Author Contributions

KKP and AR conceived the idea and planned the study. KKP performed ThT, CD, NMR, DLS, and TEM experiments. LH carried out kinetics modeling and CLBIII performed MD simulations. KKP and AR analyzed the experimental data and interpreted the results. KKP, LH, CLBIII and AR wrote the paper. AN provided the peptides. AR directed the project. All authors reviewed the results and approved the final manuscript.

2.7. References

1. Zaidi, M., Inzerillo, A. ., Moonga, B. ., Bevis, P. J. ., and Huang, C. L.-H. (2002) Forty years of calcitonin—where are we now? A tribute to the work of Iain Macintyre, FRS. *Bone*. **30**, 655–663

2. Chesnut, C. H., Azria, M., Silverman, S., Engelhardt, M., Olson, M., and Mindeholm, L. (2008) Salmon calcitonin: a review of current and future therapeutic indications. *Osteoporos. Int.* **19**, 479–91

3. Schneider, D., Hofmann, M. T., and Peterson, J. A. (2002) Diagnosis and treatment of Paget's disease of bone. *Am. Fam. Physician*. **65**, 2069–72

4. Singer, F. R., Fredericks, R. S., and Minkin, C. (1980) Salmon calcitonin therapy for paget's disease of bone the problem of acquired clinical resistance. *Arthritis Rheum.* **23**, 1148–1154

5. Cudd, A., Arvinte, T., Gaines Das, R. E., Chinni, C., and MacIntyre, I. (1995) Enhanced Potency of Human Calcitonin When Fibrillation is Avoided. *J. Pharm. Sci.* **84**, 717–719

6. Kamgar-Parsi, K., Tolchard, J., Habenstein, B., Loquet, A., Naito, A., and Ramamoorthy, A. (2016) Structural Biology of Calcitonin: From Aqueous Therapeutic Properties to

Amyloid Aggregation. *Isr. J. Chem.* **57**, 634–650

7. Harrison, R. S., Sharpe, P. C., Singh, Y., and Fairlie, D. P. (2007) Amyloid peptides and proteins in review. *Rev. Physiol. Biochem. Pharmacol.* **159**, 1–77

8. DeToma, A. S., Salamekh, S., Ramamoorthy, A., and Lim, M. H. (2012) Misfolded proteins in Alzheimer's disease and type II diabetes. *Chem. Soc. Rev.* **41**, 608–21

9. Spillantini, M. G., Schmidt, M. L., Lee, V. M., Trojanowski, J. Q., Jakes, R., and Goedert, M. (1997) Alpha-synuclein in Lewy bodies. *Nature*. **388**, 839–40

10. Mok, K. H., Pettersson, J., Orrenius, S., and Svanborg, C. (2007) HAMLET, protein folding, and tumor cell death. *Biochem. Biophys. Res. Commun.* **354**, 1–7

11. Pettersson-Kastberg, J., Aits, S., Gustafsson, L., Mossberg, A., Storm, P., Trulsson, M., Persson, F., Mok, K. H., and Svanborg, C. (2009) Can misfolded proteins be beneficial? The HAMLET case. *Ann. Med.* **41**, 162–76

12. Murphy, M. P., and LeVine, H. (2010) Alzheimer's disease and the amyloid-beta peptide. *J. Alzheimers. Dis.* **19**, 311–23

13. Westermark, P., Andersson, A., and Westermark, G. T. (2011) Islet amyloid polypeptide, islet amyloid, and diabetes mellitus. *Physiol. Rev.* **91**, 795–826

14. Fowler, S. B., Poon, S., Muff, R., Chiti, F., Dobson, C. M., and Zurdo, J. (2005) Rational design of aggregation-resistant bioactive peptides: reengineering human calcitonin. *Proc. Natl. Acad. Sci. U. S. A.* **102**, 10105–10

15. Feletti, C., and Bonomini, V. (1979) Effect of calcitonin on bone lesions in chronic dialysis patients. *Nephron*. **24**, 85–8

16. Singer, F. R., Aldred, J. P., Neer, R. M., Krane, S. M., Potts, J. T., and Bloch, K. J. (1972) An evaluation of antibodies and clinical resistance to salmon calcitonin. *J. Clin. Invest.* **51**, 2331–8

17. Grauer, A., Reinel, H. H., Ziegler, R., and Raue, F. (1993) Neutralizing antibodies against calcitonin. *Horm. Metab. Res.* **25**, 486–8

18. Avidan-Shpalter, C., and Gazit, E. (2006) The early stages of amyloid formation: biophysical and structural characterization of human calcitonin pre-fibrillar assemblies. *Amyloid*. **13**, 216–25

19. Sabaté, R., and Estelrich, J. (2005) Evidence of the existence of micelles in the fibrillogenesis of beta-amyloid peptide. *J. Phys. Chem. B.* **109**, 11027–32

20. Brender, J. R., Krishnamoorthy, J., Sciacca, M. F. M., Vivekanandan, S., D'Urso, L., Chen, J., La Rosa, C., and Ramamoorthy, A. (2015) Probing the Sources of the Apparent Irreproducibility of Amyloid Formation: Drastic Changes in Kinetics and a Switch in

Mechanism Due to Micellelike Oligomer Formation at Critical Concentrations of IAPP. *J. Phys. Chem. B*. **119**, 2886–2896

21. Hong, L., Qi, X., and Zhang, Y. (2012) Dissecting the kinetic process of amyloid fiber formation through asymptotic analysis. *J. Phys. Chem. B*. **116**, 6611–7

22. Hingant, E., Fontes, P., Alvarez-Martinez, M. T., Arnaud, J.-D., Liautard, J.-P., and Pujo-Menjouet, L. (2014) A micellar on-pathway intermediate step explains the kinetics of prion amyloid formation. *PLoS Comput. Biol.* **10**, e1003735

23. Wälti, M. A., Orts, J., Vögeli, B., Campioni, S., and Riek, R. (2015) Solution NMR studies of recombinant Aβ(1-42): from the presence of a micellar entity to residual β-sheet structure in the soluble species. *Chembiochem*. **16**, 659–69

24. Wei, Y., Lu, J., Lu, T., Meng, F., Xu, J., Wang, L., Li, Y., Wang, L., and Li, F. (2016) Formation of lamellar micelle-like oligomers and membrane disruption revealed by the study of short peptide hIAPP 18–27. *Phys. Chem. Chem. Phys.* **18**, 29847–29857

25. Rhoades, E., and Gafni, A. (2003) Micelle formation by a fragment of human islet amyloid polypeptide. *Biophys. J.* **84**, 3480–7

26. Batzli, K. M., and Love, B. J. (2015) Agitation of amyloid proteins to speed aggregation measured by ThT fluorescence: a call for standardization. *Mater. Sci. Eng. C. Mater. Biol. Appl.* **48**, 359–64

27. Guo, C., Ma, L., Zhao, Y., Peng, A., Cheng, B., Zhou, Q., Zheng, L., and Huang, K. (2015) Inhibitory effects of magnolol and honokiol on human calcitonin aggregation. *Sci. Rep.* **5**, 13556

28. Younan, N. D., and Viles, J. H. (2015) A comparison of three fluorophores (ThT, ANS, bis-ANS) for the detection of amyloid fibers and prefibrillar oligomeric assemblies. *Biochemistry*. **54**, 4297–4306

29. Khurana, R., Coleman, C., Ionescu-Zanetti, C., Carter, S. A., Krishna, V., Grover, R. K., Roy, R., and Singh, S. (2005) Mechanism of thioflavin T binding to amyloid fibrils. *J. Struct. Biol.* **151**, 229–238

30. Robbins, K. J., Liu, G., Lin, G., and Lazo, N. D. (2011) Detection of Strongly Bound Thioflavin T Species in Amyloid Fibrils by Ligand-Detected 1H NMR. *J. Phys. Chem. Lett.* **2**, 735–740

31. Milton, N. G. N., and Harris, J. R. (2013) Fibril formation and toxicity of the non-amyloidogenic rat amylin peptide. *Micron*. **44**, 246–53

32. Itoh-Watanabe, H., Kamihira-Ishijima, M., Kawamura, I., Kondoh, M., Nakakoshi, M., Sato, M., and Naito, A. (2013) Characterization of the spherical intermediates and fibril formation of hCT in HEPES solution using solid-state 13C-NMR and transmission electron microscopy. *Phys. Chem. Chem. Phys.* **15**, 16956–64

33. Huang, R., Vivekanandan, S., Brender, J. R., Abe, Y., Naito, A., and Ramamoorthy, A. (2012) NMR characterization of monomeric and oligomeric conformations of human calcitonin and its interaction with EGCG. *J. Mol. Biol.* **416**, 108–20

34. Wagner, K., Van Mau, N., Boichot, S., Kajava, A. V., Krauss, U., Le Grimellec, C., Beck-Sickinger, A., and Heitz, F. (2004) Interactions of the Human Calcitonin Fragment 9–32 with Phospholipids: A Monolayer Study. *Biophys. J.* **87**, 386–395

35. Diociaiuti, M., Macchia, G., Paradisi, S., Frank, C., Camerini, S., Chistolini, P., Gaudiano, M. C., Petrucci, T. C., and Malchiodi-Albedi, F. (2014) Native metastable prefibrillar oligomers are the most neurotoxic species among amyloid aggregates. *Biochim. Biophys. Acta*. **1842**, 1622–9

36. Gaudiano, M. C., Colone, M., Bombelli, C., Chistolini, P., Valvo, L., and Diociaiuti, M. (2005) Early stages of salmon calcitonin aggregation: effect induced by ageing and oxidation processes in water and in the presence of model membranes. *Biochim. Biophys. Acta*. **1750**, 134–45

37. Arosio, P., Knowles, T. P. J., and Linse, S. (2015) On the lag phase in amyloid fibril formation. *Phys. Chem. Chem. Phys.* **17**, 7606–18

38. Dean, D. N., Das, P. K., Rana, P., Burg, F., Levites, Y., Morgan, S. E., Ghosh, P., and Rangachari, V. (2017) Strain-specific Fibril Propagation by an Aβ Dodecamer. *Sci. Rep.* **7**, 40787

39. Ban, T., Hoshino, M., Takahashi, S., Hamada, D., Hasegawa, K., Naiki, H., and Goto, Y. (2004) Direct Observation of Aβ Amyloid Fibril Growth and Inhibition. *J. Mol. Biol.* **344**, 757–767

40. Ogi, H., Fukukshima, M., Hamada, H., Noi, K., Hirao, M., Yagi, H., and Goto, Y. (2014) Ultrafast propagation of β-amyloid fibrils in oligomeric cloud. *Sci. Rep.* **4**, 6960

41. Kim, H. J., Chatani, E., Goto, Y., and Paik, S. R. (2007) Seed-dependent accelerated fibrillation of alpha-synuclein induced by periodic ultrasonication treatment. *J. Microbiol. Biotechnol.* **17**, 2027–32

42. Shoffner, S. K., and Schnell, S. (2016) Estimation of the lag time in a subsequent monomer addition model for fibril elongation. *Phys. Chem. Chem. Phys.* **18**, 21259–21268

43. Palhano, F. L., Lee, J., Grimster, N. P., and Kelly, J. W. (2013) Toward the Molecular Mechanism(s) by Which EGCG Treatment Remodels Mature Amyloid Fibrils. *J. Am. Chem. Soc.* **135**, 7503–7510

44. Wang, Q., Guo, J., Jiao, P., Liu, H., and Yao, X. (2014) Exploring the Influence of EGCG on the β-Sheet-Rich Oligomers of Human Islet Amyloid Polypeptide (hIAPP1–37) and Identifying Its Possible Binding Sites from Molecular Dynamics Simulation. *PLoS One*. **9**, e94796

45. Soong, R., Brender, J. R., Macdonald, P. M., and Ramamoorthy, A. (2009) Association of highly compact type II diabetes related islet amyloid polypeptide intermediate species at physiological temperature revealed by diffusion NMR spectroscopy. *J. Am. Chem. Soc.* **131**, 7079–85

46. Kamihira, M., Naito, A., Tuzi, S., Nosaka, A. Y., and Saitô, H. (2000) Conformational transitions and fibrillation mechanism of human calcitonin as studied by high-resolution solid-state 13C NMR. *Protein Sci.* **9**, 867–77

47. Aguiar, J., Carpena, P., Molina-Bolıivar, J. A., and Carnero Ruiz, C. (2003) On the determination of the critical micelle concentration by the pyrene 1:3 ratio method. *J. Colloid Interface Sci.* **258**, 116–122

48. Kalyanasundaram, K., and Thomas, J. K. (1977) Environmental effects on vibronic band intensities in pyrene monomer fluorescence and their application in studies of micellar systems. *J. Am. Chem. Soc.* **99**, 2039–2044

49. Cohen, S. I. A., Linse, S., Luheshi, L. M., Hellstrand, E., White, D. A., Rajah, L., Otzen, D. E., Vendruscolo, M., Dobson, C. M., and Knowles, T. P. J. (2013) Proliferation of amyloid-β42 aggregates occurs through a secondary nucleation mechanism. *Proc. Natl. Acad. Sci. U. S. A.* **110**, 9758–63

50. Andreotti, G., Méndez, B. L., Amodeo, P., Morelli, M. A. C., Nakamuta, H., and Motta, A. (2006) Structural determinants of salmon calcitonin bioactivity: the role of the Leu-based amphipathic alpha-helix. *J. Biol. Chem.* **281**, 24193–203

51. Amodeo, P., Motta, A., Strazzullo, G., and Castiglione Morelli, M. A. (1999) Conformational flexibility in calcitonin: the dynamic properties of human and salmon calcitonin in solution. *J. Biomol. NMR.* **13**, 161–74

52. Itoh-Watanabe, H., Kamihira-Ishijima, M., Javkhlantugs, N., Inoue, R., Itoh, Y., Endo, H., Tuzi, S., Saitô, H., Ueda, K., and Naito, A. (2013) Role of aromatic residues in amyloid fibril formation of human calcitonin by solid-state 13C NMR and molecular dynamics simulation. *Phys. Chem. Chem. Phys.* **15**, 8890–901

53. Metrangolo, P., Terraneo, G., Cavallo, G., Pizzi, A., Morra, G., Bertolani, A., Gazzera, L., Pirrie, L., Meli, M., Colombo, G., and Genoni, A. (2016) Crystal structure of the DFNKF segment of human calcitonin unveils aromatic interactions between phenylalanines. *Chem. - A Eur. J.* **23**, 2051–2058

54. Blancas-Mejía, L. M., Misra, P., and Ramirez-Alvarado, M. (2017) Differences in protein concentration dependence for nucleation and elongation in light chain amyloid formation. *Biochemistry*. **56**, 757–766

55. Zhijie Qin, Dongmei Hu, Min Zhu, A., and Fink, A. L. (2007) Structural Characterization of the Partially Folded Intermediates of an Immunoglobulin Light Chain Leading to Amyloid Fibrillation and Amorphous Aggregation. *Biochemistry*. **46**, 3521–3531

56. Andreotti, G., and Motta, A. (2003) Modulating calcitonin fibrillogenesis: an antiparallel alpha-helical dimer inhibits fibrillation of salmon calcitonin. *J. Biol. Chem.* **279**, 6364–6370

57. Kashchiev, D. (2017) Modeling the Effect of Monomer Conformational Change on the Early Stage of Protein Self-Assembly into Fibrils. *J. Phys. Chem. B.* **121**, 35–46

58. Levin, A., Mason, T. O., Adler-Abramovich, L., Buell, A. K., Meisl, G., Galvagnion, C., Bram, Y., Stratford, S. A., Dobson, C. M., Knowles, T. P. J., and Gazit, E. (2014) Ostwald's rule of stages governs structural transitions and morphology of dipeptide supramolecular polymers. *Nat. Commun.* **5**, 5219

59. So, M., Hall, D., and Goto, Y. (2016) Revisiting supersaturation as a factor determining amyloid fibrillation. *Curr. Opin. Struct. Biol.* **36**, 32–39

60. Bauer, H. H., Aebi, U., Häner, M., Hermann, R., Müller, M., Arvinte, T., and Merkle, H. P. (1995) Architecture and Polymorphism of Fibrillar Supramolecular Assemblies Produced by in Vitro Aggregation of Human Calcitonin. *J. Struct. Biol.* **115**, 1–15

61. Reches, M., Porat, Y., and Gazit, E. (2002) Amyloid fibril formation by pentapeptide and tetrapeptide fragments of human calcitonin. *J. Biol. Chem.* **277**, 35475–80

62. Shtainfeld, A., Sheynis, T., and Jelinek, R. (2010) Specific Mutations Alter Fibrillation Kinetics, Fiber Morphologies, and Membrane Interactions of Pentapeptides Derived from Human Calcitonin. *Biochemistry*. **49**, 5299–5307

63. Kanaori, K., and Nosaka, A. Y. (1995) Study of human calcitonin fibrillation by proton nuclear magnetic resonance spectroscopy. *Biochemistry*. **34**, 12138–43

64. Chou, P. Y., and Fasman, G. D. (1974) Prediction of protein conformation. *Biochemistry*. **13**, 222–45

65. Siligardi, G., Samorí, B., Melandri, S., Visconti, M., and Drake, A. F. (1994) Correlations between biological activities and conformational properties for human, salmon, eel, porcine calcitonins and Elcatonin elucidated by CD spectroscopy. *Eur. J. Biochem.* **221**, 1117–25

66. Lakshmanan, A., Cheong, D. W., Accardo, A., Di Fabrizio, E., Riekel, C., and Hauser, C. A. E. (2013) Aliphatic peptides show similar self-assembly to amyloid core sequences, challenging the importance of aromatic interactions in amyloidosis. *Proc. Natl. Acad. Sci. U. S. A.* **110**, 519–24

67. Arvinte, T., Cudd, A., and Drake, A. F. (1993) The structure and mechanism of formation of human calcitonin fibrils. *J. Biol. Chem.* **268**, 6415–22

68. Arvinte, T., and Drake, A. F. (1993) Comparative study of human and salmon calcitonin secondary structure in solutions with low dielectric constants. *J. Biol. Chem.* **268**, 6408–14

69. Bauer, H. H., Müller, M., Goette, J., Merkle, H. P., and Fringeli, U. P. (1994) Interfacial adsorption and aggregation associated changes in secondary structure of human calcitonin monitored by ATR-FTIR spectroscopy. *Biochemistry*. **33**, 12276–82

70. Meyer, J. P., Pelton, J. T., Hoflack, J., and Saudek, V. (1991) Solution structure of salmon calcitonin. *Biopolymers*. **31**, 233–41

71. Andreotti, G., Vitale, R. M., Avidan-Shpalter, C., Amodeo, P., Gazit, E., and Motta, A. (2011) Converting the highly amyloidogenic human calcitonin into a powerful fibril inhibitor by three-dimensional structure homology with a non-amyloidogenic analogue. *J. Biol. Chem.* **286**, 2707–18

72. Werle, M., and Takeuchi, H. (2009) Chitosan-aprotinin coated liposomes for oral peptide delivery: Development, characterisation and in vivo evaluation. *Int. J. Pharm.* **370**, 26–32

73. Gupta, V., Hwang, B. H., Lee, J., Anselmo, A. C., Doshi, N., and Mitragotri, S. (2013) Mucoadhesive intestinal devices for oral delivery of salmon calcitonin. *J. Control. Release*. **172**, 753–62

74. Umerska, A., Matougui, N., Groo, A.-C., and Saulnier, P. (2016) Understanding the adsorption of salmon calcitonin, antimicrobial peptide AP114 and polymyxin B onto lipid nanocapsules. *Int. J. Pharm.* **506**, 191–200

75. Matougui, N., Boge, L., Groo, A.-C., Umerska, A., Ringstad, L., Bysell, H., and Saulnier, P. (2016) Lipid-based nanoformulations for peptide delivery. *Int. J. Pharm.* **502**, 80–97

76. Sang Yoo, H., and Gwan Park, T. (2004) Biodegradable nanoparticles containing protein-fatty acid complexes for oral delivery of salmon calcitonin. *J. Pharm. Sci.* **93**, 488–95

77. Zapadka, K. L., Becher, F. J., Gomes dos Santos, A. L., and Jackson, S. E. (2017) Factors affecting the physical stability (aggregation) of peptide therapeutics. *Interface Focus*. **7**, 20170030

78. Surmacz-Chwedoruk, W., Babenko, V., Dec, R., Szymczak, P., and Dzwolak, W. (2016) The emergence of superstructural order in insulin amyloid fibrils upon multiple rounds of self-seeding. *Sci. Rep.* **6**, 32022

79. Brooks, B. R., Brooks, C. L., Mackerell, A. D., Nilsson, L., Petrella, R. J., Roux, B., Won, Y., Archontis, G., Bartels, C., Boresch, S., Caflisch, A., Caves, L., Cui, Q., Dinner, A. R., Feig, M., Fischer, S., Gao, J., Hodoscek, M., Im, W., Kuczera, K., Lazaridis, T., Ma, J., Ovchinnikov, V., Paci, E., Pastor, R. W., Post, C. B., Pu, J. Z., Schaefer, M., Tidor, B., Venable, R. M., Woodcock, H. L., Wu, X., Yang, W., York, D. M., and Karplus, M. (2009) CHARMM: the biomolecular simulation program. *J. Comput. Chem.* **30**, 1545–614

80. Chen, J., Im, W., and Brooks, C. L. (2006) Balancing solvation and intramolecular interactions: toward a consistent generalized Born force field. *J. Am. Chem. Soc.* **128**, 3728–36

81. Arthur, E. J., and Brooks, C. L. (2016) Parallelization and improvements of the generalized born model with a simple sWitching function for modern graphics processors. *J. Comput. Chem.* **37**, 927–39

82. Im, W., Lee, M. S., and Brooks, C. L. (2003) Generalized born model with a simple smoothing function. *J. Comput. Chem.* **24**, 1691–702

83. Srinivasan, J., Miller, J., Kollman, P. A., and Case, D. A. (1998) Continuum solvent studies of the stability of RNA hairpin loops and helices. *J. Biomol. Struct. Dyn.* **16**, 671–82

84. Brünger, A., Brooks, C. L., and Karplus, M. (1984) Stochastic boundary conditions for molecular dynamics simulations of ST2 water. *Chem. Phys. Lett.* **105**, 495–500

85. Ryckaert, J.-P., Ciccotti, G., and Berendsen, H. J. . (1977) Numerical integration of the cartesian equations of motion of a system with constraints: molecular dynamics of n-alkanes. *J. Comput. Phys.* **23**, 327–341

86. Feig, M., Karanicolas, J., and Brooks, C. L. (2004) MMTSB Tool Set: enhanced sampling and multiscale modeling methods for applications in structural biology. *J. Mol. Graph. Model.* **22**, 377–95

Chapter 3

The role of phospholipid membranes in the amyloid aggregation of human calcitonin

3.1 Introduction

Since the discovery of its skeletoprotective effects, the 32-residue peptide hormone calcitonin (CT) has been used as a therapeutic for the bone-related diseases osteoporosis and Paget's disease.(1–4) However, the propensity for human CT (hCT) to form amyloid fibrils limits its use as a therapeutic through the sequestration and remodeling of the monomeric peptide required for receptor activation and subsequent maintenance of bone mass.(5, 6) As such, the slower aggregating salmon CT (sCT) has replaced hCT as the current preferred CT peptide for therapeutic applications.(2, 7) Despite improvements in bioavailability and activity, sCT-based therapies are still limited by fiber formation, along with additional side effects like anorexia, vomiting, and immune responses.(4, 8–10) Studies have shown hCT therapies to be devoid of the negative side effects associated with sCT therapies, and have found hCT to exhibit improved biological activity under conditions where aggregation was controlled.(5, 7, 11) To date however, this kind of control has only been possible *in vitro*. There is thus significant interest in elucidating the factors which determine hCT aggregation kinetics, not only for improving therapeutic efforts, but to provide a better understanding of the general processes involved with amyloid aggregation.

Recently, lipid-based nanoparticle delivery systems have been applied to fibrillating peptide therapeutics such as insulin and sCT.(12–19) A growing number of examples in the

literature have implicated lipid membrane interactions as key modulators of the aggregation of a range of fibrillating amyloids including amyloid-β (Aβ), islet amyloid polypeptide (IAPP), and α-synuclein.(20–26) Membranes have been shown to induce and stabilize multiple secondary structural motifs, slow and accelerate aggregation kinetics, provide scaffolds for amyloid association, and alter aggregation pathways.(21–24, 27–30) All these effects are modulated by membrane characteristics including composition, curvature, surface charge, phase, and microdomain architecture.(20–22, 31–37) Owing to this complexity, systematic studies to explore the effects of membranes on amyloid aggregation are needed.(21, 23, 33, 34) The CT field in particular has a need for such studies, as lipid-based delivery systems present a means to control aggregation pre-uptake and improve uptake without peptide modifications through intelligent choice of lipid membrane characteristics.(12, 14–17, 19, 38, 39) To date, few studies have looked at CT-membrane interactions, with even fewer reporting on the effects of membranes on aggregation kinetics.(40)

Here, for the first time, the dependence of hCT aggregation on model membranes has been systematically studied using several biophysical techniques. In the presence of large unilamellar vesicles (LUVs) composed of several common phospholipids, Thioflavin-T (ThT) kinetic assays of hCT show a direct relationship between peptide concentration and lag time, in keeping with previous results observed in solution.(41) The magnitude of this concentration dependence varies with membrane charge and fluidity and appears to be heightened with more rigid and anionic phospholipid compositions that enhance surface interactions. Circular dichroism (CD) experiments suggest that this behavior is due to the adsorption of hCT to the membrane surface. Additionally, we see an apparent remodeling of amyloid fibers by LUVs, similar to a previous study on amyloid-β.(30) This remodeling appears to be due to interactions between mature fibrils

and membranes and is dependent on the peptide to lipid ratio. Overall these results exhibit an inhibitory role for hCT-membrane interactions, and present useful information for understanding membrane mediated amyloid aggregation and the design of lipid-based CT delivery systems.

3.2 Results and Discussion

3.2.1. hCT displays a direct relationship between peptide concentration and lag phase through surface mediated peptide-membrane interactions

In order to monitor aggregation in a membrane environment, hCT was allowed to aggregate in the presence of 100 nm diameter LUVs. The ease with which LUV compositions can be altered while maintaining a bilayer of consistent size and curvature allows the systematic study of the effect of membrane composition on hCT aggregation.(21, 42) The aggregation of both 10 μM and 40 μM hCT was tracked in LUVs composed of DOPC, POPC, DOPC:DOPG (7:3 molar ratio) and POPC:POPG (7:3 molar ratio) using the ThT assay, a common method for detecting amyloid formation.(21, 30, 42–45) In all membrane compositions excluding DOPC, it was found that hCT showed a direct relationship between peptide concentration and lag time (Fig. 3.1). Such a result is consistent with previous studies on the aggregation of hCT in solution.(41) In that work it was found that the direct relationship was caused by plasticity in the hCT monomer leading to growth-competent and growth-incompetent species, with growth competence being determined by α-helical secondary structural motifs. For additional details, please refer to Chapter 2.

The induction of α-helical structural motifs is a consistent feature of amyloid-membrane interactions.(22, 23, 27, 28, 46, 47) The energetic favorability of amphipathic helix association with both hydrophobic acyl chains and hydrophilic head groups could also explain the kinetic trend seen in the present study. While the induction of helical motifs by LUVs could increase the number

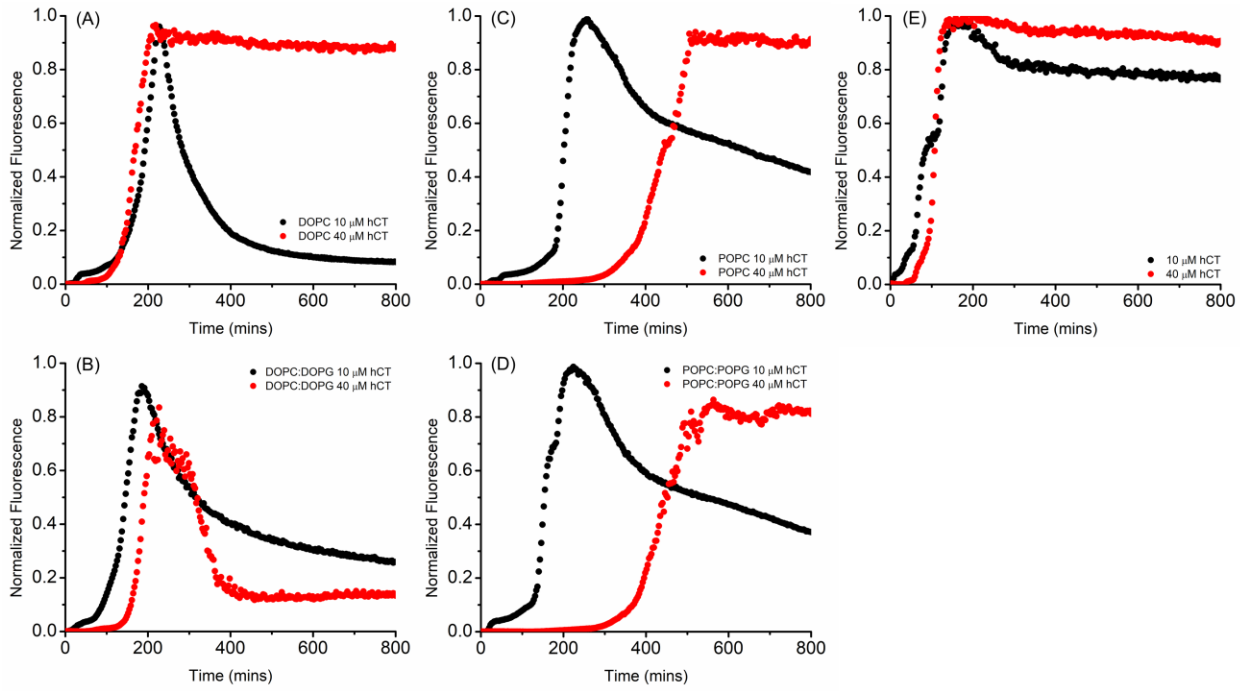

Figure 3.1. hCT exhibits a direct relationship between peptide concentration and lag phase in a membrane environment. hCT at 10 μM (black) and 40 μM (red) was allowed to aggregate in the presence of 100 μM of 100 nm LUVs composed of A) DOPC, B) DOPC:DOPG (7:3), C) POPC, and D) POPC:POPG (7:3), as well as in solution (E). All LUVs with the exception of pure DOPC showed higher concentrations of hCT to aggregate slower, consistent with hCT solution behavior. The difference between low and high peptide concentration lag times are dependent on membrane composition, with the addition of anionic lipids and increase in membrane transition temperature increasing the difference. Note the loss of signal intensity after elongation for 10 μM hCT. This phenomenon is discussed further in Section 3.2.2. Displayed curves represent normalized averages of three independent trials at 25 °C in 20 mM phosphate buffer and 100 mM NaCl, pH 7.4.

of growth-competent hCT monomers, interactions with the membrane could over-stabilize and isolate such monomers, thus decreasing their effective concentration, equivalent to a decrease in monomer conversion rate (k_{mc}) as shown previously.(41) Given the presumed role of peptide sequestration by LUVs, one would expect lag time to be dependent on LUV concentration. Indeed, the addition of higher LUV concentrations was found to increase hCT lag times in a dose dependent manner, supporting the idea that hCT sequestration is responsible for the LUV dependence of lag times (Fig. 3.2). We note that the interaction between hCT and membranes could be monomer or oligomer based, as both play a role in monomer conversion.(41) The maintenance of α-helical structures has been shown to delay hCT aggregation, thus stabilizing

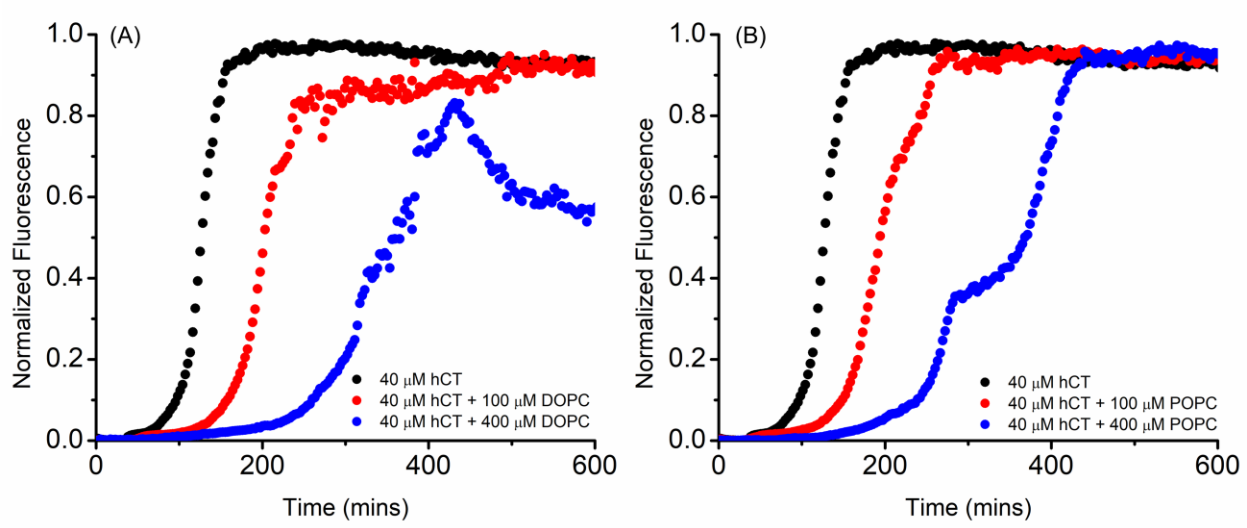

Figure 3.2. DOPC and POPC LUVs slow hCT aggregation in a dose dependent manner. hCT at 40 μM was allowed to aggregate in solution (black) and in the presence of 100 μM (red) and 400 μM (blue) of 100 nm LUVs composed of A) DOPC and B) POPC. For both membrane compositions, LUVs slowed fiber formation in a dose-dependent manner, indicating inhibition of fiber formation through peptide-membrane interactions. Displayed curves represent normalized averages of three independent trials at 25 °C in 20 mM phosphate buffer and 100 mM NaCl, pH 7.4

interactions between growth-competent monomers and the membrane are likely responsible for our observed trend.(7, 41, 48–51)

Both the addition of anionic lipids and a shift to more saturated acyl chains increase the dependence of lag time on concentration. These alterations would both be expected to promote surface interactions between lipid bilayers and amyloid peptides. Amyloids including hCT consistently show an affinity for anionic lipids regardless of peptide charge, and less fluid bilayers provide tighter packed lipids that would restrict peptide insertion.(20–22, 52, 53) Initial experiments show enhanced concentration dependent differences in lag time in more rigid DMPC LUVs (transition temperature of 24 °C as compared to -2 °C for POPC and -17 °C for DOPC), but further experiments are needed to confirm this behavior (Fig. B.1.).

The idea of increased lag times being caused by stronger interactions between amyloid peptides and the membrane surface specifically is consistent with several previous amyloid-membrane kinetics studies.(21, 34, 35, 40) A previous study on hCT-membrane interactions found

that the rigidification of membranes by cholesterol inhibited peptide insertion, and instead forced membrane-surface mediated aggregation and fibril mat formation.(40) ThT experiments with amyloid-β have shown smaller vesicles to accelerate aggregation, and more rigid membranes were found to slow the aggregation of hIAPP.(21, 34, 35) In both cases, the diminished exposure of hydrophobic patches and enhanced surface interactions were found to delay aggregation, consistent with surface interactions between helical hCT and LUVs being the driving force in the observed kinetic trend in this study.

In order to further explore this hypothesis, time-course CD experiments were performed for the four LUV compositions shown in Figure 3.1. Interestingly, the results were found to contrast with the ThT-detected kinetics, in that hCT lost its initial random coil signal more slowly in conditions shown to aggregate faster by ThT (Fig. 3.3). However, this loss of random coil signal was not correlated with a subsequent gain of β-sheet signal, indicating the decline to be independent of fibril formation. A probable explanation for this signal loss over time is the phenomenon of absorption flattening. This process occurs when particles dispersed with LUVs in solution localize to the membrane surface, leaving some regions enriched and others depleted in particles resulting in the breakdown of the Beer-Lambert Law and subsequent intensity loss (Fig. B.2).(54) We note that no signal loss is seen with the weakly interacting DOPC LUVs in the first three hours, despite DOPC being the fastest aggregating condition by ThT, further supporting the hypothesis that signal loss is caused by peptide-membrane interactions and subsequent absorption flattening rather than aggregation.(55, 56) The observation of this phenomenon in our CD experiments with the most rapid CD signal loss occurring in the slowest aggregating conditions supports the idea that differential rates of hCT association with LUVs are responsible for retarded aggregation.

CD spectra taken at intermediate time points in all four LUV conditions show the slower aggregating PO lipids to have a lower signal intensity as well as increased helical content (Fig. B.3). Such results are consistent with the idea that adsorption and stabilization of helical monomers of hCT causes an increase in lag time. CD experiments evaluating the differences between DMPC and DOPC LUVs appear consistent with this trend, but again further experiments are needed to confirm this behavior (Fig. B.4). Additionally, CD spectra taken after 24 hours of aggregation are predominantly β-sheet, implying the initial flattening to represent one of the first steps along the

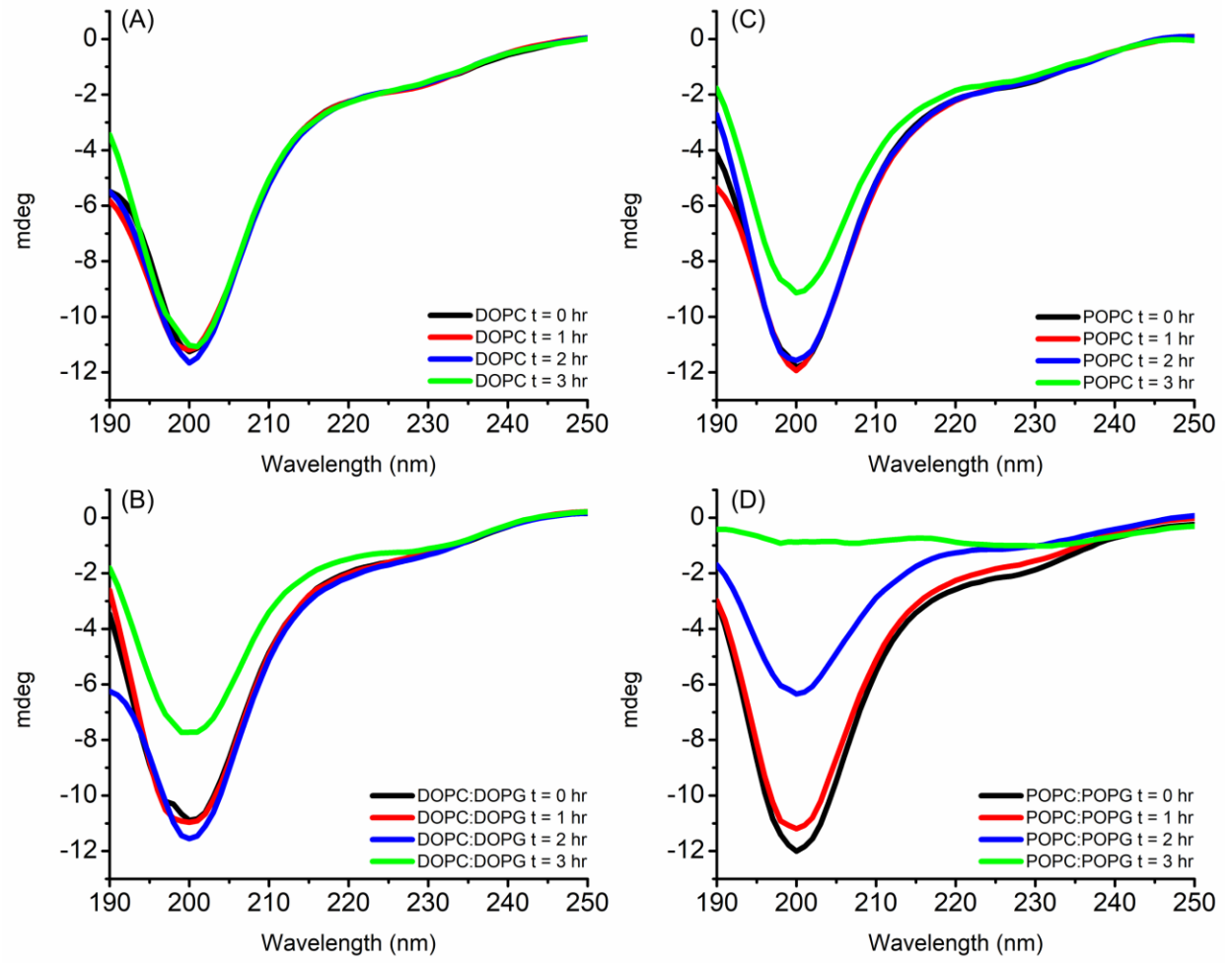

Figure 3.3. Differential absorption flattening in time-course CD experiments indicate different rates of peptide adsorption. CD spectra of hCT at 40 μM were collected at the indicated time points with 100 μM of 100 nm LUVS of A) DOPC, B) DOPC:DOPG (7:3), C) POPC, and D) POPC:POPG (7:3). The decreased intensity of the random coil peak at 200 nm over time is fastest for the slower aggregating samples. Signal loss occurs without the appearance of new peaks, suggesting spectral changes to be due to absorption flattening rather than peptide remodeling. Samples were prepared identically to those used for ThT experiments with the exception of NaF replacing NaCl. All measurements and incubations were performed at 25 °C.

fibrillation pathway rather than an uncorrelated amorphous aggregation (Fig. B.5). Taken together, the current ThT and CD results indicate that the adsorption of monomers of hCT onto the surface of LUVs delays aggregation and leads to composition dependent differences in the relationship between lag time and concentration. However, further experiments are needed to further elucidate the observed behavior and confirm the relevant species in determining LUV-mediated kinetics.

Interestingly, 10 μM hCT concentration kinetics seem relatively unaffected by lipid composition, with the major changes in lag time concentration dependence being due to 40 μM hCT conditions (Fig. B.6). In the previous study, lower concentrations of hCT exhibited smaller and shorter lived oligomeric species immediately after peptide dissolution, with such differences playing a role in lag time determination.(41) It is speculated that a possible explanation for the relative independence of 10 μM hCT lag time from lipids has to do with these differences in oligomeric reformatting. If interactions between hCT and the membrane are influenced by oligomers, as has been previously shown for hCT and other amyloids, the transience of low concentration oligomers could serve to limit these interactions and by extension the effect of lipid composition on lag time.(29, 37, 57–63) Furthermore, the sequestering behavior of hCT-LUVs interactions would be expected to have a diminished effect on 10 μM hCT as opposed to 40 μM, given that the lower concentration already experiences fewer peptide-peptide interactions. One or both of these mechanisms could be responsible, but further experiments are needed to better elucidate the cause of this phenomenon.

3.2.2. LUVs show an ability to remodel fibers of hCT in a peptide to lipid ratio dependent manner

Typically, mature amyloid fibers are highly stable, and require the introduction of significant molecular, chemical, or mechanical stresses to undergo remodeling.(64–69) This stability is reflected in the flat plateau phase of ThT fluorescence curves where the amount of β-sheet structure is constant. However, as can be seen in Figure 3.1., after reaching maximal fluorescence intensity, 10 μM samples of hCT then exhibit a decline in fluorescence intensity rather than the characteristic plateau. Previous studies on ThT-amyloid interactions have shown hydroxylation to cause a decline in fluorescent signal, especially under basic conditions.(70) However, the disparity between intensity loss in fibrils grown in the presence of LUVs and fibrils grown in solution, along with the LUV dependence of the signal decay, suggests the signal loss to be due to peptide-LUV interactions (Fig. B.6).

The presence of remodeling at 10 μM hCT and not 40 μM hCT raises the question of whether the cause was concentration dependent differences in aggregate morphology or inconsistent peptide to lipid ratio. By increasing LUV concentration from 100 to 400 μM, and thus maintaining the same peptide to lipid ratio, we were able to see signal loss in 40 μM hCT conditions, indicating this trend to be dependent on the peptide to lipid ratio rather than overall peptide concentration (Fig. 3.4). Additionally, as with 10 μM hCT in the presence of 100 μM LUVs, the decline of 40 μM hCT conditions is more rapid and pronounced in the presence of DOPC lipids as opposed to POPC lipids. Initial experiments also suggest that higher temperatures (35 °C) induce remodeling, but further experiments are needed to confirm this behavior (Fig. B.7).

Amyloid fiber growth can proceed along different pathways in lipid bilayers as compared to in solution, with such differences potentially leading to distinct polymorphs.(23, 24, 26, 35, 64, 71) The more rapid decline with DOPC as compared to POPC also suggests that polymorphs

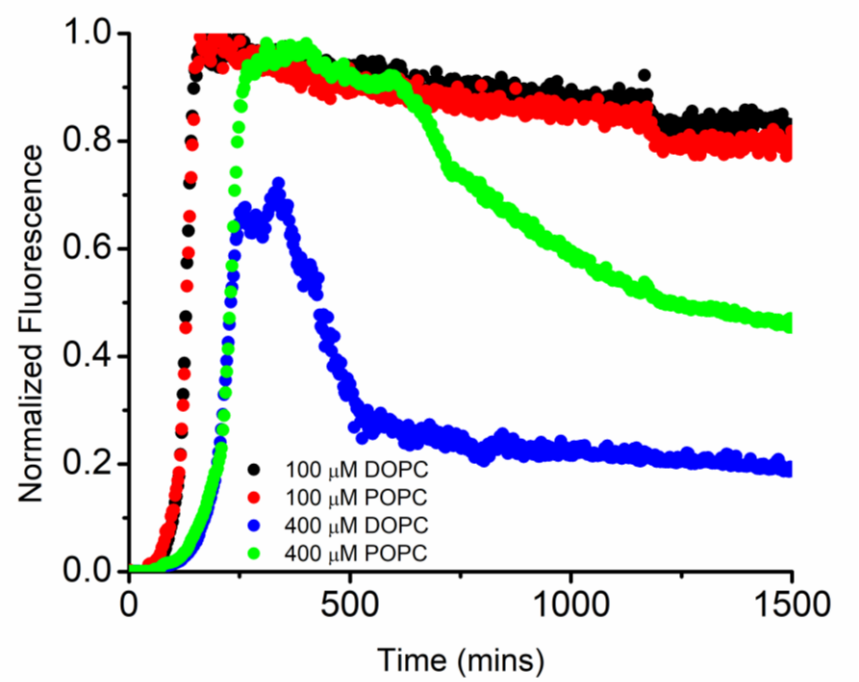

Figure 3.4. Remodeling of hCT fibers depends on peptide to lipid ratio. hCT at 40 μM was allowed to aggregate in the presence of 100 μM and 400 μM of 100 nm LUVs composed of DOPC and POPC. Fibers formed in the presence of 100 μM LUVs maintain a stable ThT signal, whereas fibers in the presence of 400 μM LUVs showed signal loss. DOPC LUVs also induced more rapid and significant loss of ThT signal as compared to POPC LUVs. Displayed curves are normalized averages of three independent trials at 25 °C in 20 mM phosphate buffer and 100 mM NaCl, pH 7.4.

grown in different LUV solutions could explain the differences in fibril stability. In order to determine whether or not hCT fiber morphologies grown in the presence of our model membranes were less stable, we tested the ability of LUVs to remodel mature fibrils grown in solution. Upon the introduction of LUVs to solution grown fibrils, the previously stable ThT signal was found to decrease in a manner similar to fibrils grown with LUVs (Fig. 3.5). The addition of DOPC LUVs resulted in a rapid decrease, while the introduction of POPC resulted in a slower and smaller decrease, consistent with the remodeling seen in LUV-grown fibers (Fig. 3.4, Fig. B.6). Noteworthy is the fact that the introduction of DOPC LUVs remodeled both the 10 μM and 40 μM fibers samples, whereas POPC LUVs could only remodel the 10 μM sample. Combined with the results shown in Figures 3.4 and B.6, this suggests DOPC-mediated remodeling of hCT fibrils to be more efficient. More significantly, the fiber remodeling is not dependent on the fiber growth

conditions, suggesting instead that the relevant interactions are between mature fibers and lipid bilayers.

The remodeling of mature amyloid fibers by lipid bilayers has been previously observed in amyloid-β, albeit with much more lipid specificity.(30) LUVs of the phospholipid DLPC were found to convert long fibrils of amyloid-β into shorter, ThT-negative amorphous aggregates. This unique behavior of DLPC was presumed to arise from its smaller hydrophobic thickness as compared to other phospholipids studied. Such an explanation seems unlikely for the present study, as the bilayer thicknesses of DOPC (26.8 Å) and POPC (27.1 Å) are similar.(72) This disparity, along with the different peptide and lipids used, means the remodeling observed in this study is likely a different mechanism. Additionally, the remodeling observed in this study could represent either changes in overall fibril architecture or changes in ThT-fiber interactions. ThT-negative amyloid fibers and ThT signal loss caused by small molecules leaving fibrils intact have both been previously reported, and we caution against the overinterpretation of ThT kinetics assays.(73, 74)

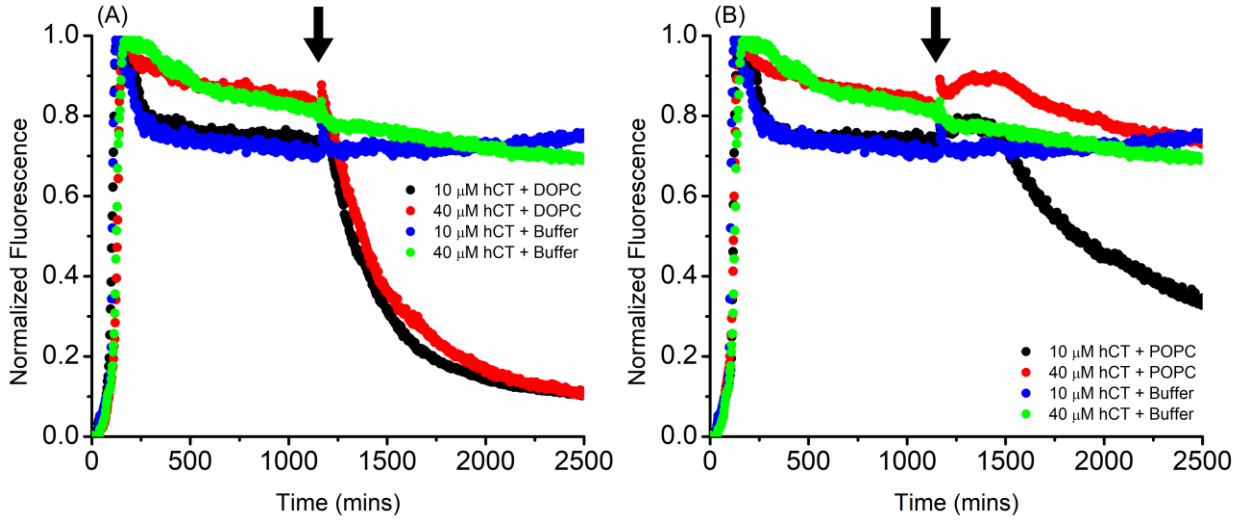

Figure 3.5. LUVs are capable of remodeling solution-grown hCT fibrils. hCT fibrils at 10 μM and 40 μM were grown in solution until fibril population was stable by ThT, at which point LUVs were introduced (black arrow). The introduction of DOPC LUVs (A) led to immediate decrease in ThT signal for 10 μM and 40 μM hCT. In contrast, POPC LUVs (B) caused smaller and slower signal loss at 10 μM and no signal loss at 40 μM. The heightened potency of DOPC LUVs to remodel fibers as compared to POPC LUVs is consistent with results for fibrils grown with LUVs (Fig. 3.4). Displayed curves represent normalized averages of three independent trials at 25 °C in 20 mM phosphate buffer and 100 mM NaCl, pH 7.4.

Future experiments to determine the nature of fibril remodeling observed in this study are needed to fully characterize the effect. The fluorescent dye bis-ANS has been previously used to detect amyloid fibers, and would help clarify if the observed signal loss was a ThT specific phenomenon.(75) TEM images of fibers before and after the addition of LUVs may provide an answer as to the degree of fiber remodeling, as any macroscopic changes in fibril morphology could be visible, and the Bradford assay could help determine the degree of protein resolubilization by LUVs, giving additional information towards the development of a more quantitative picture of fibril remodeling.(76, 77)

3.3. Conclusions

In this study, the aggregation of hCT in the presence of lipid bilayers was systematically studied for the first time. hCT was found to show a direct relationship between peptide concentration and lag time in a membrane environment, similarly to previously reported results in solution. The extent of this concentration dependence was found to depend on membrane composition, with LUVs encouraging surface interactions leading to larger concentration dependences. Comparative CD experiments showed enhanced adsorption rates of hCT to correlate with retarded aggregation, implicating the over stabilization of helical structures and peptide sequestration as causative in the trend. The degree of inhibition was found to not simply depend on membrane composition, but also on peptide and lipid concentration. Finally, LUVs showed an ability to remodel mature fibrils of hCT, whether grown in solution or a membrane environment. This remodeling was found to depend both on membrane composition and on peptide to lipid ratio. These results suggest that lipid nanoparticles for therapeutic delivery should use compositions that encourage surface interactions, specifically through the use of anionic and higher transition temperature lipids. Such choices of lipids represent a simple and non-perturbative way to delay

aggregation and maintain soluble peptide hormone without peptide modifications. This study will serve to improve our understanding of how amyloid-membrane interactions can mediate aggregation, and future directions could further inform lipid-based peptide therapeutic delivery systems.

3.4. Materials and Methods

3.4.1. Peptide preparation

Human calcitonin peptide was synthesized via Fmoc chemistry as described previously.(78) The disulfide bond between Cys1 and Cys7 of hCT was formed by air oxidation at pH 8.0-8.5 at diluted concentration and in the presence of 6 M urea to prevent fibrillation. To ensure consistent monomeric starting conditions, peptide was dissolved in hexafluoroisopropanol (HFIP) at a concentration of 1 mg/ml. Peptide was then separated into 100 μL aliquots, flash frozen in liquid nitrogen, and lyophilized for a period of 48 hours. After lyophilization, peptide aliquots were stored at -80 ºC until use. Peptide solutions were prepared by resolubilizing the lyophilized aliquots in 100 μL of HCl pH 4 at 4 °C to a concentration of ~300 μM, followed by brief sonication to ensure peptide dissolution. Peptide solutions were then warmed to room temperature and subsequently used.

3.4.2 Vesicle preparation

1,2-dioleoyl-*sn*-glycero-3-phosphocholine (DOPC), 1-palmitoyl-2-oleoyl-*sn*-glycero-3-phosphocholine (POPC), 1,2-dimyristoyl-*sn*-glycero-3-phosphocholine (DMPC), 1,2-dioleoyl-*sn*-glycero-3-phospho-(1'-rac-glycerol) (DOPG), and 1-palmitoyl-2-oleoyl-*sn*-glycero-3-phospho-(1'-rac-glycerol) (POPG) lipids were purchased from Avanti Polar Lipids *Inc.* (Alabaster, AL, USA). Large unilamellar vesicles (LUVs) were prepared of pure DOPC, POPC, and DMPC, as

well as mixtures of DOPC:DOPG and POPC:POPG in 7:3 molar ratios. Appropriate lipid compositions were prepared in chloroform and dried under nitrogen, and the resultant films were lyophilized overnight to remove residual solvent. Lipid films were rehydrated with buffer (20mM phosphate, 100mM NaCl, pH 7.4) to a final concentration of 1 mM. The resultant suspension was mixed to ensure complete film resolubilization, and subsequently extruded 21 times through 100 nm polycarbonate Nucleopore membrane filters (Whatman) mounted on a mini-extruder (Avanti Polar Lipids *Inc.*). The formation of a homogeneous population of 100 nm vesicles was confirmed via dynamic light scattering.

3.4.3. Thioflavin-T Kinetic Assay

Thioflavin-T (ThT) experiments were run on a Biotek Synergy 2 microplate reader (BioTek Instruments, Inc., Winooski, VT, USA) on uncoated Fisherbrand 96-well polystyrene plates. Peptide was added to final concentrations of 20 mM phosphate buffer, 100 mM NaCl, pH 7.4 and ThT, and immediately prior to acquisition. Experiments were performed in triplicate with two equivalents of ThT and 70 μL total volume. Wells were bottom read with an excitation wavelength of 440 nm (30 nm bandwidth) and emission wavelength of 485 nm (20 nm bandwidth). Fibril remodeling ThT assays were performed by adding 3.68 μL of 2 mM LUV stocks to the 70 μL total sample volume, to yield final LUV concentrations of 100 μM. An equivalent volume of buffer was added to control wells.

3.4.4. Circular Dichroism

Circular dichroism (CD) spectra were taken on a Jasco J-1500 Circular Dichroism Spectrometer (JASCO, Inc., Easton, MD, USA). Spectra were recorded with 40 μM hCT in 20 mM phosphate buffer, 100 mM NaF, pH 7.4 in a 1 mm quartz cuvette. Spectra were recorded with

2 nm bandwidth, 1 nm step size, scan speed of 100 nm/min, baseline corrected, and averaged over 5 scans. Smoothing was performed using the Savitzky-Golay method, with a convolution width of 15. Between reads, peptide samples were transferred to a microcentrifuge tube and shaken at ~500 rpm at the same temperature as spectra collection unless otherwise indicated.

3.5. Acknowledgements

This study was partly supported by funds from NIH.

3.6. Author Contributions

KKP and AR conceived the idea and planned the study. KKP performed ThT and CD experiments. KKP and AR analyzed the experimental data, interpreted the results, and wrote the paper. AR directed the project. All authors reviewed the results and approved the final manuscript.

3.7. References

1. Zaidi, M., Inzerillo, A. ., Moonga, B. ., Bevis, P. J. ., and Huang, C. L.-H. (2002) Forty years of calcitonin—where are we now? A tribute to the work of Iain Macintyre, FRS. *Bone*. **30**, 655–663

2. Chesnut, C. H., Azria, M., Silverman, S., Engelhardt, M., Olson, M., and Mindeholm, L. (2008) Salmon calcitonin: a review of current and future therapeutic indications. *Osteoporos. Int.* **19**, 479–91

3. Schneider, D., Hofmann, M. T., and Peterson, J. A. (2002) Diagnosis and treatment of Paget's disease of bone. *Am. Fam. Physician*. **65**, 2069–72

4. Singer, F. R., Fredericks, R. S., and Minkin, C. (1980) Salmon calcitonin therapy for paget's disease of bone the problem of acquired clinical resistance. *Arthritis Rheum.* **23**, 1148–1154

5. Cudd, A., Arvinte, T., Gaines Das, R. E., Chinni, C., and MacIntyre, I. (1995) Enhanced Potency of Human Calcitonin When Fibrillation is Avoided. *J. Pharm. Sci.* **84**, 717–719

6. Kamgar-Parsi, K., Tolchard, J., Habenstein, B., Loquet, A., Naito, A., and Ramamoorthy, A. (2016) Structural Biology of Calcitonin: From Aqueous Therapeutic Properties to Amyloid Aggregation. *Isr. J. Chem.* **57**, 634–650

7. Fowler, S. B., Poon, S., Muff, R., Chiti, F., Dobson, C. M., and Zurdo, J. (2005) Rational

design of aggregation-resistant bioactive peptides: reengineering human calcitonin. *Proc. Natl. Acad. Sci. U. S. A.* **102**, 10105–10

8. Feletti, C., and Bonomini, V. (1979) Effect of calcitonin on bone lesions in chronic dialysis patients. *Nephron*. **24**, 85–8

9. Singer, F. R., Aldred, J. P., Neer, R. M., Krane, S. M., Potts, J. T., and Bloch, K. J. (1972) An evaluation of antibodies and clinical resistance to salmon calcitonin. *J. Clin. Invest.* **51**, 2331–8

10. Cao, S., Liu, Y., Shang, H., Li, S., Jiang, J., Zhu, X., Zhang, P., Wang, X., and Li, J. (2017) Supramolecular nanoparticles of calcitonin and dipeptide for long-term controlled release. *J. Control. Release*. **256**, 182–192

11. Grauer, A., Reinel, H. H., Ziegler, R., and Raue, F. (1993) Neutralizing antibodies against calcitonin. *Horm. Metab. Res.* **25**, 486–8

12. Lin, C.-H., Chen, C.-H., Lin, Z.-C., and Fang, J.-Y. (2017) Recent advances in oral delivery of drugs and bioactive natural products using solid lipid nanoparticles as the carriers. *J. Food Drug Anal.* **25**, 219–234

13. Chono, S., Togami, K., and Itagaki, S. (2017) Aerosolized liposomes with dipalmitoyl phosphatidylcholine enhance pulmonary absorption of encapsulated insulin compared with co-administered insulin. *Drug Dev. Ind. Pharm.* **43**, 1892–1898

14. Umerska, A., Matougui, N., Groo, A.-C., and Saulnier, P. (2016) Understanding the adsorption of salmon calcitonin, antimicrobial peptide AP114 and polymyxin B onto lipid nanocapsules. *Int. J. Pharm.* **506**, 191–200

15. Matougui, N., Boge, L., Groo, A.-C., Umerska, A., Ringstad, L., Bysell, H., and Saulnier, P. (2016) Lipid-based nanoformulations for peptide delivery. *Int. J. Pharm.* **502**, 80–97

16. Werle, M., and Takeuchi, H. (2009) Chitosan-aprotinin coated liposomes for oral peptide delivery: Development, characterisation and in vivo evaluation. *Int. J. Pharm.* **370**, 26–32

17. Sang Yoo, H., and Gwan Park, T. (2004) Biodegradable nanoparticles containing protein-fatty acid complexes for oral delivery of salmon calcitonin. *J. Pharm. Sci.* **93**, 488–95

18. Sharma, G., Sharma, A. R., Nam, J.-S., Doss, G. P. C., Lee, S.-S., and Chakraborty, C. (2015) Nanoparticle based insulin delivery system: the next generation efficient therapy for Type 1 diabetes. *J. Nanobiotechnology*. **13**, 74

19. Baginski, L., Gobbo, O. L., Tewes, F., Salomon, J. J., Healy, A. M., Bakowsky, U., and Ehrhardt, C. (2012) In vitro and in vivo characterisation of PEG-lipid-based micellar complexes of salmon calcitonin for pulmonary delivery. *Pharm. Res.* **29**, 1425–34

20. Chauhan, A., Ray, I., and Chauhan, V. P. S. (2000) Interaction of Amyloid Beta-Protein with Anionic Phospholipids: Possible Involvement of Lys28 and C-Terminus Aliphatic

Amino Acids. *Neurochem. Res.* **25**, 423–429

21. Zhang, X., St. Clair, J. R., London, E., and Raleigh, D. P. (2017) Islet Amyloid Polypeptide Membrane Interactions: Effects of Membrane Composition. *Biochemistry*. **56**, 376–390

22. Eichmann, C., Campioni, S., Kowal, J., Maslennikov, I., Gerez, J., Liu, X., Verasdonck, J., Nespovitaya, N., Choe, S., Meier, B., Picotti, P., Rizo, J., Stahlberg, H., and Riek, R. (2016) Preparation and Characterization of Stable α-Synuclein Lipoprotein Particles. *J. Biol. Chem.* **291**, 8516–27

23. Korshavn, K. J., Bhunia, A., Lim, M. H., and Ramamoorthy, A. (2016) Amyloid-β adopts a conserved, partially folded structure upon binding to zwitterionic lipid bilayers prior to amyloid formation. *Chem. Commun.* **52**, 882–885

24. Ikeda, K., Yamaguchi, T., Fukunaga, S., Hoshino, M., and Matsuzaki, K. (2011) Mechanism of Amyloid β-Protein Aggregation Mediated by GM1 Ganglioside Clusters. *Biochemistry*. **50**, 6433–6440

25. Galvagnion, C., Buell, A. K., Meisl, G., Michaels, T. C. T., Vendruscolo, M., Knowles, T. P. J., and Dobson, C. M. (2015) Lipid vesicles trigger α-synuclein aggregation by stimulating primary nucleation. *Nat. Chem. Biol.* **11**, 229–234

26. Brender, J. R., Salamekh, S., and Ramamoorthy, A. (2012) Membrane disruption and early events in the aggregation of the diabetes related peptide IAPP from a molecular perspective. *Acc. Chem. Res.* **45**, 454–62

27. Epand, R. M., Epand, R. F., Orlowski, R. C., Schlueter, R. J., Boni, L. T., and Hui, S. W. (1983) Amphipathic helix and its relationship to the interaction of calcitonin with phospholipids. *Biochemistry*. **22**, 5074–5084

28. Prakash, R., Nanga, R., Brender, J. R., Xu, J., Hartman, K., Subramanian, V., and Ramamoorthy, A. (2009) Three-Dimensional Structure and Orientation of Rat Islet Amyloid Polypeptide Protein in a Membrane Environment by Solution NMR Spectroscopy. *J. Am. Chem. Soc.* **131**, 8252–8261

29. Serra-Batiste, M., Ninot-Pedrosa, M., Bayoumi, M., Gairí, M., Maglia, G., and Carulla, N. (2016) Aβ42 assembles into specific β-barrel pore-forming oligomers in membrane-mimicking environments. *Proc. Natl. Acad. Sci. U. S. A.* **113**, 10866–71

30. Korshavn, K. J., Satriano, C., Lin, Y., Zhang, R., Dulchavsky, M., Bhunia, A., Ivanova, M. I., Lee, Y.-H., Rosa, C. La, Lim, M. H., and Ramamoorthy, A. (2017) Thin Membranes Modulate Aβ Aggregation Reduced Lipid Bilayer Thickness Regulates the Aggregation and Cytotoxicity of Amyloid-β. *J. Biol. Chem.* **292**, 4638–4650

31. Amaro, M., Šachl, R., Aydogan, G., Mikhalyov, I. I., Vácha, R., and Hof, M. (2016) GM $_1$ Ganglioside Inhibits β-Amyloid Oligomerization Induced by Sphingomyelin. *Angew. Chemie Int. Ed.* **55**, 9411–9415

32. Matsuzaki, K. (2014) How Do Membranes Initiate Alzheimer's Disease? Formation of Toxic Amyloid Fibrils by the Amyloid β-Protein on Ganglioside Clusters. *Acc. Chem. Res.* **47**, 2397–2404

33. Thomaier, M., Gremer, L., Dammers, C., Fabig, J., Neudecker, P., and Willbold, D. (2016) High-Affinity Binding of Monomeric but Not Oligomeric Amyloid-β to Ganglioside GM1 Containing Nanodiscs. *Biochemistry*. **55**, 6662–6672

34. Terakawa, M. S., Yagi, H., Adachi, M., Lee, Y.-H., and Goto, Y. (2015) Small liposomes accelerate the fibrillation of amyloid β (1-40). *J. Biol. Chem.* **290**, 815–26

35. Kinoshita, M., Kakimoto, E., Terakawa, M. S., Lin, Y., Ikenoue, T., So, M., Sugiki, T., Ramamoorthy, A., Goto, Y., and Lee, Y.-H. (2017) Model membrane size-dependent amyloidogenesis of Alzheimer's amyloid-β peptides. *Phys. Chem. Chem. Phys.* **19**, 16257–16266

36. Malchiodi-Albedi, F., Paradisi, S., Matteucci, A., Frank, C., and Diociaiuti, M. (2011) Amyloid oligomer neurotoxicity, calcium dysregulation, and lipid rafts. *Int. J. Alzheimers. Dis.* **2011**, 906964

37. Malchiodi-Albedi, F., Contrusciere, V., Raggi, C., Fecchi, K., Rainaldi, G., Paradisi, S., Matteucci, A., Santini, M. T., Sargiacomo, M., Frank, C., Gaudiano, M. C., and Diociaiuti, M. (2010) Lipid raft disruption protects mature neurons against amyloid oligomer toxicity. *Biochim. Biophys. Acta*. **1802**, 406–15

38. Herbig, M. E., Weller, K., Krauss, U., Beck-Sickinger, A. G., Merkle, H. P., and Zerbe, O. (2005) Membrane surface-associated helices promote lipid interactions and cellular uptake of human calcitonin-derived cell penetrating peptides. *Biophys. J.* **89**, 4056–66

39. Schmidt, M. C., Rothen-Rutishauser, B., Rist, B., Beck-Sickinger, A., Wunderli-Allenspach, H., Rubas, W., Sadée, W., and Merkle, H. P. (1998) Translocation of Human Calcitonin in Respiratory Nasal Epithelium Is Associated with Self-Assembly in Lipid Membrane. *Biochemistry*. **37**, 16582–90

40. Sheynis, T., and Jelinek, R. (2010) Lipid-Induced Calcitonin Fibrillation Blocks Membrane Interactions of a Peptide Antibiotic. *J. Phys. Chem. B*. **114**, 15530–15535

41. Kamgar-Parsi, K., Hong, L., Naito, A., Brooks, C. L., and Ramamoorthy, A. (2017) Growth-incompetent monomers of human calcitonin lead to a noncanonical direct relationship between peptide concentration and aggregation lag time. *J. Biol. Chem.* **292**, 14963–14976

42. Caillon, L., Lequin, O., and Khemtémourian, L. (2013) Evaluation of membrane models and their composition for islet amyloid polypeptide-membrane aggregation. *Biochim. Biophys. Acta - Biomembr.* **1828**, 2091–2098

43. Sciacca, M. F. M., Milardi, D., Messina, G. M. L., Marletta, G., Brender, J. R., Ramamoorthy, A., and La Rosa, C. (2013) Cations as switches of amyloid-mediated

membrane disruption mechanisms: calcium and IAPP. *Biophys. J.* **104**, 173–84

44. Sciacca, M. F. M., Kotler, S. A., Brender, J. R., Chen, J., Lee, D., and Ramamoorthy, A. (2012) Two-step mechanism of membrane disruption by Aβ through membrane fragmentation and pore formation. *Biophys. J.* **103**, 702–10

45. Kotler, S. A., Walsh, P., Brender, J. R., and Ramamoorthy, A. (2014) Differences between amyloid-β aggregation in solution and on the membrane: insights into elucidation of the mechanistic details of Alzheimer's disease. *Chem. Soc. Rev.* **43**, 6692–700

46. Motta, A., Andreotti, G., Amodeo, P., Strazzullo, G., and Castiglione Morelli, M. A. (1998) Solution structure of human calcitonin in membrane-mimetic environment: the role of the amphipathic helix. *Proteins.* **32**, 314–23

47. Soria, M. A., Cervantes, S. A., Bajakian, T. H., and Siemer, A. B. (2017) The Functional Amyloid Orb2A Binds to Lipid Membranes. *Biophys. J.* **113**, 37–47

48. Andreotti, G., Vitale, R. M., Avidan-Shpalter, C., Amodeo, P., Gazit, E., and Motta, A. (2011) Converting the highly amyloidogenic human calcitonin into a powerful fibril inhibitor by three-dimensional structure homology with a non-amyloidogenic analogue. *J. Biol. Chem.* **286**, 2707–18

49. Andreotti, G., and Motta, A. (2003) Modulating calcitonin fibrillogenesis: an antiparallel alpha-helical dimer inhibits fibrillation of salmon calcitonin. *J. Biol. Chem.* **279**, 6364–6370

50. Itoh-Watanabe, H., Kamihira-Ishijima, M., Javkhlantugs, N., Inoue, R., Itoh, Y., Endo, H., Tuzi, S., Saitô, H., Ueda, K., and Naito, A. (2013) Role of aromatic residues in amyloid fibril formation of human calcitonin by solid-state 13C NMR and molecular dynamics simulation. *Phys. Chem. Chem. Phys.* **15**, 8890–901

51. Micelli, S., Meleleo, D., Picciarelli, V., Stoico, M. G., and Gallucci, E. (2004) Effect of nanomolar concentrations of sodium dodecyl sulfate, a catalytic inductor of alpha-helices, on human calcitonin incorporation and channel formation in planar lipid membranes. *Biophys. J.* **87**, 1065–75

52. Wong, P. T., Schauerte, J. A., Wisser, K. C., Ding, H., Lee, E. L., Steel, D. G., and Gafni, A. (2009) Amyloid-β Membrane Binding and Permeabilization are Distinct Processes Influenced Separately by Membrane Charge and Fluidity. *J. Mol. Biol.* **386**, 81–96

53. Sciacca, M. F. M., Lolicato, F., Di Mauro, G., Milardi, D., D'Urso, L., Satriano, C., Ramamoorthy, A., and La Rosa, C. (2016) The Role of Cholesterol in Driving IAPP-Membrane Interactions. *Biophys. J.* **111**, 140–151

54. Miles, A. J., and Wallace, B. A. (2016) Circular dichroism spectroscopy of membrane proteins. *Chem. Soc. Rev.* **45**, 4859–4872

55. Wagner, K., Van Mau, N., Boichot, S., Kajava, A. V., Krauss, U., Le Grimellec, C., Beck-

Sickinger, A., and Heitz, F. (2004) Interactions of the Human Calcitonin Fragment 9–32 with Phospholipids: A Monolayer Study. *Biophys. J.* **87**, 386–395

56. Stipani, V., Gallucci, E., Micelli, S., Picciarelli, V., and Benz, R. (2001) Channel formation by salmon and human calcitonin in black lipid membranes. *Biophys. J.* **81**, 3332–8

57. Zhang, M., Ren, B., Liu, Y., Liang, G., Sun, Y., Xu, L., and Zheng, J. (2017) Membrane Interactions of hIAPP Monomer and Oligomer with Lipid Membranes by Molecular Dynamics Simulations. *ACS Chem. Neurosci.* **8**, 1789–1800

58. Johnson, R. D., Schauerte, J. A., Chang, C.-C., Wisser, K. C., Althaus, J. C., Carruthers, C. J. L., Sutton, M. A., Steel, D. G., and Gafni, A. (2013) Single-molecule imaging reveals aβ42:aβ40 ratio-dependent oligomer growth on neuronal processes. *Biophys. J.* **104**, 894–903

59. Das, A. K., Rawat, A., Bhowmik, D., Pandit, R., Huster, D., and Maiti, S. (2015) An Early Folding Contact between Phe19 and Leu34 is Critical for Amyloid-β Oligomer Toxicity. *ACS Chem. Neurosci.* **6**, 1290–1295

60. Bode, D. C., Baker, M. D., and Viles, J. H. (2016) Ion Channel Formation by Amyloid-β42 Oligomers but not Amyloid-β40 in Cellular Membranes. *J. Biol. Chem.* **292**, 1404–1413

61. Diociaiuti, M., Macchia, G., Paradisi, S., Frank, C., Camerini, S., Chistolini, P., Gaudiano, M. C., Petrucci, T. C., and Malchiodi-Albedi, F. (2014) Native metastable prefibrillar oligomers are the most neurotoxic species among amyloid aggregates. *Biochim. Biophys. Acta*. **1842**, 1622–9

62. Kayed, R., Sokolov, Y., Edmonds, B., McIntire, T. M., Milton, S. C., Hall, J. E., and Glabe, C. G. (2004) Permeabilization of Lipid Bilayers Is a Common Conformation-dependent Activity of Soluble Amyloid Oligomers in Protein Misfolding Diseases. *J. Biol. Chem.* **279**, 46363–46366

63. Evangelisti, E., Cascella, R., Becatti, M., Marrazza, G., Dobson, C. M., Chiti, F., Stefani, M., and Cecchi, C. (2016) Binding affinity of amyloid oligomers to cellular membranes is a generic indicator of cellular dysfunction in protein misfolding diseases. *Sci. Rep.* **6**, 32721

64. Eisenberg, D. S., and Sawaya, M. R. (2017) Structural Studies of Amyloid Proteins at the Molecular Level. *Annu. Rev. Biochem.* **86**, 69–95

65. Pithadia, A. S., Bhunia, A., Sribalan, R., Padmini, V., Fierke, C. A., and Ramamoorthy, A. (2016) Influence of a curcumin derivative on hIAPP aggregation in the absence and presence of lipid membranes. *Chem. Commun. (Camb).* **52**, 942–5

66. Zhao, J., Liang, Q., Sun, Q., Chen, C., Xu, L., Ding, Y., Zhou, P., Oh, W. M., Kim, S. H., and Kim, W. T. (2017) (−)-Epigallocatechin-3-gallate (EGCG) inhibits fibrillation,

disaggregates amyloid fibrils of α-synuclein, and protects PC12 cells against α-synuclein-induced toxicity. *RSC Adv.* **7**, 32508–32517

67. Song, Y., Moore, E. G., Guo, Y., and Moore, J. S. (2017) Polymer–Peptide Conjugates Disassemble Amyloid β Fibrils in a Molecular-Weight Dependent Manner. *J. Am. Chem. Soc.* **139**, 4298–4301

68. Yagi, H., Mizuno, A., So, M., Hirano, M., Adachi, M., Akazawa-Ogawa, Y., Hagihara, Y., Ikenoue, T., Lee, Y.-H., Kawata, Y., and Goto, Y. (2015) Ultrasonication-dependent formation and degradation of α-synuclein amyloid fibrils. *Biochim. Biophys. Acta*. **1854**, 209–17

69. Baumketner, A. (2014) Electric Field as a Disaggregating Agent for Amyloid Fibrils. *J. Phys. Chem. B*. **118**, 14578–14589

70. Foderà, V., Groenning, M., Vetri, V., Librizzi, F., Spagnolo, S., Cornett, C., Olsen, L., van de Weert, M., and Leone, M. (2008) Thioflavin T Hydroxylation at Basic pH and Its Effect on Amyloid Fibril Detection. *J. Phys. Chem. B.* **112**, 15174–15181

71. Chiti, F., and Dobson, C. M. (2017) Protein Misfolding, Amyloid Formation, and Human Disease: A Summary of Progress Over the Last Decade. *Annu. Rev. Biochem.* **86**, 27–68

72. Kučerka, N., Tristram-Nagle, S., and Nagle, J. F. (2006) Structure of Fully Hydrated Fluid Phase Lipid Bilayers with Monounsaturated Chains. *J. Membr. Biol.* **208**, 193–202

73. Wong, A. G., Wu, C., Hannaberry, E., Watson, M. D., Shea, J.-E., and Raleigh, D. P. (2015) Analysis of the Amyloidogenic Potential of Pufferfish (Takifugu rubripes) Islet Amyloid Polypeptide Highlights the Limitations of Thioflavin-T Assays and the Difficulties in Defining Amyloidogenicity. *Biochemistry*. **55**, 510–518

74. Kroes-Nijboer, A., Lubbersen, Y. S., Venema, P., and van der Linden, E. (2009) Thioflavin T fluorescence assay for β-lactoglobulin fibrils hindered by DAPH. *J. Struct. Biol.* **165**, 140–145

75. Younan, N. D., and Viles, J. H. (2015) A comparison of three fluorophores (ThT, ANS, bis-ANS) for the detection of amyloid fibers and prefibrillar oligomeric assemblies. *Biochemistry*. **54**, 4297–4306

76. Harlow, E., and Lane, D. (2006) Bradford Assay. *Cold Spring Harb. Protoc.* **2006**, pdb.prot4644-prot4644

77. Ku, H.-K., Lim, H.-M., Oh, K.-H., Yang, H.-J., Jeong, J.-S., and Kim, S.-K. (2013) Interpretation of protein quantitation using the Bradford assay: Comparison with two calculation models. *Anal. Biochem.* **434**, 178–180

78. Huang, R., Vivekanandan, S., Brender, J. R., Abe, Y., Naito, A., and Ramamoorthy, A. (2012) NMR characterization of monomeric and oligomeric conformations of human calcitonin and its interaction with EGCG. *J. Mol. Biol.* **416**, 108–20

Chapter 4
Conclusions and Perspectives

4.1. General Conclusions

Amyloid aggregation remains a poorly understood biological process, despite its ubiquity and the breadth of scientific efforts to understand it. The complexity of the process, particularly in the early stages with several metastable and heterogeneous species, likely has obfuscated certain pathways and features of the amyloid cascade. The study of CT holds the potential to elucidate previously undetected amyloid aggregation pathways, as well as providing information valuable in improving its activity as a therapeutic. While early events in hCT aggregation have received more attention recently, as with all amyloid peptides, further studies are required before a functional understanding of the aggregation intermediates can be constructed.(1–4) The results of this thesis provide new insights into the aggregation of hCT in both solution and membrane environments, and have the potential to inform future efforts to influence amyloid aggregation in both hCT and other amyloids.

In Chapter 2, a novel direct relationship between initial monomer concentration and lag time for hCT was demonstrated for the first time, in contrast to previous results in the amyloid literature. ThT kinetic assays revealed this trend to exist in a range of aggregation environments, and the differential rates in fibril formation were confirmed by CD and TEM measurements. The micelle-like oligomers detected in hCT do not influence its aggregation kinetics, unlike the strong effects reported for similar oligomers in other amyloids.(5–9) Seeded ThT assays along with DLS

and solution NMR results suggested an origin for the aggregation behavior in the early steps of aggregation. Kinetic modeling provided a novel aggregation mechanism whereby monomer conformation conversion and subsequent inhibition slows aggregation in a concentration dependent process. hCT at low pH and sCT were both found to show the canonical inverse relationship between peptide concentration and lag time. MD simulations comparing hCT and sCT suggest that relative levels of helical secondary structure distinguish growth-competent and growth-incompetent monomers, explaining the differences in the peptide concentration versus lag time relationship between hCT and sCT. These results suggest that small structural elements in the mostly unstructured monomers of CT are necessary for fibril formation and crucial in determining aggregation kinetics. Further, the kinetic model represents a novel aggregation pathway, and synthesizes several previously disparate phenomenon into one cogent mechanism, while still incorporating the canonical nucleation-elongation-fragmentation kinetic model of Knowles and colleagues.(10–18) Future efforts to ascertain a more detailed structural understanding of this atypical behavior of hCT and overcome the difficulties inherent in detecting such monomeric reformatting in the heterogeneous amyloid environment are needed to fully characterize the aggregation process.

In Chapter 3, the first study of the effects of model membranes on hCT aggregation kinetics was performed. Using LUVs composed of several different common phospholipids, it was found that hCT maintained its direct relationship between peptide concentration and lag time independently of membrane composition. The quantitative difference between low and high concentration lag times varied with membrane composition, with lipid compositions encouraging stronger surface interactions most significantly retarding aggregation. CD showed slower aggregating conditions to correspond with more significant partitioning of hCT to the membrane

surface. Combining this with previously known interactions of amyloids with membranes, a mechanism is proposed whereby surface interactions pull helical growth-competent monomers off pathway, thus depleting the population of monomers able to aggregate and delaying fibrillation. LUVs also showed an ability to remodel hCT in both a membrane composition and peptide to lipid ratio dependent manner. This behavior is reminiscent of a previously reported behavior of DLPC LUVs with the amyloid-β peptide, and hints that this phenomenon could be more general than previously believed.(22)

These results help to address several questions in the amyloid and CT therapeutic fields. The results from Chapter 2 highlight the importance of monomer structure and intramolecular interactions in the amyloid aggregation of intrinsically disordered peptides, which has been an area of controversy in the amyloid field.(11, 19–21) The relative transience of intramolecular forces compared to intermolecular forces, especially in intrinsically disordered peptides, has relegated the former to an afterthought in considering mediators of aggregation kinetics, a viewpoint which will hopefully be reformed by these results. Given the desire for oral delivery of CT therapeutics, and the early promise of lipid-based delivery systems, the composition- and concentration-dependent modulation of hCT aggregation kinetics by lipid membranes shown in Chapter 3 is of interest for therapeutic development. The trends discovered provide valuable guidance in intelligently designing lipid-based delivery system to enhance bioavailability and limit pre-uptake aggregation, thus improving therapeutic efficacy. Additionally, the remodeling results in Chapter 3 are in contrast to the typical picture of membrane assisted amyloid aggregation, where membranes can influence kinetics and morphology but play a limited role once the mature stable fibers are formed.(21, 23–28) This behavior points to a richer picture for amyloid fibril-membrane interactions, and could bear relevance to the development of amyloid associated pathologies

through novel secondary nucleation and fragmentation pathways. Further work would be required however to gauge the biological and pathological relevance of this reformatting.

4.2. Future Directions

While the work presented in this thesis provides new information on mechanisms of amyloid aggregation both in solution and in the membrane, the complexity and heterogeneity of the aggregation process presents numerous opportunities for further study. In both Chapter 2 and Chapter 3, helical motifs in hCT monomers were suggested to play a major role in determining aggregation kinetics and the relationship between peptide concentration and lag phase. As such, the induction of helical structure in hCT presents a way to further evaluate the role of such motifs in aggregation. The addition of 2,2,2-trifluoroethanol (TFE) has the ability to dose-dependently induce enhanced helical structure in the monomeric peptide, granting some control over the monomeric structure and allow for a more systematic analysis on the role of α-helical monomers in hCT aggregation.(29–31) Further, mutation studies with hCT have yielded slower aggregating and more stable α-helical mutants that could experimentally elucidate the specific residues or regions that are key for determining hCT monomer growth-competence and the dependence of lag time on concentration.(14, 32–34)

Additionally, while helical monomer motifs appear to be key mediating factors in the aggregation of hCT, it remains undetermined whether or not this is unique to hCT or a general property for all amyloids. While helical intermediates have been demonstrated in a number of other amyloids, it remains unclear what roles these intermediates play in influencing monomer growth-competence and aggregation.(26, 35–46) For example, the formation and stabilization of helical monomers of α-synuclein by membrane mimetics has been shown to both accelerate and delay

aggregation, calling into question the generality of the trends presented in this dissertation.(47–49) By repeating the experiments in Chapter 2 and 3 in other model amyloids such as IAPP, amyloid-β, and α-synuclein, and exerting control over their helical propensity, the applicability of our kinetic mechanism to other amyloids in solution and in the presence of membrane could be explored. Considering the toxicity of oligomeric intermediates and the struggles currently faced in their characterization, the prospect of identifying key aggregation modifiers at the monomer level provides an attractive alternative for drug targets.

Given the presumed importance of interactions between helical hCT and the membrane surface presented in Chapter 3, future studies aimed at interrogating this behavior at a higher structural resolution are crucial. The field of NMR spectroscopy provides a number of techniques well suited to the study of membrane bound amyloids, even in unlabeled peptides. Line broadening in ^{1}H NMR spectra of hCT in the presence of LUVs would provide further confirmation of peptide adsorption, and transferred ^{1}H–^{1}H nuclear Overhauser effect spectroscopy (tr-NOESY) would allow direct confirmation of the degree of structure present in bound hCT populations, given the likelihood of exchange between the bound and free form.(50–52) Due to the slow tumbling speed of LUVs however, NMR spectra of membrane-associated peptides experience significant signal broadening due to longer correlation times, limiting the number of applicable experiments. Smaller, NMR-suitable membrane mimetics have typically required the incorporation of detergents or short chain lipids, which can interfere with the native peptide behavior.(53–56) Recent advances in membrane mimetics systems have given rise to small lipid bilayer patches called nanodiscs that tumble on the NMR timescale and form without detergents.(57, 58) Nanodiscs thus are ideally suited for structural characterizations of membrane bound hCT species through solution-state NMR methods, as has been demonstrated.(59–61) The use of nanodiscs with

NMR spectroscopy presents a new tool to probe amyloid-membrane interactions in a native environment, and could greatly improve our understanding of the role the membrane plays in influencing the early stages of amyloid aggregation.

Chapter 3 also demonstrated an ability for LUVs to remodel mature amyloid fibers of hCT, but relatively little is known about this behavior. The loss of ThT signal does not necessarily imply a loss of overall fiber structure, and could rather be reflective of side chain remodeling and subsequently reduced ThT binding. TEM provides a straightforward way to compare fibers before and after reformatting to determine the extent and nature of fibril structure loss. The clear differences in reformatting between DOPC and POPC lipids along with the enhanced remodeling seen at higher temperatures suggests membrane fluidity to play a crucial role in fibril reformatting. ThT experiments with more rigid DMPC LUVs, along with other LUVs incorporating anionic lipids would help confirm and discover additional mediators of this behavior. Comparative solid-state HSQC NMR experiments on labeled hCT during reformatting would allow for the determination of residue specific insights into the reformatting process. Given previous studies, the remodeling of mature amyloid fibrils by model membranes could represent a more general phenomenon than previously believed.(22) Residue specific information on this behavior could not only elucidate previously unknown structural features in amyloid fibrils in a membrane system, but also inform the design of novel amyloid inhibitors.

4.3. References

1. Diociaiuti, M., Polzi, L. Z., Valvo, L., Malchiodi-Albedi, F., Bombelli, C., and Gaudiano, M. C. (2006) Calcitonin forms oligomeric pore-like structures in lipid membranes. *Biophys. J.* **91**, 2275–81

2. Diociaiuti, M., Macchia, G., Paradisi, S., Frank, C., Camerini, S., Chistolini, P., Gaudiano, M. C., Petrucci, T. C., and Malchiodi-Albedi, F. (2014) Native metastable prefibrillar oligomers are the most neurotoxic species among amyloid aggregates. *Biochim. Biophys.*

Acta. **1842**, 1622–9

3. Huang, R., Vivekanandan, S., Brender, J. R., Abe, Y., Naito, A., and Ramamoorthy, A. (2012) NMR characterization of monomeric and oligomeric conformations of human calcitonin and its interaction with EGCG. *J. Mol. Biol.* **416**, 108–20

4. Avidan-Shpalter, C., and Gazit, E. (2006) The early stages of amyloid formation: biophysical and structural characterization of human calcitonin pre-fibrillar assemblies. *Amyloid*. **13**, 216–25

5. Wei, Y., Lu, J., Lu, T., Meng, F., Xu, J., Wang, L., Li, Y., Wang, L., and Li, F. (2016) Formation of lamellar micelle-like oligomers and membrane disruption revealed by the study of short peptide hIAPP 18–27. *Phys. Chem. Chem. Phys.* **18**, 29847–29857

6. Brender, J. R., Krishnamoorthy, J., Sciacca, M. F. M., Vivekanandan, S., D'Urso, L., Chen, J., La Rosa, C., and Ramamoorthy, A. (2015) Probing the Sources of the Apparent Irreproducibility of Amyloid Formation: Drastic Changes in Kinetics and a Switch in Mechanism Due to Micellelike Oligomer Formation at Critical Concentrations of IAPP. *J. Phys. Chem. B*. **119**, 2886–2896

7. Wälti, M. A., Orts, J., Vögeli, B., Campioni, S., and Riek, R. (2015) Solution NMR studies of recombinant Aβ(1-42): from the presence of a micellar entity to residual β-sheet structure in the soluble species. *Chembiochem*. **16**, 659–69

8. Hingant, E., Fontes, P., Alvarez-Martinez, M. T., Arnaud, J.-D., Liautard, J.-P., and Pujo-Menjouet, L. (2014) A micellar on-pathway intermediate step explains the kinetics of prion amyloid formation. *PLoS Comput. Biol.* **10**, e1003735

9. Sabaté, R., and Estelrich, J. (2005) Evidence of the existence of micelles in the fibrillogenesis of beta-amyloid peptide. *J. Phys. Chem. B*. **109**, 11027–32

10. Shoffner, S. K., and Schnell, S. (2016) Estimation of the lag time in a subsequent monomer addition model for fibril elongation. *Phys. Chem. Chem. Phys.* **18**, 21259–21268

11. Kashchiev, D. (2017) Modeling the Effect of Monomer Conformational Change on the Early Stage of Protein Self-Assembly into Fibrils. *J. Phys. Chem. B*. **121**, 35–46

12. Blancas-Mejía, L. M., Misra, P., and Ramirez-Alvarado, M. (2017) Differences in protein concentration dependence for nucleation and elongation in light chain amyloid formation. *Biochemistry*. **56**, 757–766

13. Zhijie Qin, Dongmei Hu, Min Zhu, A., and Fink, A. L. (2007) Structural Characterization of the Partially Folded Intermediates of an Immunoglobulin Light Chain Leading to Amyloid Fibrillation and Amorphous Aggregation. *Biochemistry*. **46**, 3521–3531

14. Andreotti, G., and Motta, A. (2003) Modulating calcitonin fibrillogenesis: an antiparallel alpha-helical dimer inhibits fibrillation of salmon calcitonin. *J. Biol. Chem.* **279**, 6364–6370

15. Amodeo, P., Motta, A., Strazzullo, G., and Castiglione Morelli, M. A. (1999) Conformational flexibility in calcitonin: the dynamic properties of human and salmon calcitonin in solution. *J. Biomol. NMR*. **13**, 161–74

16. Meisl, G., Yang, X., Hellstrand, E., Frohm, B., Kirkegaard, J. B., Cohen, S. I. A., Dobson, C. M., Linse, S., and Knowles, T. P. J. (2014) Differences in nucleation behavior underlie the contrasting aggregation kinetics of the Aβ40 and Aβ42 peptides. *Proc. Natl. Acad. Sci. U. S. A.* **111**, 9384–9

17. Meisl, G., Kirkegaard, J. B., Arosio, P., Michaels, T. C. T., Vendruscolo, M., Dobson, C. M., Linse, S., and Knowles, T. P. J. (2016) Molecular mechanisms of protein aggregation from global fitting of kinetic models. *Nat. Protoc.* **11**, 252–72

18. Arosio, P., Knowles, T. P. J., and Linse, S. (2015) On the lag phase in amyloid fibril formation. *Phys. Chem. Chem. Phys.* **17**, 7606–18

19. Roche, J., Shen, Y., Lee, J. H., Ying, J., and Bax, A. (2016) Monomeric Aβ(1-40) and Aβ(1-42) Peptides in Solution Adopt Very Similar Ramachandran Map Distributions That Closely Resemble Random Coil. *Biochemistry*. **55**, 762–75

20. Qiao, Q., Qi, R., Wei, G., and Huang, X. (2016) Dynamics of the conformational transitions during the dimerization of an intrinsically disordered peptide: a case study on the human islet amyloid polypeptide fragment. *Phys. Chem. Chem. Phys.* **7**, 824–826

21. Chiti, F., and Dobson, C. M. (2017) Protein Misfolding, Amyloid Formation, and Human Disease: A Summary of Progress Over the Last Decade. *Annu. Rev. Biochem.* **86**, 27–68

22. Korshavn, K. J., Satriano, C., Lin, Y., Zhang, R., Dulchavsky, M., Bhunia, A., Ivanova, M. I., Lee, Y.-H., Rosa, C. La, Lim, M. H., and Ramamoorthy, A. (2017) Thin Membranes Modulate Aβ Aggregation Reduced Lipid Bilayer Thickness Regulates the Aggregation and Cytotoxicity of Amyloid-β. *J. Biol. Chem.* **292**, 4638–4650

23. Zhang, X., St. Clair, J. R., London, E., and Raleigh, D. P. (2017) Islet Amyloid Polypeptide Membrane Interactions: Effects of Membrane Composition. *Biochemistry*. **56**, 376–390

24. Eisenberg, D. S., and Sawaya, M. R. (2017) Structural Studies of Amyloid Proteins at the Molecular Level. *Annu. Rev. Biochem.* **86**, 69–95

25. Ikeda, K., Yamaguchi, T., Fukunaga, S., Hoshino, M., and Matsuzaki, K. (2011) Mechanism of Amyloid β-Protein Aggregation Mediated by GM1 Ganglioside Clusters. *Biochemistry*. **50**, 6433–6440

26. Korshavn, K. J., Bhunia, A., Lim, M. H., and Ramamoorthy, A. (2016) Amyloid-β adopts a conserved, partially folded structure upon binding to zwitterionic lipid bilayers prior to amyloid formation. *Chem. Commun.* **52**, 882–885

27. Brender, J. R., Salamekh, S., and Ramamoorthy, A. (2012) Membrane disruption and

early events in the aggregation of the diabetes related peptide IAPP from a molecular perspective. *Acc. Chem. Res.* **45**, 454–62

28. Sheynis, T., and Jelinek, R. (2010) Lipid-Induced Calcitonin Fibrillation Blocks Membrane Interactions of a Peptide Antibiotic. *J. Phys. Chem. B.* **114**, 15530–15535

29. Myers, J. K., Nick Pace, C., and Martin Scholtz, J. (2008) Trifluoroethanol effects on helix propensity and electrostatic interactions in the helical peptide from ribonuclease T1. *Protein Sci.* **7**, 383–388

30. Luo, P., and Baldwin, R. L. (1997) Mechanism of Helix Induction by Trifluoroethanol: A Framework for Extrapolating the Helix-Forming Properties of Peptides from Trifluoroethanol/Water Mixtures Back to Water †. *Biochemistry*. **36**, 8413–8421

31. Otzen, D. E. (2010) Amyloid formation in surfactants and alcohols: membrane mimetics or structural switchers? *Curr. Protein Pept. Sci.* **11**, 355–71

32. Fowler, S. B., Poon, S., Muff, R., Chiti, F., Dobson, C. M., and Zurdo, J. (2005) Rational design of aggregation-resistant bioactive peptides: reengineering human calcitonin. *Proc. Natl. Acad. Sci. U. S. A.* **102**, 10105–10

33. Andreotti, G., Vitale, R. M., Avidan-Shpalter, C., Amodeo, P., Gazit, E., and Motta, A. (2011) Converting the highly amyloidogenic human calcitonin into a powerful fibril inhibitor by three-dimensional structure homology with a non-amyloidogenic analogue. *J. Biol. Chem.* **286**, 2707–18

34. Itoh-Watanabe, H., Kamihira-Ishijima, M., Javkhlantugs, N., Inoue, R., Itoh, Y., Endo, H., Tuzi, S., Saitô, H., Ueda, K., and Naito, A. (2013) Role of aromatic residues in amyloid fibril formation of human calcitonin by solid-state 13C NMR and molecular dynamics simulation. *Phys. Chem. Chem. Phys.* **15**, 8890–901

35. Chen, Y.-C. (2017) Impact of a discordant helix on β-amyloid structure, aggregation ability and toxicity. *Eur. Biophys. J.* **46**, 681–687

36. Kumar, S., and Hamilton, A. D. (2017) α-Helix Mimetics as Modulators of Aβ Self-Assembly. *J. Am. Chem. Soc.* **139**, 5744–5755

37. Abedini, A., Cao, P., and Raleigh, D. P. (2016) Detection of Helical Intermediates During Amyloid Formation by Intrinsically Disordered Polypeptides and Proteins. *Methods Mol. Biol.* **1345**, 55–66

38. Saraogi, I., Hebda, J. A., Becerril, J., Estroff, L. A., Miranker, A. D., and Hamilton, A. D. (2010) Synthetic α-Helix Mimetics as Agonists and Antagonists of Islet Amyloid Polypeptide Aggregation. *Angew. Chemie Int. Ed.* **49**, 736–739

39. Williamson, J. A., Loria, J. P., and Miranker, A. D. (2009) Helix Stabilization Precedes Aqueous and Bilayer-Catalyzed Fiber Formation in Islet Amyloid Polypeptide. *J. Mol. Biol.* **393**, 383–396

40. Abedini, A., and Raleigh, D. P. (2009) A critical assessment of the role of helical intermediates in amyloid formation by natively unfolded proteins and polypeptides. *Protein Eng. Des. Sel.* **22**, 453–9

41. Yang, M., and Teplow, D. B. (2008) Amyloid β-Protein Monomer Folding: Free-Energy Surfaces Reveal Alloform-Specific Differences. *J. Mol. Biol.* **384**, 450–464

42. Epand, R. M., Epand, R. F., Orlowski, R. C., Schlueter, R. J., Boni, L. T., and Hui, S. W. (1983) Amphipathic helix and its relationship to the interaction of calcitonin with phospholipids. *Biochemistry*. **22**, 5074–5084

43. Eichmann, C., Campioni, S., Kowal, J., Maslennikov, I., Gerez, J., Liu, X., Verasdonck, J., Nespovitaya, N., Choe, S., Meier, B., Picotti, P., Rizo, J., Stahlberg, H., and Riek, R. (2016) Preparation and Characterization of Stable α-Synuclein Lipoprotein Particles. *J. Biol. Chem.* **291**, 8516–27

44. Prakash, R., Nanga, R., Brender, J. R., Xu, J., Hartman, K., Subramanian, V., and Ramamoorthy, A. (2009) Three-Dimensional Structure and Orientation of Rat Islet Amyloid Polypeptide Protein in a Membrane Environment by Solution NMR Spectroscopy. *J. Am. Chem. Soc.* **131**, 8252–8261

45. Motta, A., Andreotti, G., Amodeo, P., Strazzullo, G., and Castiglione Morelli, M. A. (1998) Solution structure of human calcitonin in membrane-mimetic environment: the role of the amphipathic helix. *Proteins.* **32**, 314–23

46. Soria, M. A., Cervantes, S. A., Bajakian, T. H., and Siemer, A. B. (2017) The Functional Amyloid Orb2A Binds to Lipid Membranes. *Biophys. J.* **113**, 37–47

47. Galvagnion, C., Buell, A. K., Meisl, G., Michaels, T. C. T., Vendruscolo, M., Knowles, T. P. J., and Dobson, C. M. (2015) Lipid vesicles trigger α-synuclein aggregation by stimulating primary nucleation. *Nat. Chem. Biol.* **11**, 229–234

48. Iyer, A., Roeters, S. J., Schilderink, N., Hommersom, B., Heeren, R. M. A., Woutersen, S., Claessens, M. M. A. E., and Subramaniam, V. (2016) The Impact of N-terminal Acetylation of Alpha Synuclein on Phospholipid Membrane Binding and Fibril Structure. *J. Biol. Chem.* **291**, 21110–21122

49. Zhu, M., and Fink, A. L. (2003) Lipid Binding Inhibits α-Synuclein Fibril Formation. *J. Biol. Chem.* **278**, 16873–16877

50. Wang, Z., Jones, J. D., Rizo, J., and Gierasch, L. M. (1993) Membrane-bound conformation of a signal peptide: a transferred nuclear Overhauser effect analysis. *Biochemistry*. **32**, 13991–9

51. Bhunia, A., Mohanram, H., and Bhattacharjya, S. (2009) Lipopolysaccharide bound structures of the active fragments of fowlicidin-1, a cathelicidin family of antimicrobial and antiendotoxic peptide from chicken, determined by transferred nuclear overhauser effect spectroscopy. *Biopolymers.* **92**, 9–22

52. Clore, G. M., and Gronenborn, A. M. (1982) Theory and applications of the transferred nuclear overhauser effect to the study of the conformations of small ligands bound to proteins. *J. Magn. Reson.* **48**, 402–417

53. Caillon, L., Lequin, O., and Khemtémourian, L. (2013) Evaluation of membrane models and their composition for islet amyloid polypeptide-membrane aggregation. *Biochim. Biophys. Acta - Biomembr.* **1828**, 2091–2098

54. Serra-Batiste, M., Ninot-Pedrosa, M., Bayoumi, M., Gairí, M., Maglia, G., and Carulla, N. (2016) Aβ42 assembles into specific β-barrel pore-forming oligomers in membrane-mimicking environments. *Proc. Natl. Acad. Sci. U. S. A.* **113**, 10866–71

55. Sanders, C. R., and Sönnichsen, F. (2006) Solution NMR of membrane proteins: practice and challenges. *Magn. Reson. Chem.* **44**, S24–S40

56. Columbus, L., Lipfert, J., Jambunathan, K., Fox, D. A., Sim, A. Y. L., Doniach, S., and Lesley, S. A. (2009) Mixing and Matching Detergents for Membrane Protein NMR Structure Determination. *J. Am. Chem. Soc.* **131**, 7320–7326

57. Hagn, F., Etzkorn, M., Raschle, T., and Wagner, G. (2013) Optimized phospholipid bilayer nanodiscs facilitate high-resolution structure determination of membrane proteins. *J. Am. Chem. Soc.* **135**, 1919–25

58. Orwick, M. C., Judge, P. J., Procek, J., Lindholm, L., Graziadei, A., Engel, A., Gröbner, G., and Watts, A. (2012) Detergent-Free Formation and Physicochemical Characterization of Nanosized Lipid-Polymer Complexes: Lipodisq. *Angew. Chemie Int. Ed.* **51**, 4653–4657

59. Nath, A., Miranker, A. D., and Rhoades, E. (2011) A membrane-bound antiparallel dimer of rat islet amyloid polypeptide. *Angew. Chem. Int. Ed. Engl.* **50**, 10859–62

60. Thomaier, M., Gremer, L., Dammers, C., Fabig, J., Neudecker, P., and Willbold, D. (2016) High-Affinity Binding of Monomeric but Not Oligomeric Amyloid-β to Ganglioside GM1 Containing Nanodiscs. *Biochemistry*. **55**, 6662–6672

61. Rodriguez Camargo, D. C., Korshavn, K. J., Jussupow, A., Raltchev, K., Goricanec, D., Fleisch, M., Sarkar, R., Xue, K., Aichler, M., Mettenleiter, G., Walch, A. K., Camilloni, C., Hagn, F., Reif, B., and Ramamoorthy, A. (2017) Stabilization and structural analysis of a membrane-associated hIAPP aggregation intermediate. *Elife.* 10.7554/eLife.31226

Appendix A

Supporting Information for Chapter 2

A.1. Supplementary Figures

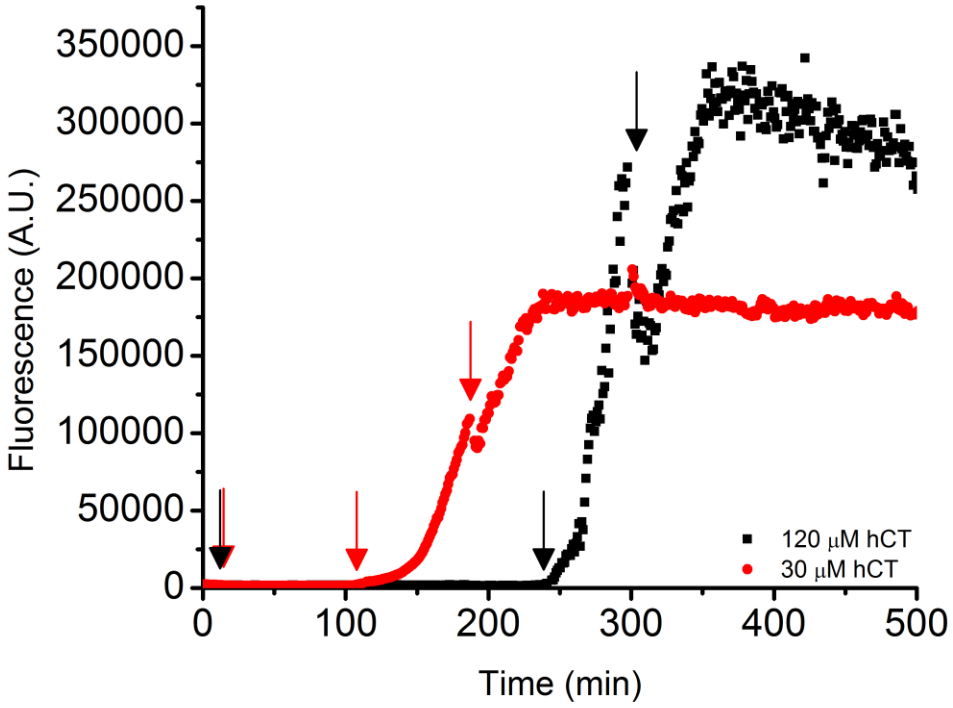

Figure A.1. ThT fluorescence curves of hCT aggregation for TEM. ThT assay conditions identical to those for Figure 2.1. Arrows indicate time point of removal of samples for TEM. Initial removal for both samples corresponds to t = 15 mins for both conditions. Discontinuities arise from removal of sample from wells/disturbance of solution.

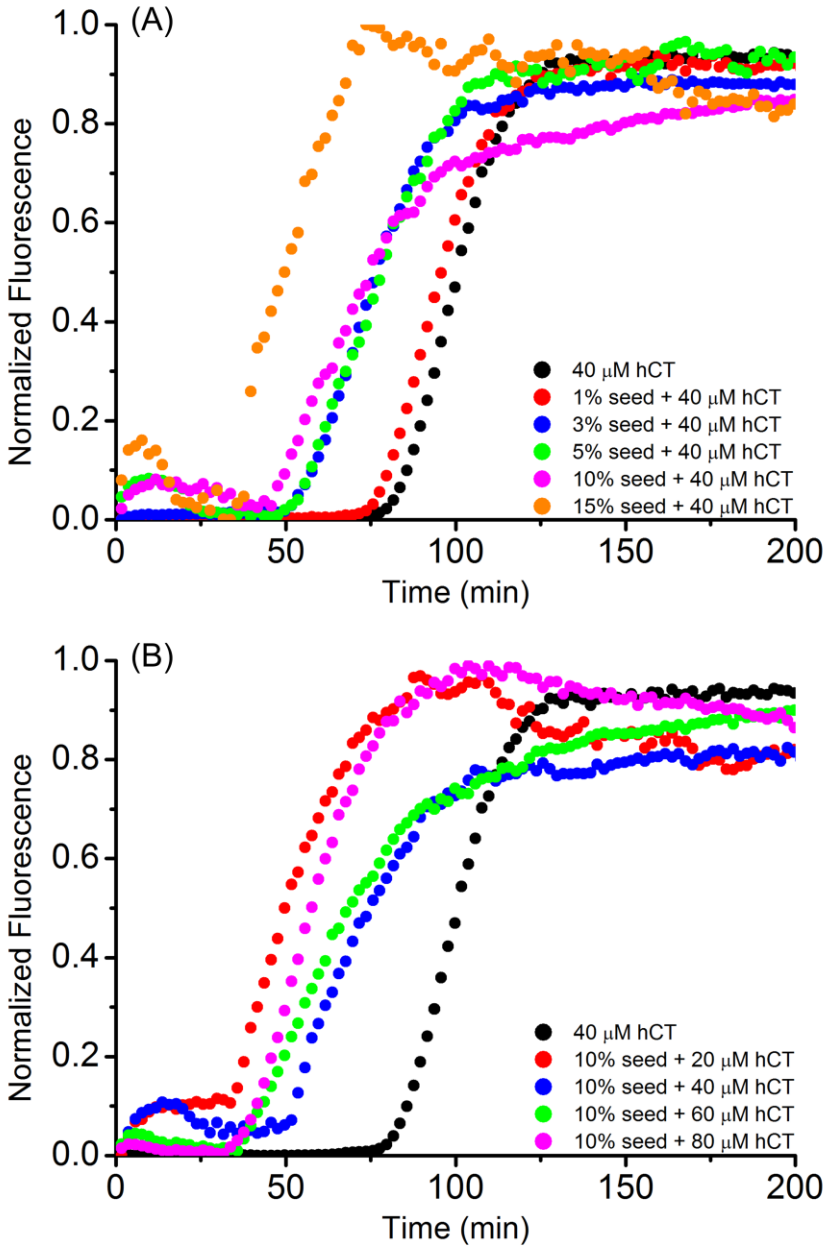

Figure A.2. Seeded ThT assays reveal lag time to not be entirely primary nucleus dependent. ThT assay conditions identical to those for Figure 2.1. A) Varying of seed percentage by volume with fixed hCT monomer concentration shows dose-dependent decrease of lag time with seed concentration, but does not show full abolition of lag time. B) Varying of hCT monomer concentration with fixed 10% seed by volume shows decrease in lag time versus pure monomer. The relationship between monomer concentration and lag time from the unseeded experiments is lost with seeding.

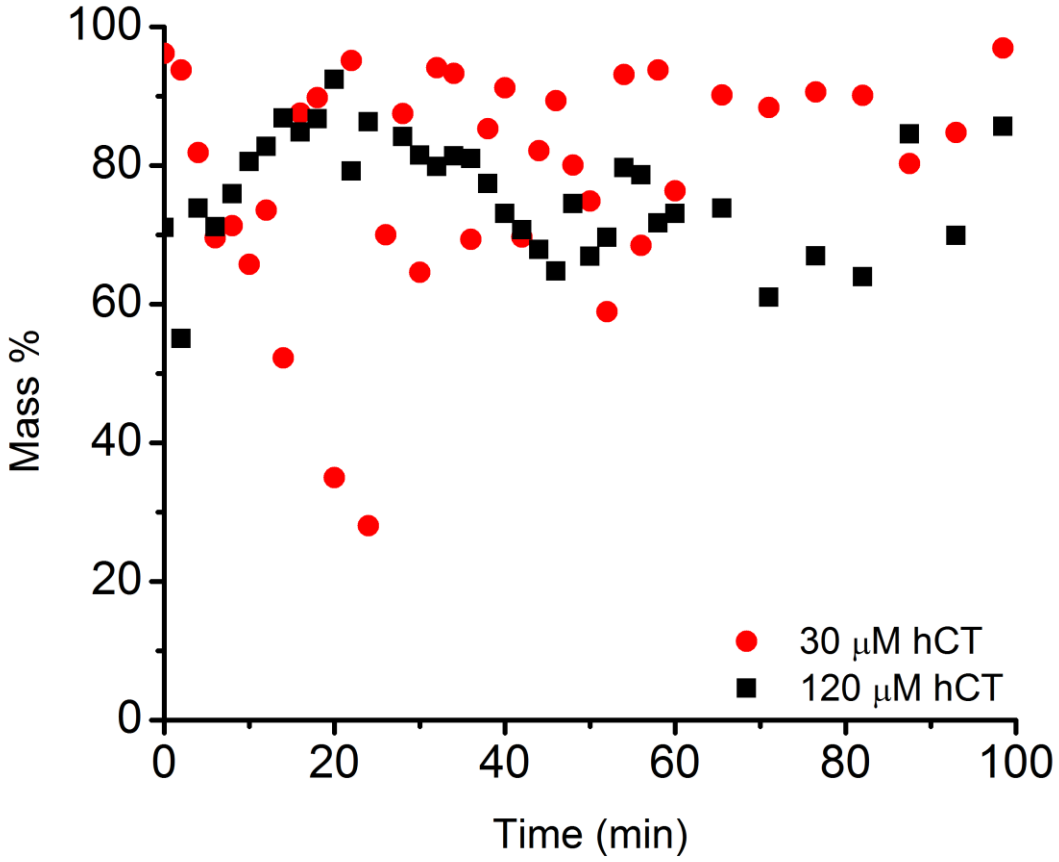

Figure A.3. DLS measurements show no time- or concentration-dependent differences in mass distribution over time between peaks. Both 120 μM and 30 μM DLS time course experiments show constant and equivalent percentage of total peptide mass in small oligomer peak (Fig. 2.3.A, peak I, shown above). Remaining peptide mass is contained in larger aggregate peak (Fig. 2.3.A, peak II). As would be expected early in the aggregation process, the majority of peptide mass is still in smaller oligomeric aggregates.

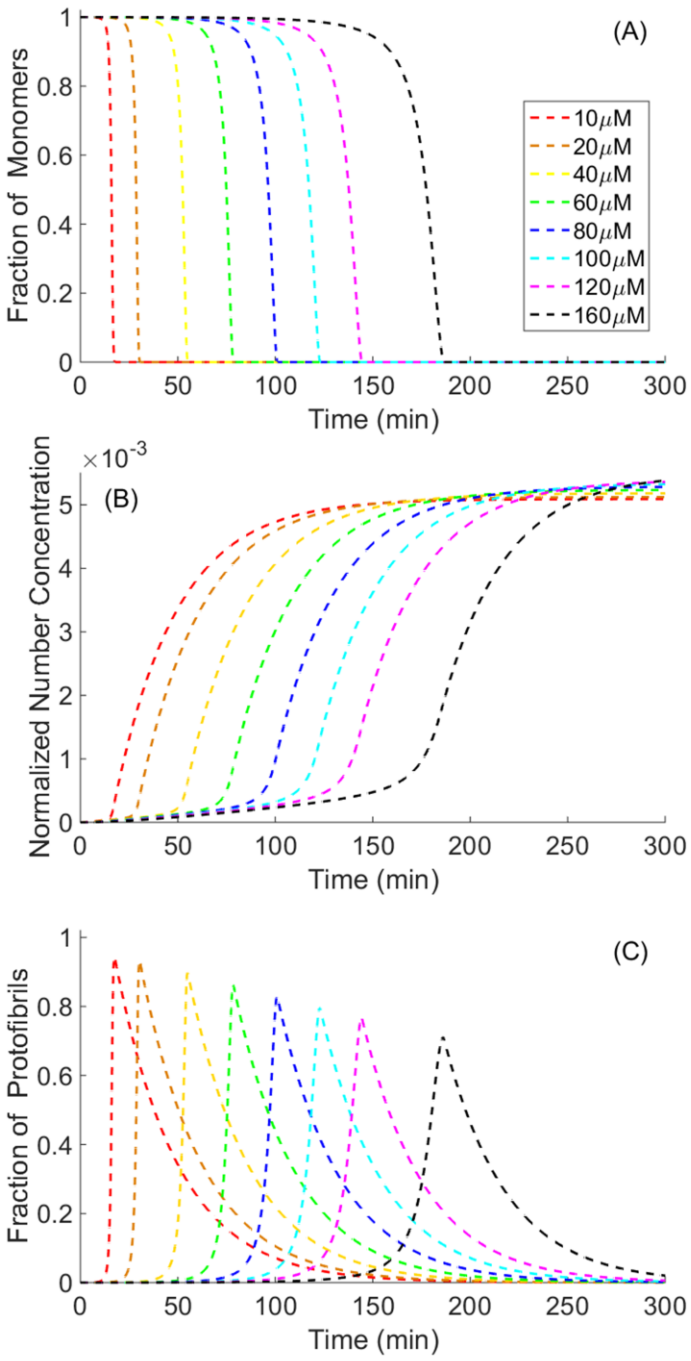

Figure A.4. Predictions on (a) fraction of monomers, (b) normalized number concentration of protofibrils, and (c) normalized mass concentration of protofibrils (all with respect to total hCT peptide concentration) under different initial hCT peptide concentration based on the kinetic model.

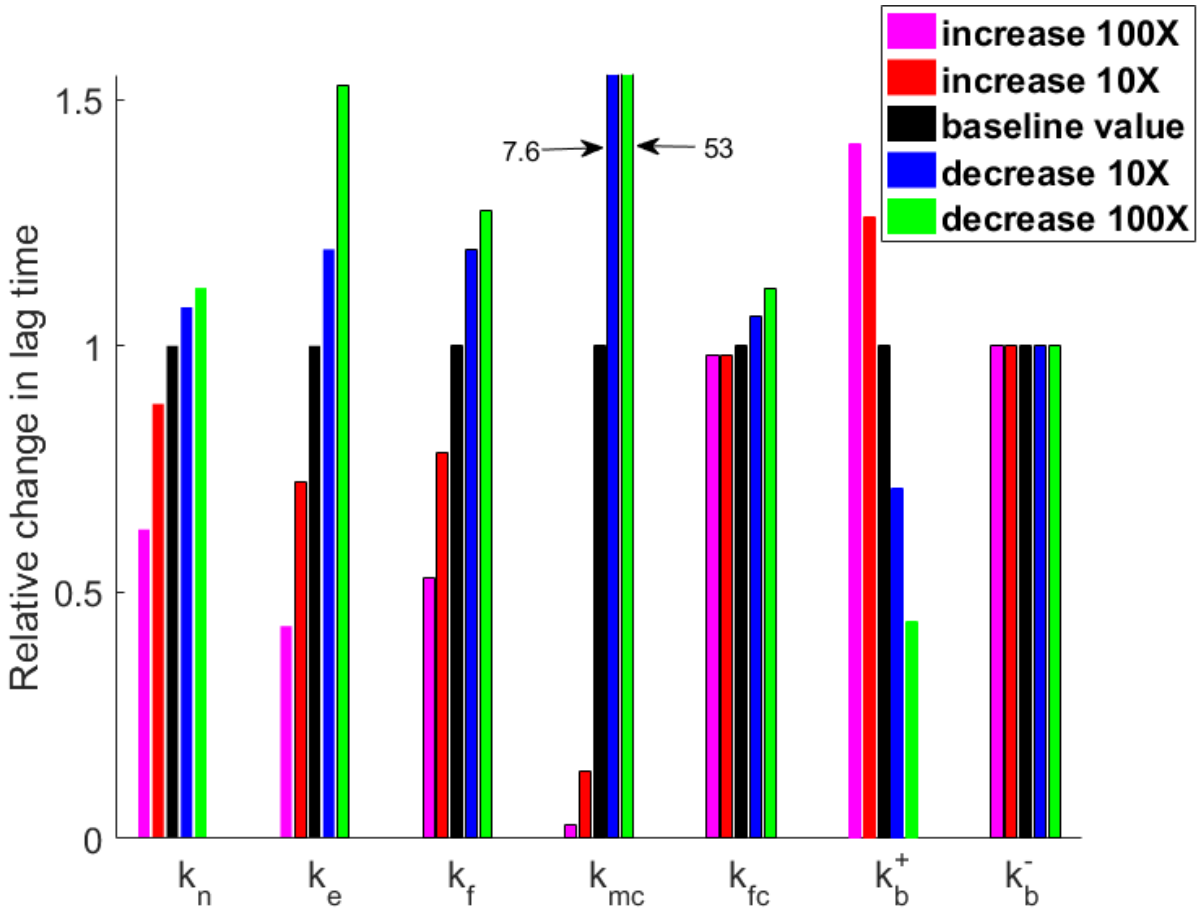

Figure A.5. The influence of reaction rate constants on the lag time of hCT fibrillation. In each group, the relative change of lag time is drawn when the marked rate constant is varied independently by one or two orders of magnitude higher or lower with respect to its default values given in the main text. The initial hCT peptide concentration is taken as 40 μM.

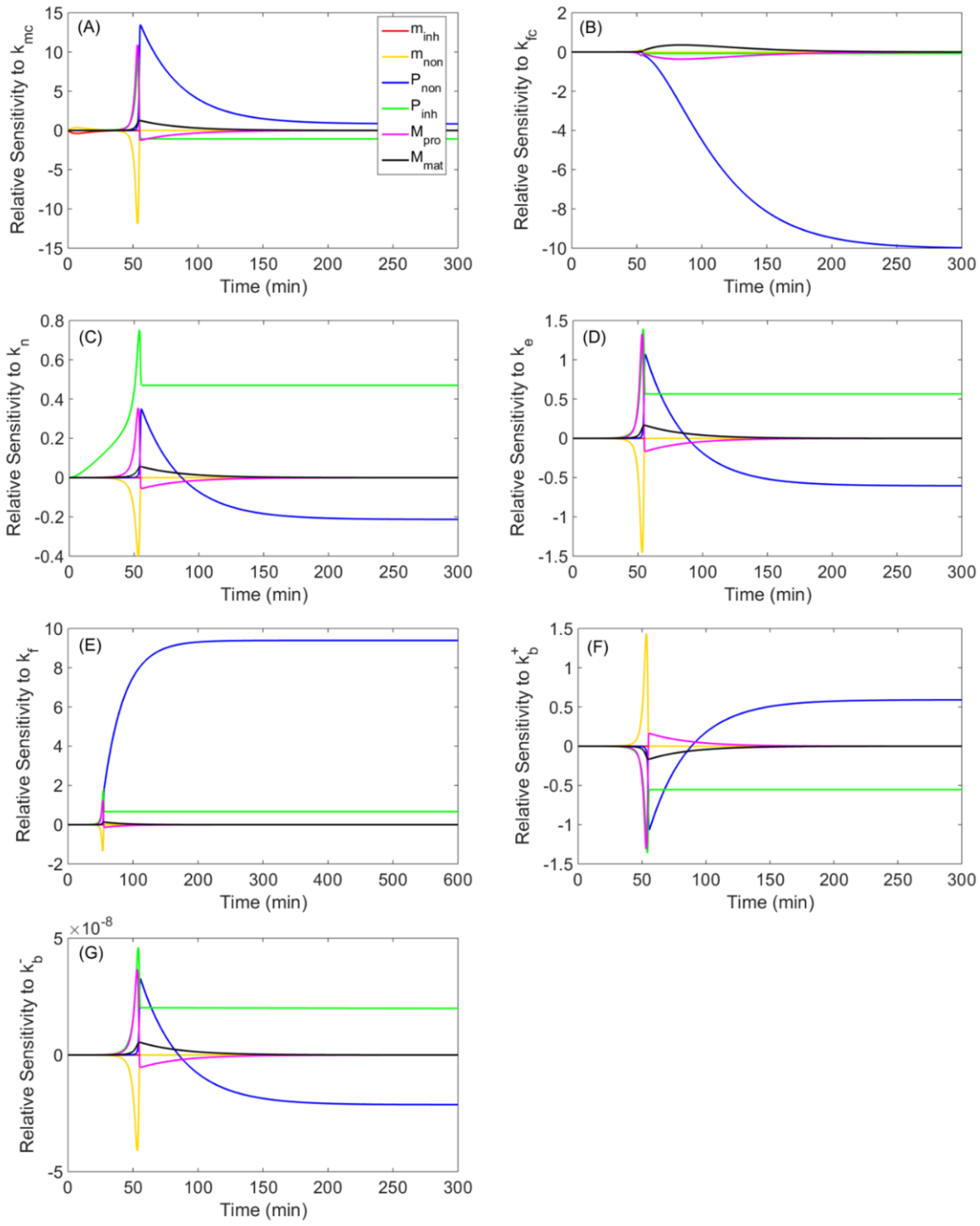

Figure A.6. Local sensitivity analysis on reaction rates. Let $\mathrm{Y(t)} = (m_{\mathrm{i}}, m_n, P_{\mathrm{n}}, P_{\mathrm{b}}, M_{\mathrm{p}}, M_{\mathrm{f}})$ and $\mathrm{K(t)} = (k_{mc}, k_{fc}, k_n, k_e, k_f, k_b^+, k_b^-)$. Then the relative local sensitivity of Y with respect to K drawn in each subplot is defined as $\mathrm{S(Y;K)} = \frac{K}{Y_{max}}\frac{dY}{dK}$. Here $Y_{max} = \max\{Y(t)|t \geq 0\}$ is adopted instead of Y in order to avoid singularities in Y. Based on local sensitivity analysis, following conclusions could be reached, i.e. i) m_{i} mainly depends on k_{mc}; ii) m_{n} mainly depends on k_b^+; iii) M_{p} *and* M_{f} depend not only on k_{fc}, but also on k_{mc}, k_e in an indirect way; iv) P_{n} and P_{b} not only depend on k_n, k_f, but also are influenced by all parameters; vi) k_b^- has no apparent effect on Y.

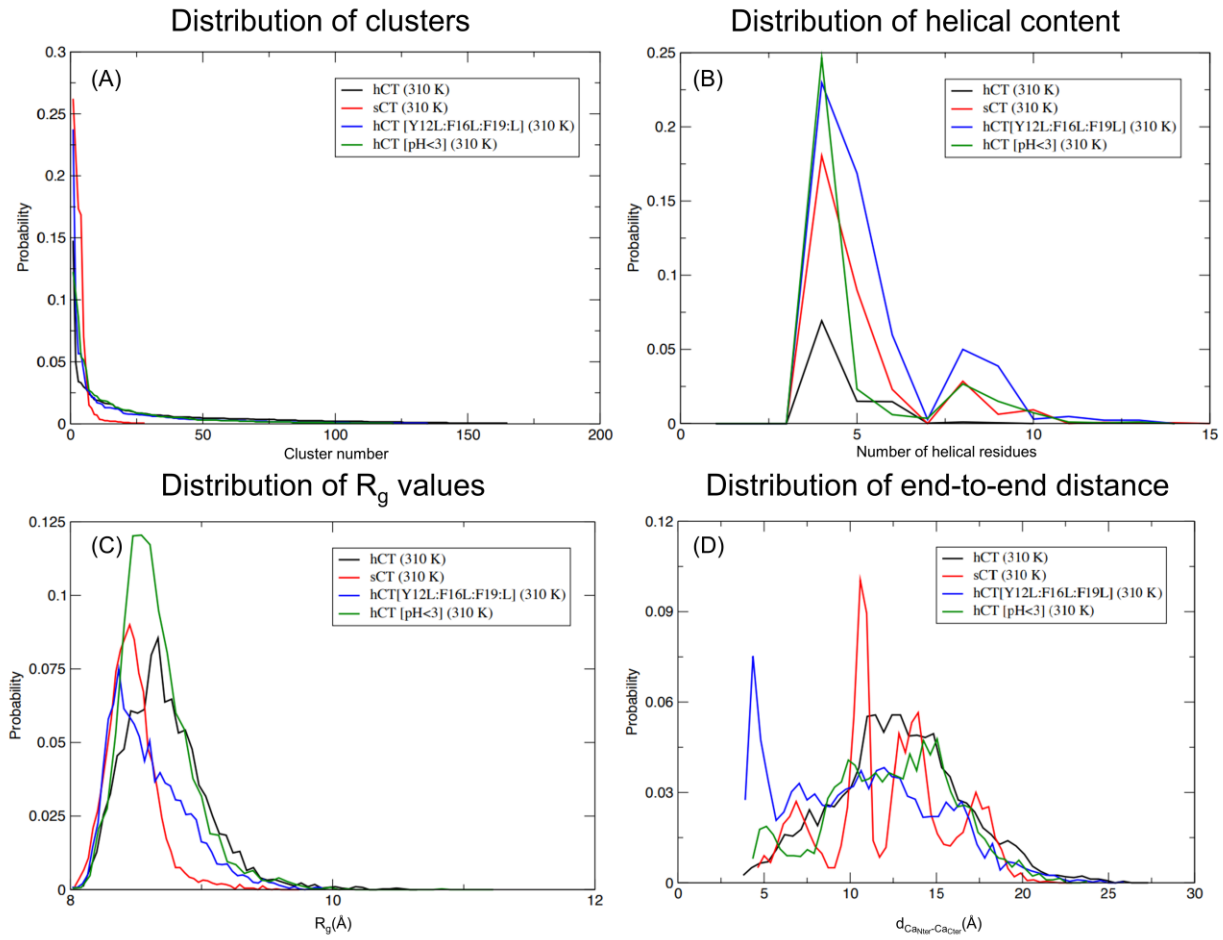

Figure A.7. sCT displays lower structural heterogeneity and inreased helical content when compared to hCT, with mutations to the aromatic residues in hCT and hCT at low pH inducing a more sCT-like behavior. A) Relative probability of hCT, sCT, hCT-mutant, and hCT (low pH) monomer conformations versus cluster number. sCT monomers sample a smaller section of conformational space than hCT, while mutated and low pH hCT occupy an intermediate amount of conformational space. B) sCT shows higher propensity for helical content than hCT, with mutated and low pH hCT showing intermediate levels of helical secondary structure. C) Radius of gyration and D) end-to-end distance values in monomer clusters for hCT, sCT, hCT mutant, and hCT at pH 3. sCT shows a sharper distribution with lower average radius of gyration when compared with hCT. sCT also has a lower average end to end distance, while showing distinct peaks in the end-to-end distances distribution, indicating its existence in several discreet clusters/conformations. Our hCT mutant and hCT at low pH behave in a more sCT like way. In particular, mutant hCT becomes significantly more favorable for compact structures as indicated by the increased probability for short end to end distances and radii of gyration.

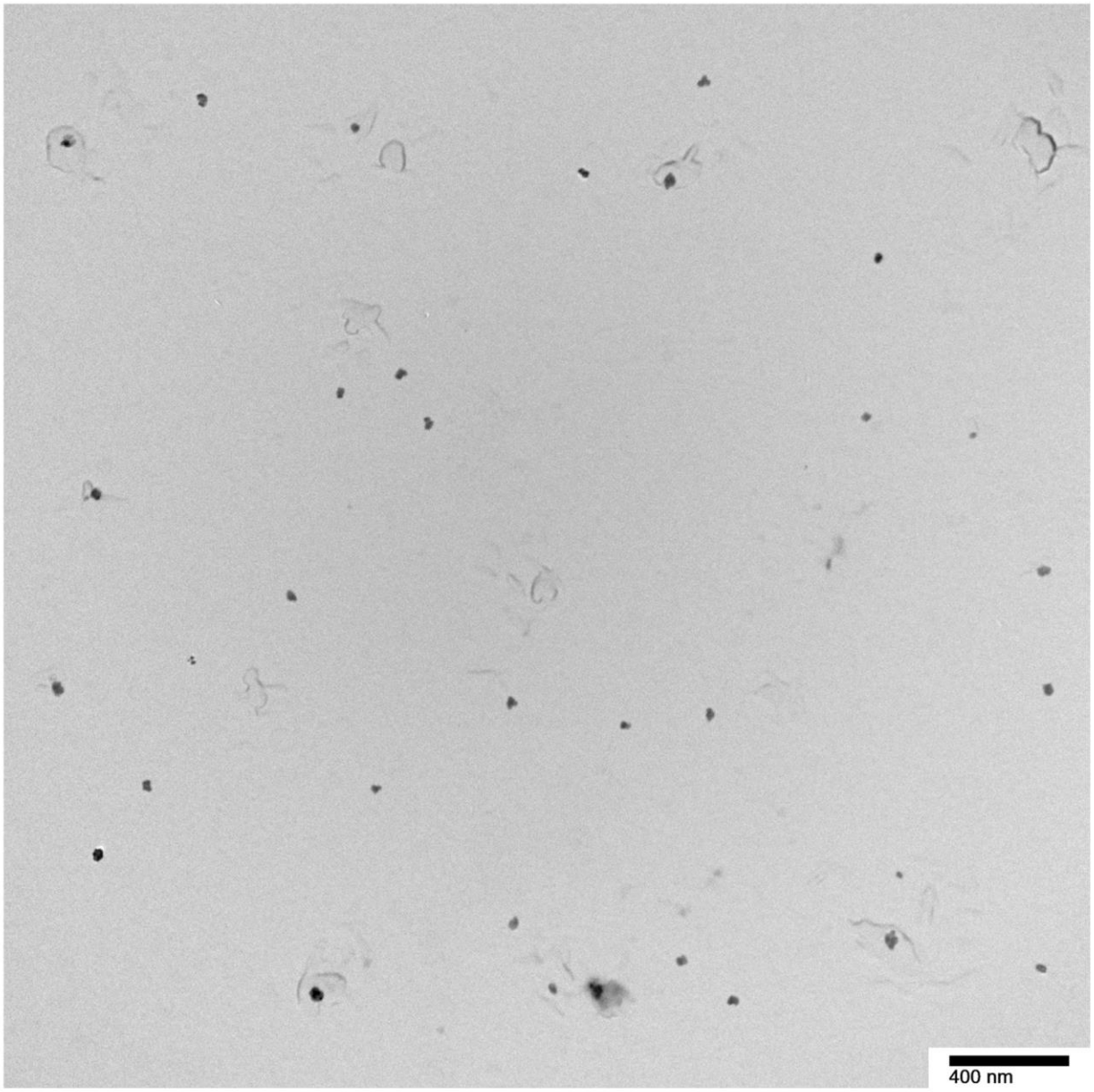

Figure A.8. TEM image of 120 μM hCT aggregates in late lag phase (same sample as Fig. 2.1.). Image shows the presence of a number of punctate, proteinaceous aggregates presumed to be micelle-like oligomers, due to their shape, size, and presence only above the CMC. Aggregates appear to be ~20 nm in size, with relatively uniform size distribution. Aggregates don't show any preference for or association with protofibrillar or fibrillar species.

Appendix B

Supporting Information for Chapter 3

B.1. Supplementary Figures

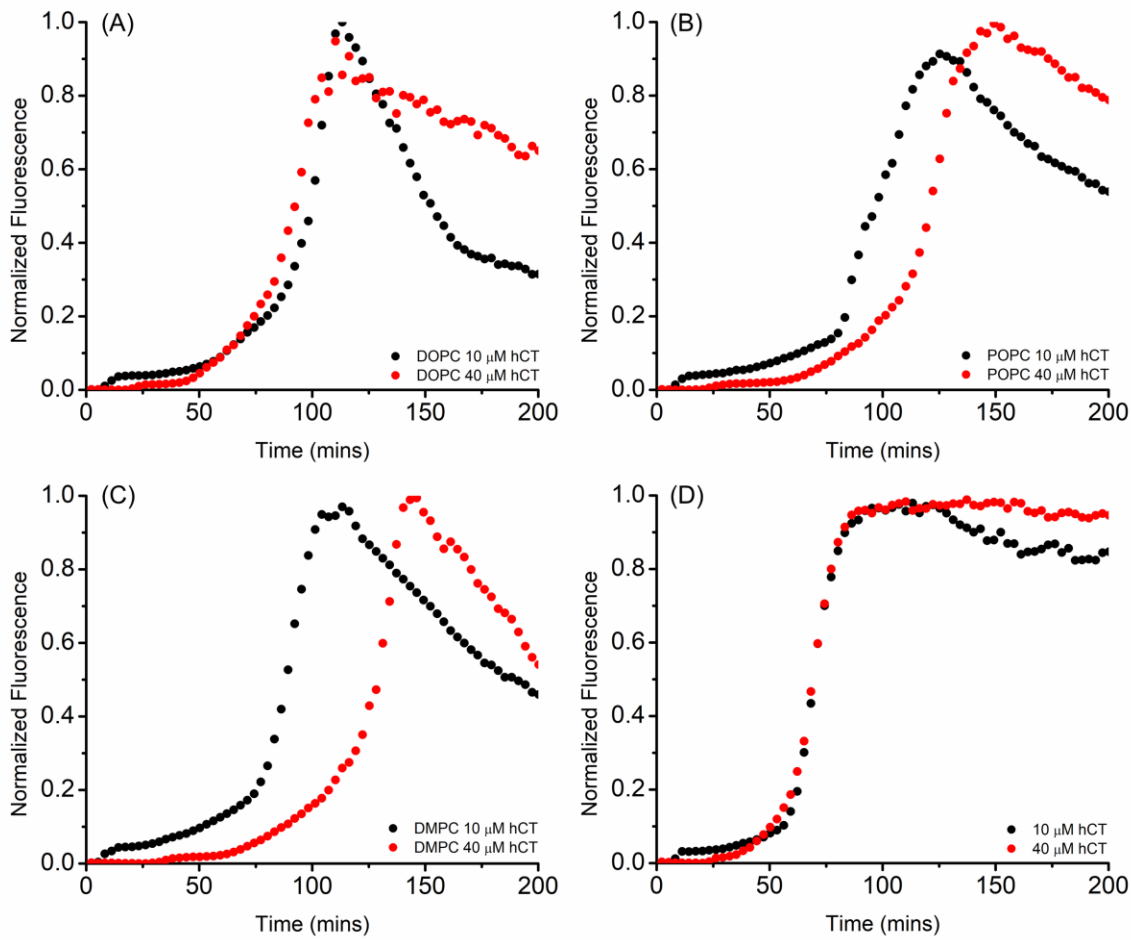

Figure B.1. LUVs with higher transition temperatures induce correspondingly larger concentration dependent increases in lag time. hCT at 10 μM and 40 μM was allowed to aggregate in the presence of 100 μM of 100 nm LUVs composed of A) DOPC, B) POPC, and C) DMPC. Moving to LUVs with higher transition temperatures leads to greater differences between low and high concentration lag times and slower aggregation. Due to the high transition temperature of DMPC (24 °C), experiments were run at 35 °C to ensure all LUVs were in the same phase. Increased temperature was found to accelerate aggregation under all conditions, and also remove concentration dependent differences in aggregation rate in solution (D). Displayed curves represent normalized averages of three independent trials in 20 mM phosphate buffer and 100 mM NaCl, pH 7.4.

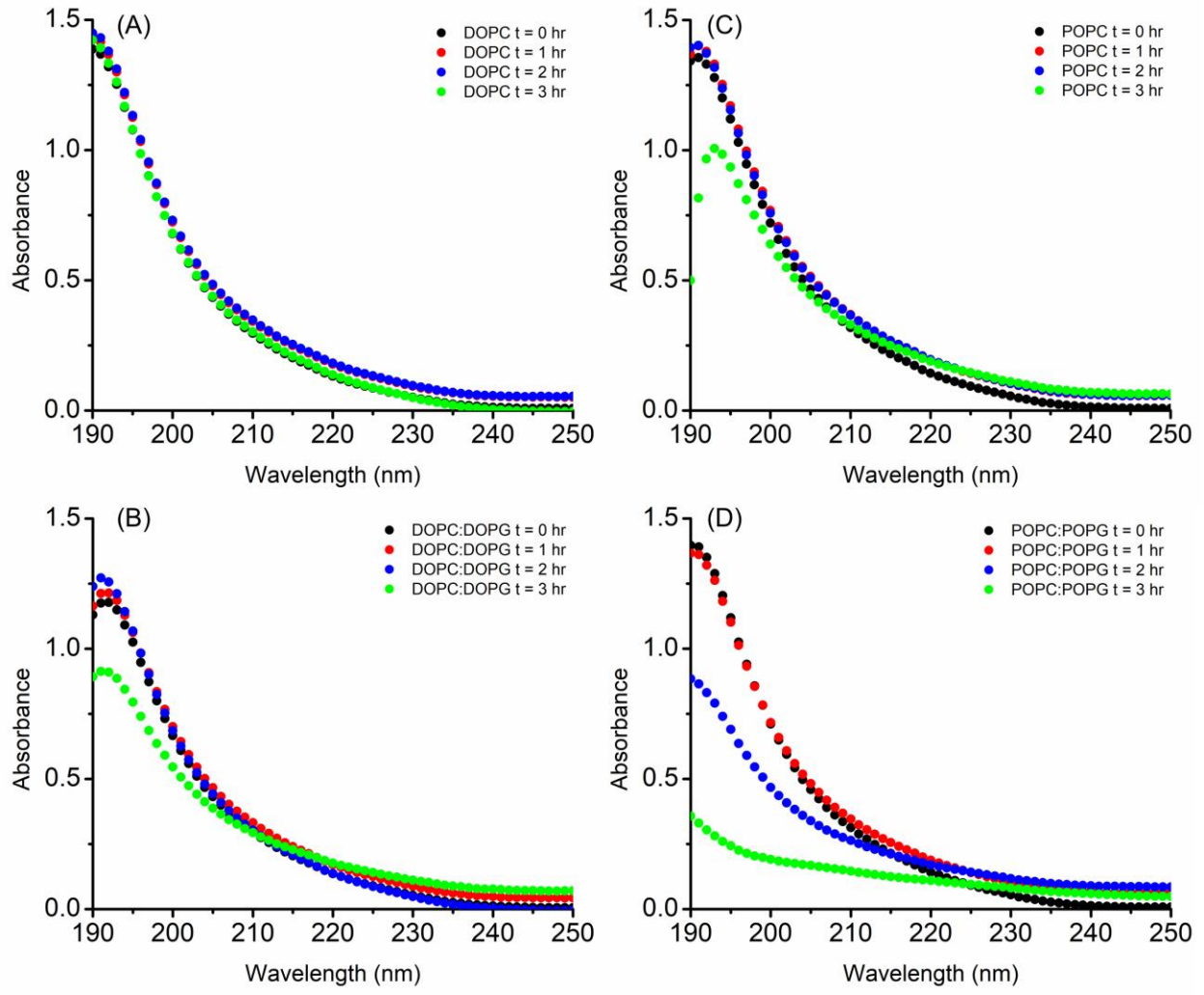

Figure B.2. CD absorbance over time confirms absorption flattening and signal loss. Absorption spectra of hCT at 40 μM were collected at the indicated timepoints with 100 μM of 100 nm LUVS of A) DOPC, B) DOPC:DOPG (7:3), C) POPC, and D) POPC:POPG (7:3). The rate of absorption loss is consistent with CD signal loss seen in Figure 3.3, indicating signal loss to be due to absorption flattening rather than peptide remodeling. Samples were prepared identically to those used for ThT experiments with the exception of NaF replacing NaCl. All measurements and incubations were performed at 25 °C.

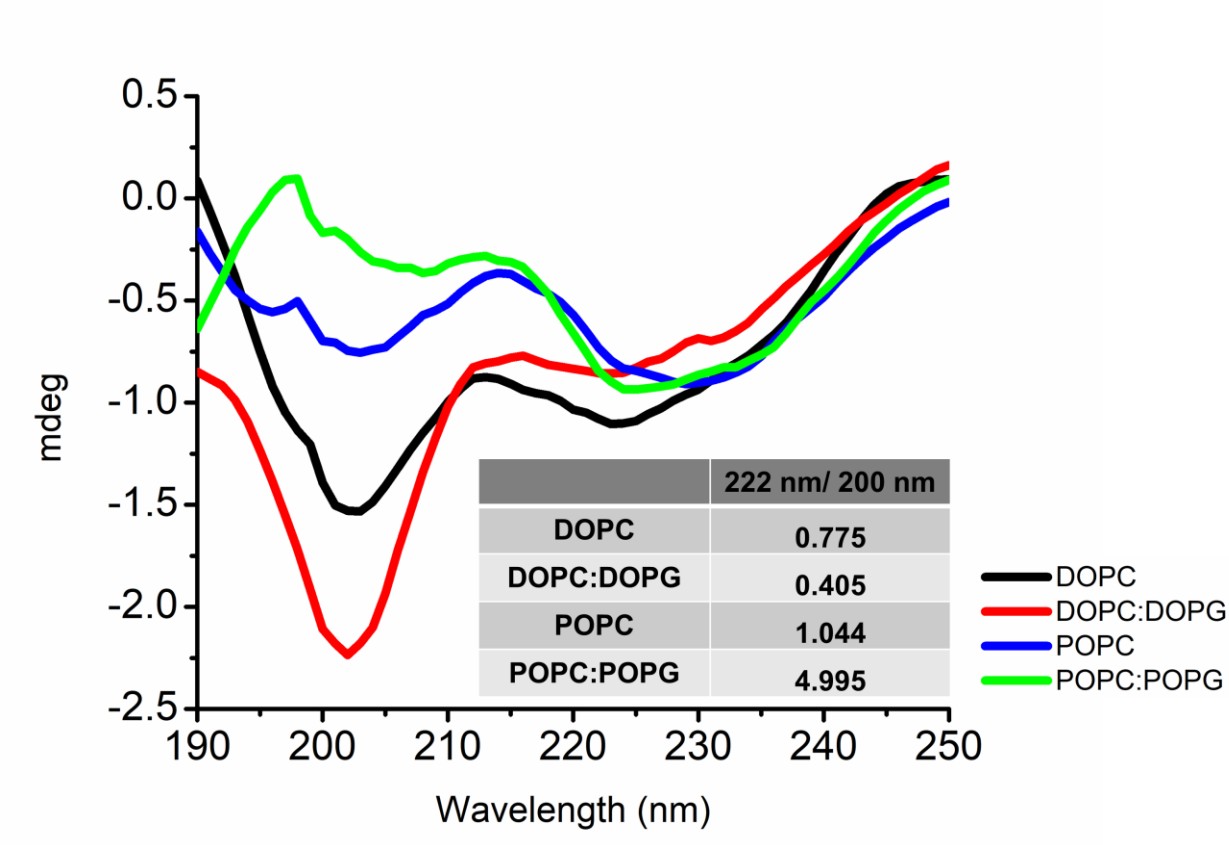

Figure B.3. LUVs that slow aggregation increase adsorption and induce enhanced helical structure in hCT at intermediate time points. CD spectra of hCT at 40 μM were collected after three hours of incubation with 100 μM of 100 nm LUVS of the indicated lipid compositions under 1000 rpm shaking. The faster aggregating DO lipid conditions show higher intensity and greater random coil propensity when compared to the slower aggregating PO lipids, which show a stronger helical propensity. This difference is quantified in the table showing the ratio between helical signal at 222 nm and random coil signal at 200 nm. The increased absorption flattening and helical propensity indicate the enhanced stabilization of growth-competent hCT monomers by PO lipids as compared to DO lipids. Samples were prepared identically to those used for ThT experiments with the exception of NaF replacing NaCl. All measurements and incubations were performed at 25 °C.

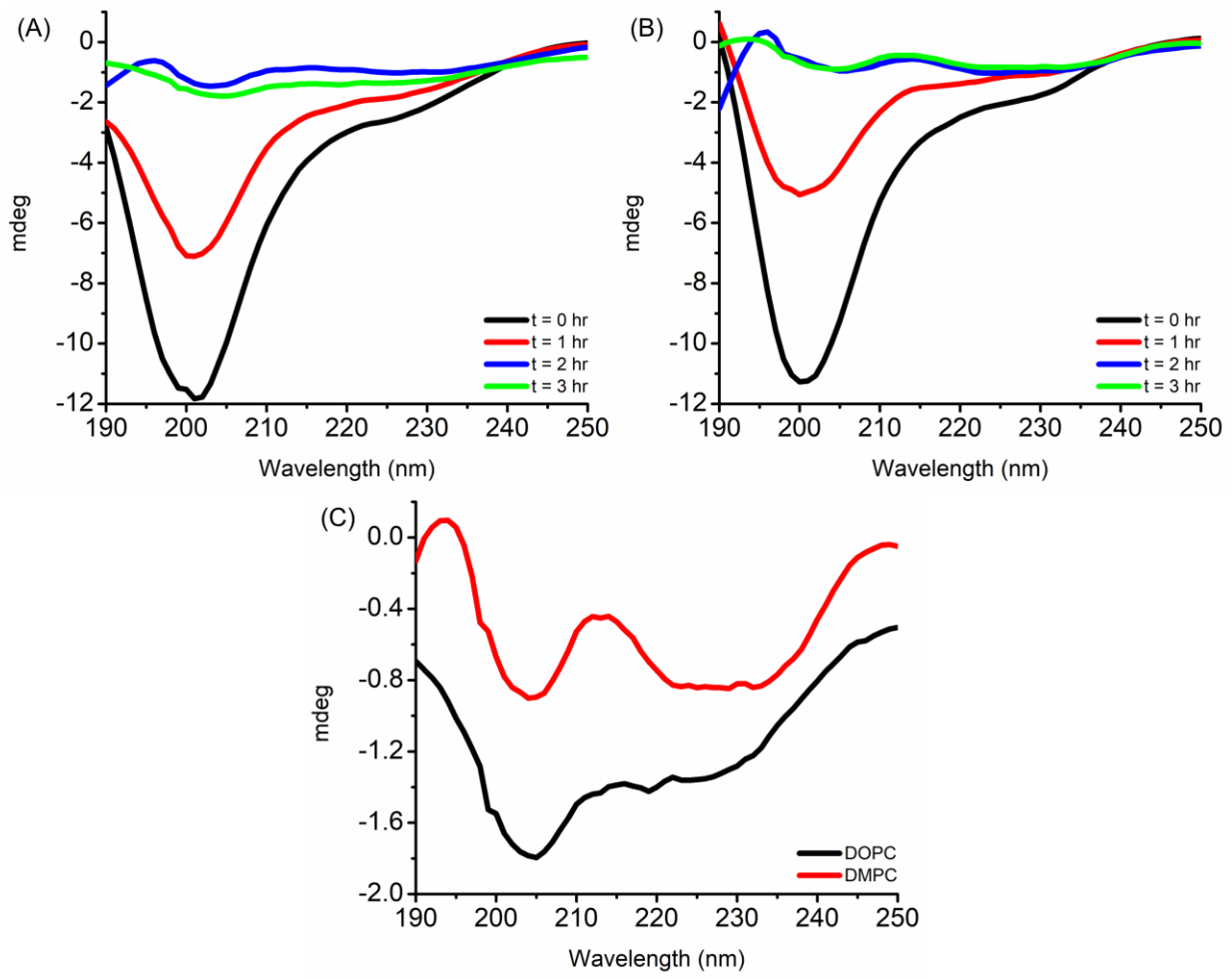

Figure B.4. DMPC LUVs show more rapid absorption flattening and induce greater helical structure in hCT than DOPC LUVs. CD spectra of 40 μM hCT were collected at the indicated timepoints in 100 μM of 100 nm LUVs of A) DOPC and B) DMPC. Signal loss is more rapid for DMPC LUVs, again consistent with the idea that more rigid bilayers encourage surface interactions and faster absorption flattening. C) The CD spectra for DOPC and DMPC at t = 3hr show weaker signal intensity and enhanced helical propensity for DMPC, consistent with similar comparisons between DO and PO lipids. The faster loss of CD signal as compared to Figure 3.2. is due to the overall aggregation acceleration at 35 °C compared with 25 °C. Samples were prepared identically to those used for ThT experiments with the exception of NaF replacing NaCl. All measurements and incubations were performed at 35 °C.

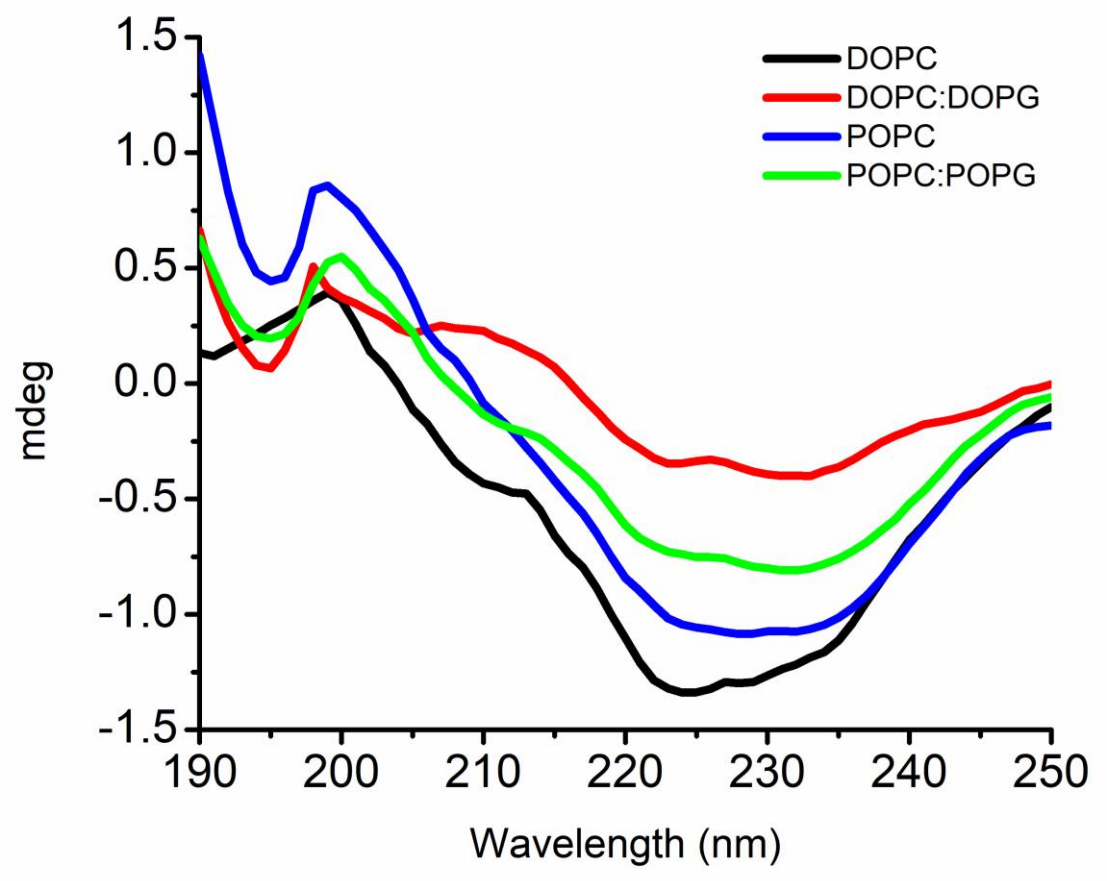

Figure B.5. CD spectra taken after 24 hours of aggregation for hCT grown in a membrane environment show primarily β-sheet structures. Spectra taken from same samples as shown in Figure 3.2. All measurements and incubations were performed at 25 °C. Slight variations in mature β-sheet signals are likely due to different polymorphs and degrees of membrane association.(1)

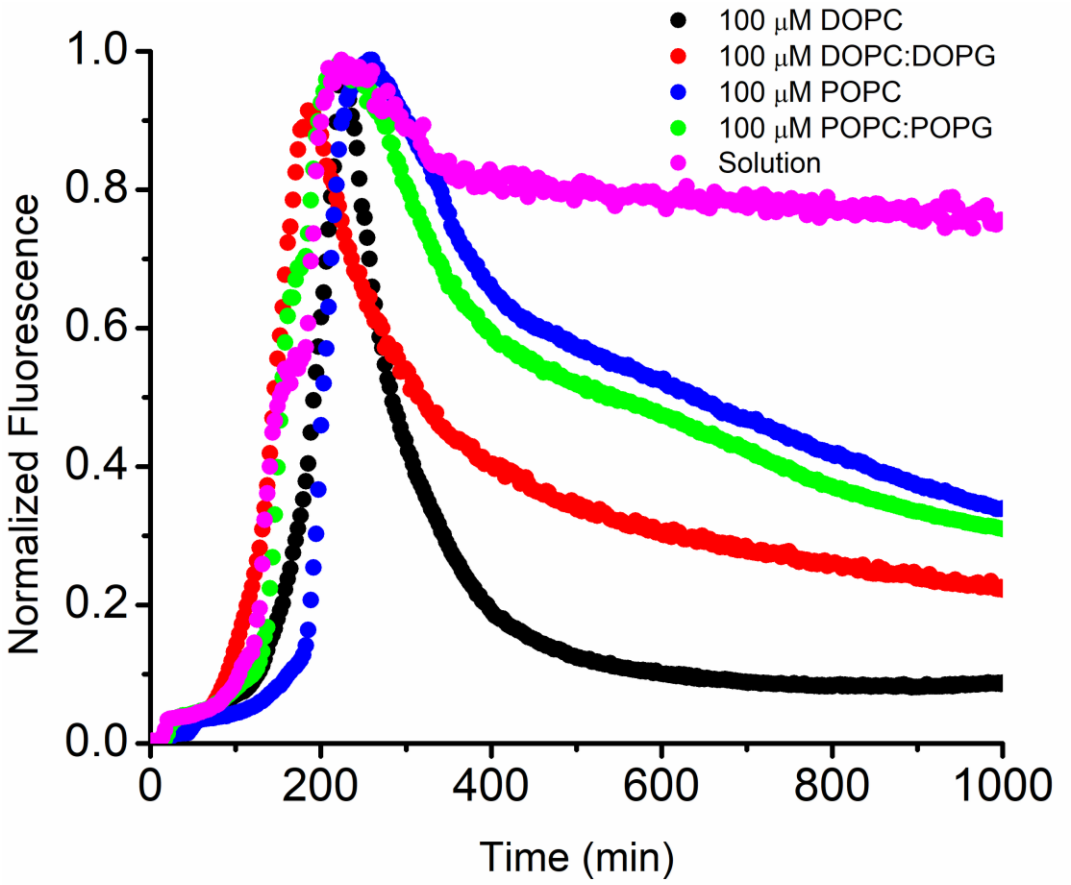

Figure B.6. ThT signal loss for 10 μM hCT fibers is significantly greater than that seen in solution. LUV curves are the same as those shown in Figure 3.1. with the solution curve having been taken from the same plate. While 10 μM hCT fibrils grown in solution maintain a stable plateau, fibrils in the presence of LUVs experience significant intensity loss. DO lipids show a more significant intensity loss than PO lipids. Displayed curves represent normalized averages of three independent trials at 25 °C in 20 mM phosphate buffer and 100 mM NaCl, pH 7.4.

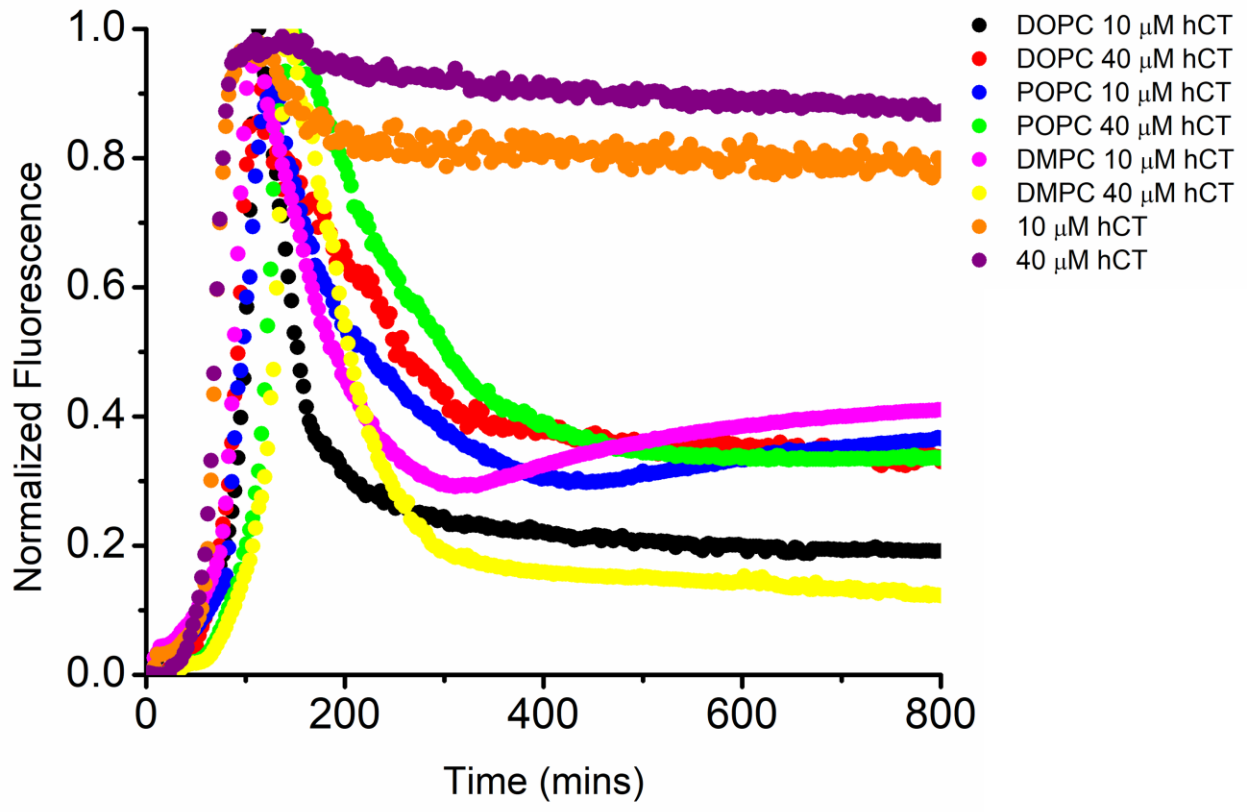

Figure B.7. Higher temperatures induce fibril remodeling in all LUV compositions and peptide to lipid ratios. hCT at 10 μM and 40 μM was allowed to aggregate in the presence of 100 μM of 100 nm LUVs composed of DOPC, POPC, and DMPC lipids at 35 °C. While both 10 μM and 40 μM hCT fibrils in solution show no appreciable signal loss, all LUV conditions show rapid and significant decline in ThT signal regardless of composition or peptide to lipid ratio. The uniform signal loss at higher temperatures suggests that such temperatures could overcome LUV-dependent energy barriers to fibril remodeling responsible for the different remodeling behaviors of PO and DO lipids. Displayed curves represent normalized averages of three independent trials in 20 mM phosphate buffer and 100 mM NaCl, pH 7.4.

B.2. References

1. Lomont, J. P., Ostrander, J. S., Ho, J.-J., Petti, M. K., and Zanni, M. T. (2017) Not All β-Sheets Are the Same: Amyloid Infrared Spectra, Transition Dipole Strengths, and Couplings Investigated by 2D IR Spectroscopy. *J. Phys. Chem. B.* **121**, 8935–8945